



Innovative separation and detection protocols for compounds of forensic importance

AUTHOR(S)

Ashton Theakstone

PUBLICATION DATE

01-05-2019

HANDLE

[10536/DRO/DU:30146632](https://hdl.handle.net/10536/DRO/DU:30146632)

Downloaded from Deakin University's Figshare repository

Deakin University CRICOS Provider Code: 00113B

Innovative separation and detection protocols for compounds of forensic importance

by

Ashton Gwendolyn Theakstone

Bachelor of Forensic Science (Honours)

Submitted in fulfilment of the requirements for the degree of
Doctor of Philosophy

Deakin University

May, 2019



DEAKIN UNIVERSITY
ACCESS TO THESIS - A

I am the author of the thesis entitled:

'Innovative separation and detection protocols for compounds of forensic importance'

Submitted for the degree of Doctor of Philosophy

This thesis may be made available for consultation, loan and limited copying in accordance with the Copyright Act 1968.

'I certify that I am the student named below and that the information provided in the form is correct'

Full Name: Ashton Gwendolyn Theakstone

Signed: Signature Redacted by Library

Date: 03/05/2019



DEAKIN UNIVERSITY
CANDIDATE DECLARATION

I certify the following about the thesis entitled:

‘Innovative separation and detection protocols for compounds of forensic importance’

submitted for the degree of Doctor of philosophy

- a. I am the creator of all or part of the whole work(s) (including content and layout) and that where reference is made to the work of others, due acknowledgment is given.
- b. The work(s) are not in any way a violation or infringement of any copyright, trademark, patent, or other rights whatsoever of any person.
- c. That if the work(s) have been commissioned, sponsored or supported by any organisation, I have fulfilled all of the obligations required by such contract or agreement.
- d. That any material in the thesis which has been accepted for a degree or diploma by any university or institution is identified in the text.
- e. All research integrity requirements have been complied with.

‘I certify that I am the student named below and that the information provided in the form is correct’

Full Name: Ashton Gwendolyn Theakstone

Signed: Signature Redacted by Library

Date: 03/05/2019

TABLE OF CONTENTS

Table of contents.....	IV
Abstract.....	VII
Acknowledgements.....	IX
Publications.....	XI
Abbreviations.....	XII
Chapter one:.....	1
General introduction and literature review	1
1.1 Forensically important compounds.....	2
1.2 Amphetamine type stimulants.....	3
1.2.1 Synthetic pathways	5
1.2.1.1 Amphetamine.....	5
1.2.1.2 Methamphetamine.....	5
1.2.1.3 3,4-Methylenedioxymethamphetamine (MDMA).....	7
1.2.2 History and appeal	9
1.2.3 Current separation and detection methods.....	14
1.2.3.1 Preliminary testing	14
1.2.3.2 Confirmatory testing	16
1.3 Synthetic cannabinoids	18
1.3.1 Synthetic pathways	21
1.3.2 History and appeal	23
1.3.3 Current separation and detection methods.....	27
1.4 Proposed separation and detection methods	29
1.4.1 Flow injection analysis (FIA)	29
1.4.2 High performance liquid chromatography (HPLC).....	30
1.4.3 Chemiluminescence (CL) detection.....	30
1.4.4 Electrochemiluminescence (ECL) detection.....	32
1.4.5 Solid-state nuclear magnetic resonance (SSNMR) spectroscopy detection	38
1.5 Project aims.....	40
Chapter two:.....	42
Chemiluminescence detection of illicit substances.....	42
Chapter overview	43
2.1 Introduction.....	44

2.1.1 Amphetamine type stimulants.....	44
2.1.2 Synthetic cannabinoids	47
2.2 Experimental.....	49
2.2.1 Chemicals.....	49
2.2.2 Instrumentation	51
2.2.2.1 Amphetamine type stimulants.....	51
2.2.2.2 Synthetic cannabinoids	53
2.3 Results and discussion	55
2.3.1 Amphetamine type stimulants.....	55
2.3.2 Synthetic cannabinoids	62
2.4 Conclusions.....	71
2.4.1 Amphetamine type stimulants.....	71
2.4.2 Synthetic cannabinoids	72
Chapter three:.....	73
Electrochemiluminescence detection in aqueous environments.....	73
Chapter overview	74
3.1 Introduction.....	75
3.2 Experimental.....	79
3.2.1 Chemicals.....	79
3.2.2 Instrumentation	79
3.3 Results and discussion	82
3.4 Conclusions.....	89
Chapter four:	90
Electrochemiluminescence detection in organic environments.....	90
Chapter overview	91
4.1 Introduction.....	93
4.2 Experimental.....	98
4.2.1 Chemicals.....	98
4.2.2 Instrumentation	99
4.3 Results and discussion	100
4.4 Conclusions.....	122
Chapter five:.....	124
Determination of synthetic cannabinoids in real samples.....	124
Chapter overview	125

5.1 Introduction.....	126
5.2 Experimental.....	129
5.2.1 Chemicals.....	129
5.2.2 Instrumentation	130
5.2.2.1 Electrochemiluminescence (ECL)	130
5.2.2.2 Solid-state nuclear magnetic resonance (SSNMR) spectroscopy	130
5.3 Results and discussion	131
5.3.1 Electrochemiluminescence (ECL) detection.....	131
5.3.2 Solid-state nuclear magnetic resonance (SSNMR) spectroscopy detection	151
5.4 Conclusions.....	160
Chapter six:	162
Concluding remarks and future work	162
6.1 Concluding remarks	163
6.2 Future work.....	164
References.....	167

ABSTRACT

Amphetamine type stimulants and synthetic cannabinoid compounds are forensically important as they are a social and health problem worldwide. Amphetamine type stimulants continue to be the second highest abused substance after cannabis and have been so for many years. Synthetic cannabinoids however, have recently emerged as a “legal” and “natural” alternative to cannabis, promising similar psychoactive effects to users. Detection systems for amphetamine type stimulants have been well established including a number of preliminary and confirmatory tests. Nevertheless, there is room for development in elucidation of these compounds based on the improvements seen in recently emerging analytical technologies. Due to the synthetic cannabinoids being a relatively new illicit substance, there is limited research around detection methods that can accurately identify specific compounds without extensive run times or sample preparations.

The research described herein explores utilising a tris(2,2'-bipyridine)ruthenium(II) chemiluminescence (CL) detection for both amphetamines and synthetic cannabinoids, *via* flow injection analysis (FIA) as well as post column high performance liquid chromatography (HPLC) separations. This approach has been taken to afford simple separation and detection protocols that have the capacity to be useful for forensic practitioners. Initial condition optimisations were performed with FIA for amphetamines and applied to post column HPLC. Five seizure samples were obtained with known concentrations of active ingredients that confirmed the viability of this technique for the selective detection of amphetamine type stimulants. The reaction conditions for synthetic cannabinoids were obtained from previous research conducted at Deakin University and further explored with post-column HPLC separations. This method of detection proved less selective towards these synthetic cannabinoid substances therefore research was then targeted towards electrochemiluminescence.

Electrochemiluminescence (ECL) was explored as an alternative novel technique with initial research focusing on a model compound (TPrA) to better understand the reaction mechanisms for co-reactant ECL, with the aim of applying to illicit substances. Three metal centered luminophores (Ir(ppy)_3 , $[\text{Ir(df-ppy)}_2(\text{ptb})]^+$ and $[\text{Ru(bpy)}_3]^{2+}$) were studied to gain an understanding into the redox processes occurring to elicit an ECL response with TPrA. These were subjected to both cyclic voltammetry and chronoamperometry experiments to establish the range of emitting potentials as well as location of the ECL response (at the counter or working electrode). Dual emission or multi-coloured systems were explored to exhibit a potential secondary emission location for a bi-detection model.

Once the fundamental knowledge of luminophore emissions were understood it was applied to synthetic cannabinoid substances acting as the co-reactant. A photomultiplier tube (PMT) and a Canon EOS 6D DSLR digital camera were utilised as the emission detectors to establish the range of emitting potentials and location indicating the specific reaction pathways (anodic or cathodic). Thirteen synthetic cannabinoid standards and twelve samples containing known compounds were subjected to both cyclic voltammetry and chronoamperometry experiments and displayed promising results for a potential screening tool, without the need for a sample extraction.

Solid-state nuclear magnetic resonance (SSNMR) spectroscopy was explored alongside the ECL experiments as a complementary technique for the determination of synthetic cannabinoids. The determination of synthetic cannabinoids was viable without interferences from the herbal substrate that illustrates a potential non-destructive technique without extractions and ensures sample integrity is maintained for further analysis if needed.

ACKNOWLEDGEMENTS

There are many people all over the world that I am very grateful for and would not have made it this far without their love and support.

Firstly, to my supervisor Associate Professor Xavier Conlan. Thank you for always encouraging me to follow my dreams, even if that means temporarily leaving to the other side of the world and supporting a football team that will never be promoted. I would not be here without your support and advice and will forever be grateful.

To my co-supervisor Professor Paul Francis. Thank you for your hard work, advice and recommendations with laboratory work and writing up. I appreciate any time you spend helping me learn and expand my knowledge within the chemistry world. You were my honours supervisor, so I definitely wouldn't be here without that initial support within research and I am appreciative for your huge contributions towards my research.

To Dr Lynn Dennany, thank you for this international collaboration and becoming such an important role model and friend. I appreciate everything you have taught me and the opportunities you have provided. Majority of the work within this thesis would not have been completed without your on-going guidance.

To Alfred Deakin Professor Neil Barnett and Dr Zoe Smith, you have supported me since day one and I will forever be grateful of all your love and support. I appreciate every laugh we've had together and thank you for believing in me and welcoming me back with open arms.

To everyone that has helped me within the laboratory and with this thesis (Lachlan Soulsby, Egan Doeven and Luke O'Dell), I appreciate all your efforts especially when I ask for help in a last-minute panic.

To my close friends at Deakin University, past and present (Nat Gasz, Kim Quayle, Niki Burns, Luke Andrighetto, Hannah Brozinski and the Greyling street fam), you are the reasons I enjoy my work. Thank you for always making me laugh and keeping me sane in tough times.

To my parents, you are the reason I am who I am today. I am grateful for you both and I appreciate every phone call and text and I know that you'll always be there for me, as I will for you.

PUBLICATIONS

Ashton G. Theakstone, Zoe M. Smith, Jessica M. Terry, Neil W. Barnett and Paul S. Francis, Chemiluminescence detection of MDMA in street drug samples using tris(2,2'-bipyridine)ruthenium(III), *Drug Testing and Analysis* 7(5): 428-432 (2015). DOI: 10.1002/dta.1780

This paper is a result of the work presented in **Chapter two** of this thesis.

Ashton G. Theakstone, Egan H. Doeven, Xavier A. Conlan, Lynn Dennany and Paul S. Francis, 'Cathodic' electrochemiluminescence of $[\text{Ru}(\text{bpy})_3]^{2+}$ and tri-*n*-propylamine revealed as emission at the counter electrode. Submitted to the Journal of Chemical Communications 25/04/2019.

This paper is a result of the work presented in **Chapter three** of this thesis.

Niki K. Burns, **Ashton G. Theakstone**, Haijin. Zhu, Luke A. O'Dell, James R. Pearson, Trent D. Ashton, Fred M. Pfeffer and Xavier A. Conlan, Solid-state NMR detection and identification of synthetic cannabinoids surface coated on herbal substrates. To be submitted to the Analyst (May 2019)

This paper is a result of the work present in **Chapter five** of this thesis.

Other publications not presented in this thesis include:

A.F. Clarke, **A.G. Theakstone**, X.A. Conlan. Environmental recirculation of ketamine. Australian Veterinary Journal. 92(7), N21, (2014)

Mitchell T. Montgomery, Xavier A. Conlan, Neil W. Barnett, **Ashton G. Theakstone**, Kim Quayle, and Zoe M. Smith, Determination of morphine in culinary poppy seed tea extractions using high performance liquid chromatography with chemiluminescence detection. *Australian Journal of Forensic Sciences*, 2019: p. 1-4.

Mitchell T. Montgomery, Xavier A. Conlan, **Ashton G. Theakstone**, Stuart D. Purcell, Neil W. Barnett, and Zoe M. Smith, Extraction and determination of morphine present on the surface of Australian food grade poppy seeds using acidic potassium permanganate chemiluminescence detection. Submitted to the Journal of Food Chemistry 29/04/2019.

ABBREVIATIONS

λ	Wavelength
5F-AKB48	N-(adamantan-1-yl)-1-(5-fluoropentyl)-1H-indazole-3-carboxamide
AB-CHMINACA	N-[(1S)-1-(aminocarbonyl)-2-methylpropyl]-1-(cyclohexylmethyl)-1H-indazole-3-carboxamide
ACN	Acetonitrile
AM-1220	[1-[(1-methyl-2-piperidinyl)methyl]-1H-indol-3-yl]-1-naphthalenyl-methanone
AM-2201	1-[(5-fluoropentyl)-1H-indol-3-yl]-(naphthalen-1-yl)methanone
ATS	Amphetamine type stimulants
Au	Absorbance units
BB-22	1-(cyclohexylmethyl)-8-quinolinyl ester-1H-indole-3-carboxylic acid
CCD	Charge coupled device
CE	Counter electrode
CL	Chemiluminescence
CT	Charge transfer
CV	Cyclic voltammetry
E	Applied potential
ECL	Electrochemiluminescence
eV	Electron volt
FIA	Flow injection analysis
FTIR	Fourier transform infrared spectroscopy
GC	Glassy carbon
HOMO	Highest occupied molecular orbital
HPLC	High performance liquid chromatography
$h\nu$	Photon

<i>i</i>	Current
Ir(ppy) ₃	Tris(2-phenylpyridine-C ² ,N)iridium(III)
Ir(df-ppy) ₂ (ptb)	Bis[3,5-difluoro-2-(2-pyridinyl-κN)phenyl-κC][2-[1-(phenylmethyl)-1H-1,2,3-triazol-4-yl-κN ₃]pyridine-κN]iridium(III)
JWH-302	2-(3-methoxyphenyl)-1-(1-pentyl-1H-indol-3-yl)-ethanone
L	Ligand
LC	Ligand centre
LMCT	Ligand to metal charge transfer
LOD	Limits of detection
LUMO	Lowest unoccupied molecular orbital
MA	Methamphetamine
MC	Metal centre
MDA	3,4-Methylenedioxyamphetamine
MDEA	3,4-Methylenedioxyethylamphetamine
MDMA	3,4-Methylenedioxymethamphetamine
MDMB-CHMICA	N-[[1-(cyclohexylmethyl)-1H-indol-3-yl]carbonyl]-3-methyl-L-valine, methyl ester
MLCT	Metal to ligand charge transfer
MO	Molecular orbital
MS	Mass spectrometry
NMR	Nuclear magnetic resonance spectroscopy
PB-22	1-pentyl-1H-indole-3-carboxylic acid 8-quinolinyl ester
PCA	Principal component analysis
PMT	Photomultiplier tube
RE	Reference electrode
RSD	Relative standard deviation
RT	Retention time

[Ru(bpy) ₃] ²⁺	Tris(2,2'-bipyridine)ruthenium(II)
[Ru(bpy) ₃] ³⁺	Tris(2,2'-bipyridine)ruthenium(III)
Ru(bpy) ₂ (CH ₃ CN) ₂	Bis(acetonitrile)bis(2,2'-bipyridine)ruthenium(II)
Ru(bpy) ₃ Cl ₂ .6H ₂ O	Tris(2,2'-bipyridine)dichlororuthenium(II) hexahydrate
Ru(bpy) ₃ (PF) ₆	Tris(2,2'-bipyridine)ruthenium(II) hexafluorophosphate
SPE	Screen printed electrode
STS-135	1-(5-fluoropentyl)-N-tricyclo[3.3.1.1 ^{3,7}]dec-1-yl-1H-indole-3-carboxamide
THC	Tetrahydrocannabinol
THJ-018	1-naphthalenyl(1-pentyl-1H-indazol-3-yl)-methanone
THJ-2201	[1-(5-fluoropentyl)-1H-indazol-3-yl]-1-naphthalenyl-methanone
TBAPF ₆	Tetrabutylammonium hexafluorophosphate
TPrA	Tri- <i>n</i> -propylamine
UR-144	(1-pentylindol-3-yl)-(2,2,3,3-tetramethylcyclopropyl)methanone
UV	Ultra violet
ν	Scan rate
V	Volt
XLR-11	(1-(5-fluoropentyl)-1H-indol-3-yl)(2,2,3,3-tetramethylcyclopropyl)methanone
WE	Working electrode

CHAPTER ONE:

GENERAL INTRODUCTION AND LITERATURE REVIEW

1.1 Forensically important compounds

Both classes of compounds (amphetamine type stimulants and synthetic cannabinoids) explored within this research are important for current forensic practices. Amphetamine type stimulants have a long history with many varieties being developed and abused over the years [1]. This chapter will introduce the history, prevalence and detection methods of amphetamine, methamphetamine and methylenedioxy ring substituted amphetamines. The research project presented here focuses on the latter, with novel detection methods being explored for methylenedioxy ring substituted amphetamines, including 3,4-methylenedioxymethamphetamine (MDMA). Synthetic cannabinoids have recently emerged as a major component of new psychoactive substances (NPS) worldwide [1]. This chapter introduces the brief history of these compounds, as well as prevalence and current analytical detection systems in place to determine synthetic cannabinoids. The research in the following chapters focuses on developing methods for screening and identifying specific synthetic cannabinoid compounds.

1.2 Amphetamine type stimulants

Amphetamine type stimulants refer to a class of compounds that are derived from the parent backbone, phenethylamine (Figure 1.1) [2-4]. Amphetamine and methamphetamine are non-ring substituted phenethylamines with methyl groups attached at the R₃ or R₁ and R₃ locations, respectively (Table 1.1) [3].

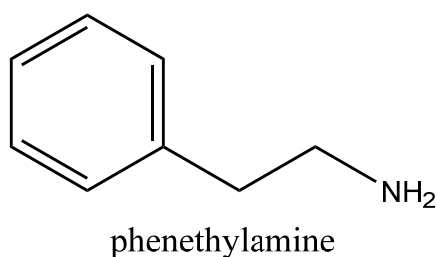
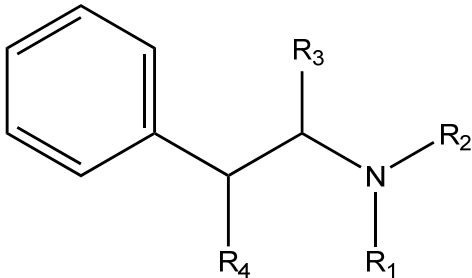


Figure 1.1. Chemical structure of phenethylamine.

Table 1.1. Locations of functional groups on non-ring substituted amphetamine type stimulants: amphetamine and methamphetamine [5].

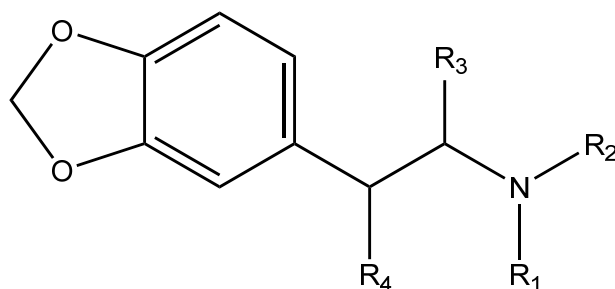


Common name	IUPAC name	R ₁	R ₂	R ₃	R ₄
Phenethylamine	2-phenylethan-1-amine	H	H	H	H
Amphetamine	1-methyl-2-phenethylamine	H	H	CH ₃	H
Methamphetamine	<i>N</i> -methyl- <i>N</i> -(1-methyl-2-phenethyl)amine	CH ₃	H	CH ₃	H

Methylenedioxy ring substituted phenethylamines involve a class of entactogen compounds, including three forensically important substances: 3,4-methylenedioxyamphetamine (MDA),

3,4-methylenedioxyethylamphetamine (MDEA) and 3,4-methylenedioxymethamphetamine (MDMA) [3]. The parent phenethylamine backbone has a methylenedioxy ring connected to the benzene with the methyl or ethyl group substitutions for these compounds displayed in Table 1.2 [3, 6].

Table 1.2. Locations of functional groups on methylenedioxy ring substituted amphetamine type stimulants: MDA, MDEA and MDMA [5].



Common name	IUPAC name	R ₁	R ₂	R ₃	R ₄
MDA	1-(1,3-benzodioxol-5-yl)propan-2-amine	H	H	CH ₃	H
MDEA	<i>N</i> -[2-(1,3-benzodioxol-5-yl)-1-methylethyl]- <i>N</i> -ethylamine	C ₂ H ₅	H	CH ₃	H
MDMA	<i>N</i> -[2-(1,3-benzodioxol-5-yl)-1-methylethyl]- <i>N</i> -methylamine	CH ₃	H	CH ₃	H

1.2.1 Synthetic pathways

1.2.1.1 Amphetamine

Commonly illicit manufacture of amphetamine follows the Leuckart reaction from the starting materials 1-phenyl-2-propanone (P2P) and formamide. The P2P ketone is converted to an amine *via* reductive amination with an *N*-formylamphetamine intermediate [5, 7] as outlined below in Figure 1.2.

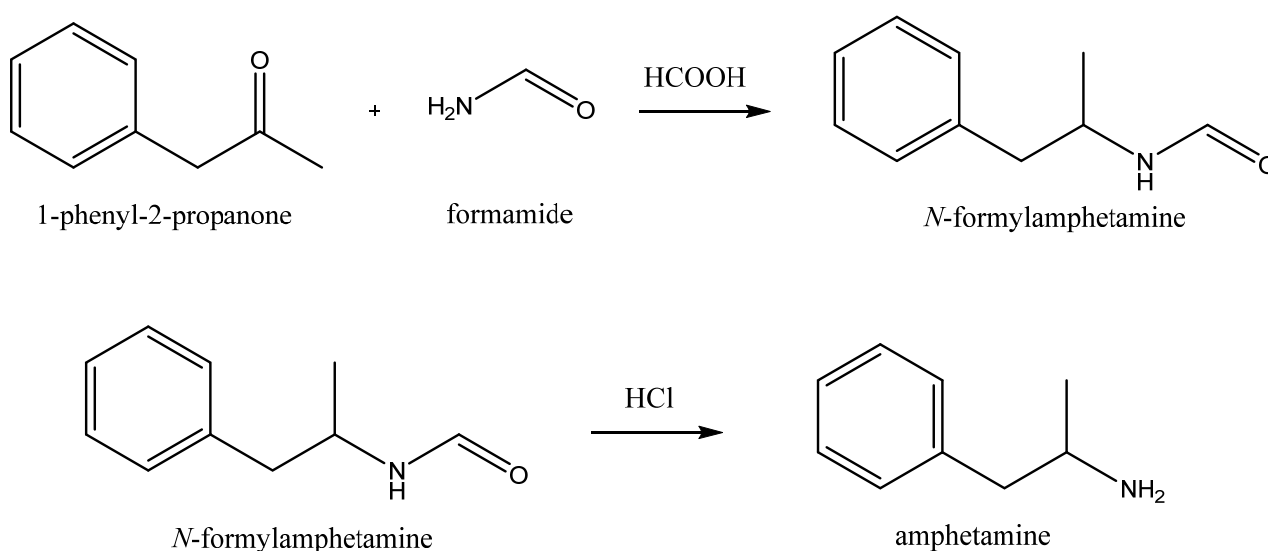


Figure 1.2. Synthetic pathway for the manufacture of illicit amphetamine *via* Leuckart reaction.

1.2.1.2 Methamphetamine

There are three common routes for the synthesis of illicit methamphetamine, each containing ephedrine or pseudoephedrine as the starting material [5, 8, 9]. Firstly the Nagai route that uses hydriodic acid and red phosphorus [8, 10], secondly the Birch reduction with anhydrous ammonia and either lithium or sodium metal and the third is the Emde route *via* heterogeneous catalytic reduction [8]. An overview of the three synthetic routes are presented in Figure 1.3.

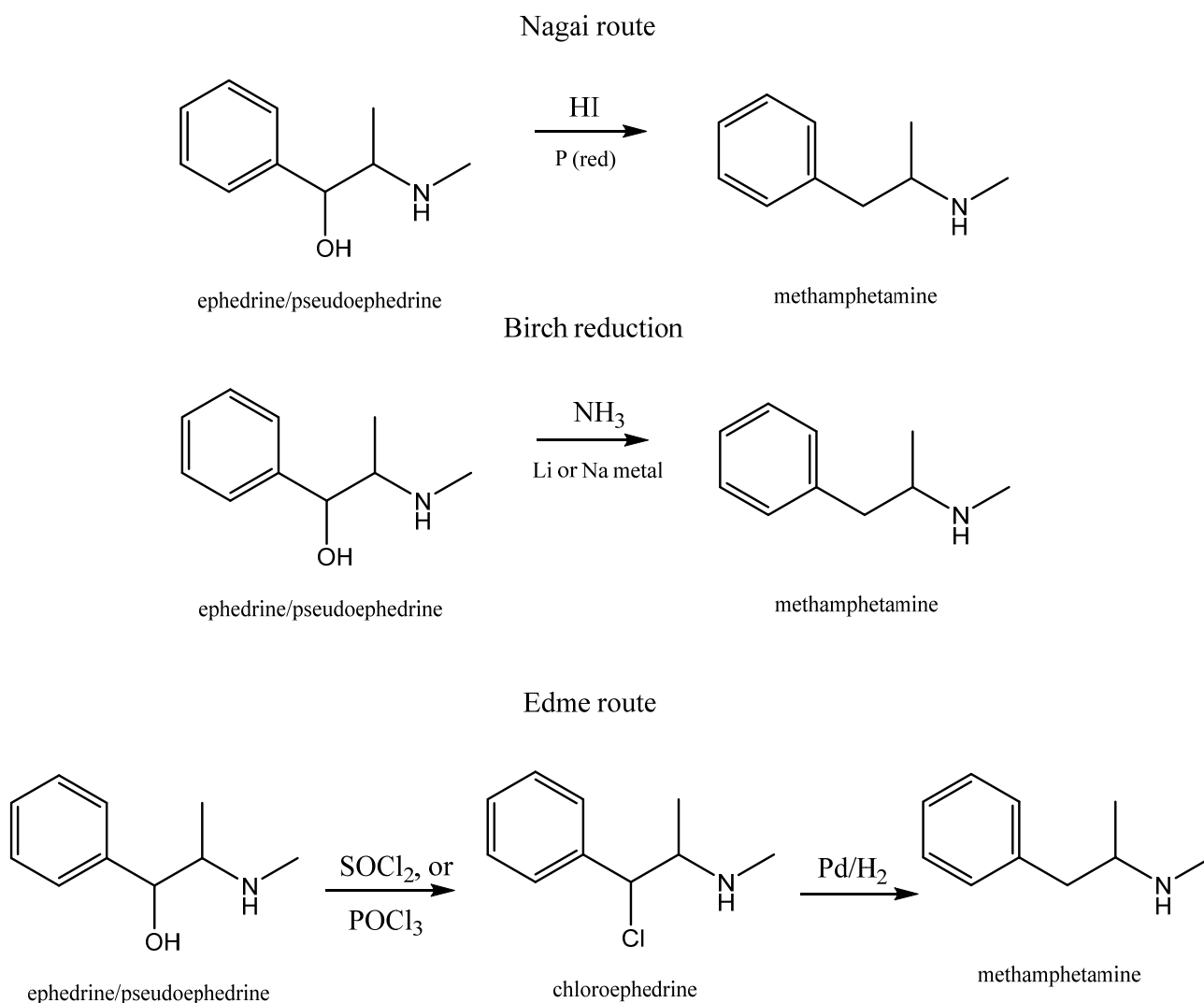


Figure 1.3. Synthetic pathway for the manufacture of illicit methamphetamine *via* Nagai route (top), Birch reduction (middle) and Edme route (bottom).

Ephedrine and pseudoephedrine (more typically pseudoephedrine) can be obtained *via* simple extractions from common cold and flu tablets available at pharmacies or purchased online [11, 12]. Due to the extent of methamphetamine production worldwide and the ease in precursor obtainment, ephedrine and pseudoephedrine are now under strict international controls [13, 14]. Within Australia, as of October 2015, they are listed as a Schedule 4 substance with purchase available *via* a prescription only process [15]. In July 2018, Australia implemented a SafeScript initiative that monitors prescription records within an online database. This enables pharmacists and doctors to identify circumstances where prescriptions are being used beyond

the medical needs and is aimed towards Schedule 8 substances and other high-risk medications, including those containing ephedrine or pseudoephedrine [16]. Since this change in scheduling, illicit methamphetamine production has started to shift towards the use of other precursor such as P2P and ephedrine that has been obtained by a fermentation process with benzaldehyde as the starting material [17]. In the case of the fermentation once it is complete and ephedrine is extracted the methamphetamine production can be achieved by the same steps illustrated above in Figure 1.3.

1.2.1.3 3,4-Methylenedioxyamphetamine (MDMA)

Illicit MDMA synthesis is similar to amphetamine synthesis involving reductive amination with a 3,4-methylenedioxyphenyl-2-propanone (3,4-MDP2P) ketone and methylamine free base as the starting materials, this occurs *via* a reversible imine intermediate [5]. The reaction mechanism is shown in Figure 1.4.

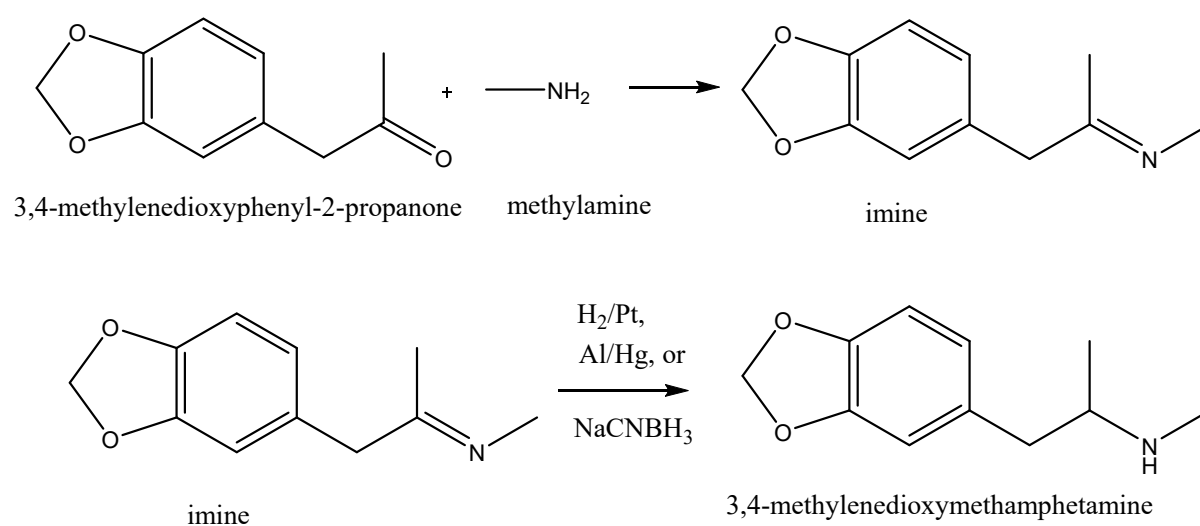


Figure 1.4. Reductive amination pathway used for illicit MDMA manufacturing.

The 3,4-MDP2P ketone is typically obtained by oxidising a plant oil (safrole) [18], that is condensed with the methylamine free base and reduced into MDMA. The MDMA produced *via* this method is a racemic mixture of R(-) and S(+) at roughly 50:50 ratios [19] that combined generate the full MDMA psychoactive effects. Typically with psychoactive compounds one stereoisomer is generally responsible for majority of effects interestingly however MDMA does not follow this trend, with R(-)-MDMA producing the psychedelic effects and S(+)-MDMA responsible for stimulation [19-21].

1.2.2 History and appeal

Amphetamines have been used pharmaceutically for the treatment of depression and narcolepsy and they have also been exploited as anti-obesity agents and decongestants [22]. In the 1930s, benzodrine (a racemic mixture of levoamphetamine and dextroamphetamine) was marketed and sold as a decongestant for asthma and common colds. It was one of the first instances where a pharmaceutical drug could be used recreationally for their stimulant effects and as a result, was banned by the Food and Drug Administration (FDA) in 1959 [22]. Dexedrine (dextroamphetamine), ritalin (methylphenidate) and adderall (dextroamphetamine and amphetamine mixture) are still used today for the treatment of narcolepsy or attention deficient hyperactive disorder (ADHD) in children, and are globally obtained *via* a prescription only [22].

MDMA was first synthesised in Germany by the pharmaceutical company Merck, and between 1912 and the mid-1970s, little to no information was available until a chemist by the name of Alexander Shulgin rediscovered it [23, 24]. From this point on, MDMA was used for psychotherapy treatments for depression, anxiety and post-traumatic stress disorder [25, 26]. In the early 1980s, MDMA or 'ecstasy' was starting to be used outside of a therapeutic context and was experimented with by individuals attending concerts, self-exploration, spiritual curiosity and in dance clubs. It became a large trend within nightclubs and dance music scenes across continental Europe, the UK and USA [23]. In 1985, MDMA was considered a schedule 1 controlled substance in the USA, from which psychotherapy treatments became illegal [27]. 3,4-Methylenedioxymethamphetamine (MDMA) intake releases serotonin (5-HT), dopamine and norepinephrine that stimulates the central nervous system (CNS) and the sympathetic nervous system (SNS) [12, 28-30]. The desired effects include a sense of euphoria and

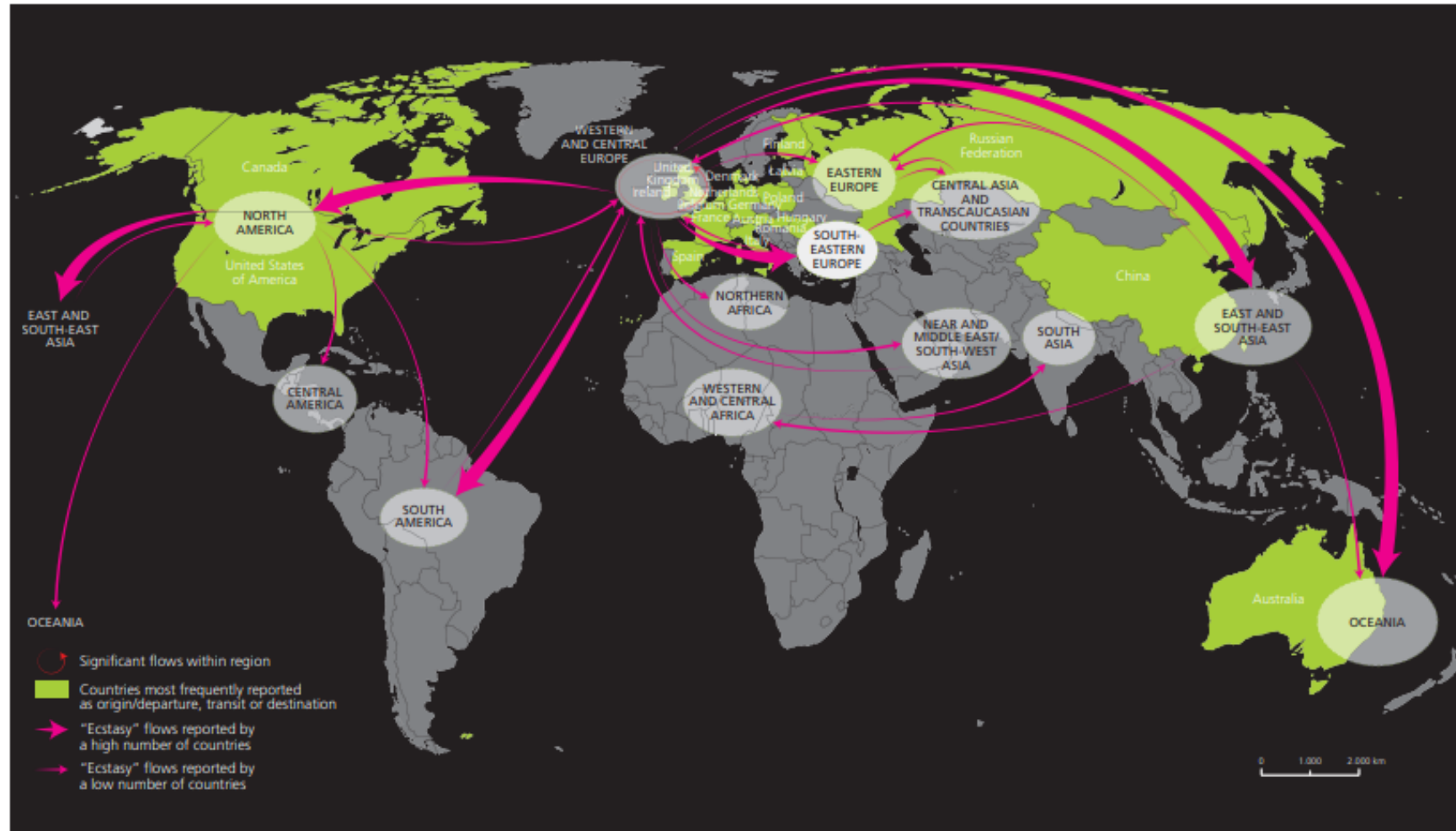
wellbeing, heightened sensors, greater sociability and closeness to others [24]. Typically, MDMA is pressed into a pill or in capsule form and is administered *via* oral ingestion [23, 31]. The daily dose of MDMA ranges between 75 mg to 150 mg, with experienced users often taking more noting that the effects begin typically within 5-20 min of ingestion [19]. The ‘rush’ associated with this drug is due to an increased heart rate and body temperature, pupil dilation, and jaw muscle tightening. The effects have been observed to typically last up to four hours, however the major effects of withdrawal such as depression, anxiety or paranoia can last several days [32]. Further, a user may notice muscle aches, energy loss, trouble sleeping and irritability during this period after use. Long term effects of using MDMA can include neurotoxicity, psychosis, cognitive functions, poor memory and depression [32] and there is extensive literature surrounding MDMA use and the persistence of psychiatric symptoms. McGuire *et al.* highlighted the prevalence of psychosis, panic attacks, depersonalisation, depression and visual distortions from long term use of MDMA that remains long after use has stopped [33]. This coincides with a study by McCann *et al.* that outlined the positive correlation between MDMA and a decrease in the 5-HT transport binding, lowering serotonin levels within the brain [34].

Illicit amphetamine samples come with a range of active ingredient(s) and a number of excipients that can be dangerous to the consumer and depending on the adulterants present, can cause serious negative side effects. Typically, they are synthesised by scientifically untrained individuals in clandestine laboratories, often with make shift, poor quality equipment [35, 36]. As a result of this, they are almost guaranteed to contain trace amounts of precursors such as ephedrine, pseudoephedrine, safrole and P2P, or intermediates such as *N*-formylamphetamine and chloroephedrine, that indicate the synthesis not reaching completion [3]. The particular precursors or intermediates present in samples can aid in monitoring illicit substances as it

provides information on specific synthetic methods that can be traced back to clandestine laboratories. Adulterants, or cutting agents, are added to bulk the sample that increases the opportunity to sell more product and gain more profits for the supplier [37]. Sugars, caffeine, paracetamol or other household products are often detected within illicit samples [38]. Any white, crystalline substance can be exploited as a cutting agent as they resemble the appearance of the drug and are used to increase sample volume without any thought to the physical consequences for the consumers [37, 39, 40]. Other illicit substances are often found within samples being sold as ecstasy that illustrates the extreme dangers and uncertainty of what is being consumed. The National Institute on Drug Abuse outlined that a large portion of ecstasy seized by the police contain substances such as cocaine, ketamine or synthetic cathinones ("bath salts") that have stimulant or psychoactive effects and combined with amphetamines can be potentially lethal [41].

According to the 2018 world drug report, global ecstasy quantities of seizures almost tripled from 2012 to 2016, reaching 14 tonnes. In Australia alone an increase from 1 tonne being seized in 2015 to 5 tonnes in 2016 was observed [1]. International supply of ecstasy is well established from Western and Central Europe as the trafficking hubs of the world [1, 42] as displayed in Figure 1.5.

MAP 3 | Interregional trafficking flows of "ecstasy", 2012-2015



MARKET ANALYSIS OF SYNTHETIC DRUGS A. Amphetamine-type stimulants

Source: UNODC, responses to annual report questionnaire, 2012-2015.

Note: The origins of the flow arrows do not necessarily indicate the source/manufacture of "ecstasy". Flow arrows represent the direction of "ecstasy" trafficking and are not an indication of the quantity trafficked. The boundaries shown on this map do not imply official endorsement or acceptance by the United Nations. Dashed lines represent undetermined boundaries. The dotted line represents approximately the Line of Control in Jammu and Kashmir agreed upon by India and Pakistan. The final status of Jammu and Kashmir has not yet been agreed upon by the parties. The final boundary between the Sudan and South Sudan has not yet been determined.

Figure 1.5. Global ecstasy flows as represented in the 2017 UNODC world drug report [42]

Between 2014 and 2016, in Australia, 35 clandestine laboratories were identified by police services for the manufacture of MDMA. In the following year, between 2016 and 2017, only 8 MDMA manufacturing clandestine laboratories were detected that is shown in Figure 1.6 [42, 43].

State/ Territory	ATS (excluding MDMA)	MDMA	Homebake heroin	Cannabis oil extraction	PSE extraction	GHB/ GBL	Other ^a	Unknown ^b	Total ^c
NSW	32	3	0	3	0	2	15	3	58
Vic	112	3	0	8	5	3	0	4	135
Qld	88	1	0	1	0	3	0	57	150
SA	48	0	0	9	4	3	7	16	87
WA	19	0	1	0	2	0	8	7	37
Tas	2	0	0	0	1	0	0	0	3
NT	4	1	0	0	0	0	0	0	5
ACT	0	0	0	0	0	0	0	0	0
Total	305	8	1	21	12	11	30	87	475

a. 'Other' refers to the detection of other illicit manufacture.

b. 'Unknown' includes seized substances which were unable to be identified or are awaiting analysis.

c. Total may exceed the number of clandestine laboratory detections due to multiple drug production types being identified in a single laboratory.

Figure 1.6. Number of clandestine laboratories detections, by drug production type, per state and territory between 2016 and 2017. Image from reference [43].

This decrease in the number of clandestine laboratories identified suggests that MDMA supply has shifted towards international importation rather than local manufacturing. The amount of MDMA consumed annually is much higher than the amount that can be produced by the number of local laboratories so the consumption must be sourced from both local and international supply [1]. Importation of MDMA and/or its precursors occurs primarily through international mail, that accounts for 75% of the number detected at the border, and air cargo providing the other 25%. The weight of MDMA and/or its precursors samples is 98.2% through air cargo and only 1.8% *via* international mail [43].

1.2.3 Current separation and detection methods

In 1987, the United Nations Office on Drugs and Crime (UNODC) published recommended methods for the testing of illicit ring-substituted amphetamine derivatives [38]. These recommended methods were revised and updated in 2006 and include a number of presumptive/preliminary and confirmatory tests [5]. The presumptive tests are a preliminary screening to provide information on specific classes of compounds. Confirmatory testing is required as specific identification and quantification is needed for forensic purposes [5, 38].

1.2.3.1 Preliminary testing

Colour tests are usually the first screening on any seizure drug material as they are quick and quite sensitive so only require small amounts of sample [5, 38, 39]. These typically involve reacting the sample with a known reagent and observing any colour change [44] as displayed in Figure 1.7 with an unknown sample giving a positive response for ecstasy when reacted with a Marquis reagent.

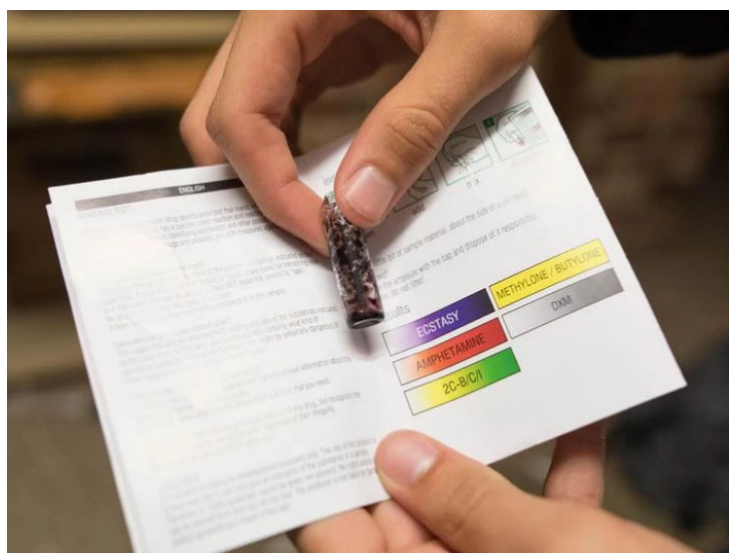


Figure 1.7. Positive test result for ecstasy utilising the Marquis reagent. Image from reference [45].

There are a number of reagents that have been developed towards being selective to the class of drug. For amphetamines there are four widely used colour test reagents [5, 38] including the Marquis test that is utilised to distinguish between amphetamine and their ring-substituted derivatives. The Simon's test is used for secondary amines such as MDEA and MDMA, however other secondary amines can give false positive results so a further test is needed for these compounds reducing its analytical utility [37]. The Chen's test distinguishes between starting materials such as ephedrine or pseudoephedrine with amphetamine or methamphetamine while the gallic acid test reacts specifically with the methylenedioxy substructure and can distinguish between MDA, MDEA and MDMA from amphetamine and methamphetamine. Common precursors such as safrole also react with the gallic acid test therefore it is not commonly utilised in the field [5, 38]. The range of compounds that are targets for the colour test reagents are summarised in Table 1.3.

Table 1.3. Colour test results for amphetamine, ephedrine/pseudoephedrine, methamphetamine, MDA, MDEA and MDMA using Marquis, Simon or Chen reagents.

Compound	Marquis	Simon	Chen
Amphetamine	Orange, slowly turning brown	NR*	NR*
Ephedrine/pseudoephedrine	NR	NR*	Purple
Methamphetamine	Orange, slowly turning brown	Deep blue	NR*
MDA	Dark blue/black	NR*	NR*
MDEA	Dark blue/black	Deep blue to brown	NR*
MDMA	Dark blue/black	Deep blue	NR*

NR = no reaction.

* donates colour of reagent to be considered as negative [5].

Beyond the colour tests Fourier transform infrared spectroscopy (FTIR) is another preliminary analysis technique commonly utilised for the presumptive indication of specific compounds

present in unknown samples. It is a qualitative method that can determine structural information of single or mixed materials by comparison to a reference material [5, 38, 46]. Currently, the most common FTIR approach includes the use of attenuated total reflectance (ATR), that is preferred over other approaches because it requires no sample preparation [37, 47]. The ATR method involves passing infrared light through a crystal that reflects off the internal surface and makes contact with the sample placed above. The reflective beam leaves the crystal and transmittance of light is recorded. The resulting spectrum indicates specific functional groups within samples by assigning them to specific wavenumber regions [37, 47]. The reference FTIR-ATR spectra for MDMA is shown in Figure 1.8.

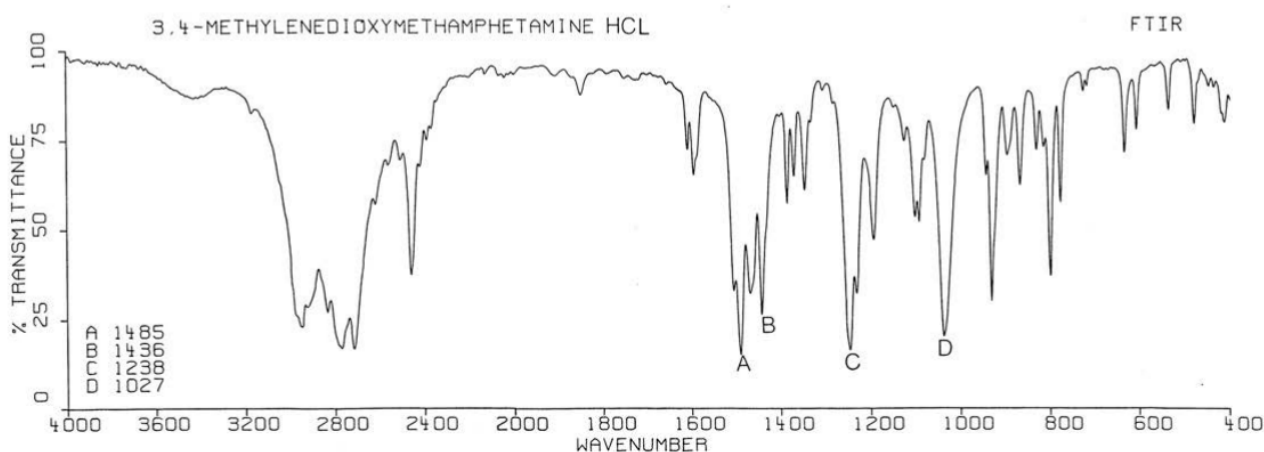


Figure 1.8. Reference FTIR-ATR spectrum for MDMA HCl (Instrumental Data for Drug Analysis) [48].

Other preliminary testing for amphetamine type stimulants, particularly methylenedioxy substituted, include anion tests, microcrystal tests and thin layer chromatography (TLC) [5, 38]. These presumptive tests are not as commonly used therefore they will not be included in greater detail in this thesis.

1.2.3.2 Confirmatory testing

The preliminary tests give information on classes of compounds or an indication of structural moieties however confirmatory testing is needed to identify and quantify specific compounds

within an unknown sample [5, 38]. Amphetamine seizure samples are often quite complex, including the presence of multiple active components and numerous adulterants [40, 49]. Due to their complex nature, analytical separations are performed in order to separate individual components. Gas chromatography and high performance liquid chromatography (HPLC) are the preferred separation techniques, often coupled with one of three detectors – flame ionisation detector (FID) or mass spectrometry (MS) for gas chromatography and UV absorbance for HPLC [5, 38, 50-52].

For amphetamines, including ring substituted amphetamines, HPLC is preferred over gas chromatography as they are non-volatile and polar compounds [53]. The UN recommended methods suggest an isocratic technique with UV absorbance detection at wavelengths of 200-210 nm for amphetamines and 280-290 nm for the ring substituted derivatives. The presence of specific compounds is confirmed by comparisons with known standards and quantified using a standard calibration curve [5, 38, 54-56].

1.3 Synthetic cannabinoids

Synthetic cannabinoids were originally designed to help in aiding the study of the endocannabinoid system in the 1980s [57]. They are CB₁ and CB₂ receptor agonists that results in similar effects to Δ^9 -tetrahydrocannabinol (Δ^9 -THC), the psychoactive ingredient in cannabis [58]. There are several structural differences between Δ^9 -THC and synthetic cannabinoids (shown in Figure 1.9), therefore the typical psychoactive effects can come with unwanted side effects [59]. These side effects can include nausea, agitation, anxiety, paranoia, convulsions and can lead to addiction. It has also been reported that withdrawal symptoms from synthetic cannabinoid addiction is harsher than cannabis and similar to cocaine or opiate substances [59, 60].

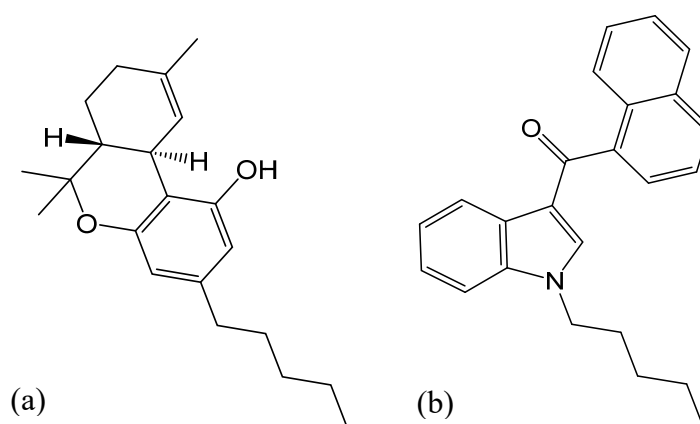


Figure 1.9. Chemical structure of Δ^9 -THC (a), and a synthetic cannabinoid: JWH-018 (b).

In order to be taken by the user synthetic cannabinoids are dissolved in an appropriate volatile solvent (typically acetone) and sprayed onto an herbal substrate and the solvent is allowed to dry off [57]. Inert dried plant material make up these herbal substrates and commonly included indian warrior (*Pedicularis Densiflora*), lion's ear (*Leonotis Leonuris*), damiana (*Turnera Diffusa*), marshmallow leaf (*Althaea Officinalis*) and mullein leaf (*Verbascum Thapsus*) [61-63].

Structurally, synthetic cannabinoids can vary quite considerably with each one made up of four components; the core, head, a linker and tail (Figure 1.10) [64]. The core of the structure, being the centre component, is typically an indole or indazole. The head is quite bulky and varies dependant on synthetic cannabinoid series. A linker (sometimes referred to as a bridge) joins the bulky head to the core and is often a carboxamine, carboxylate or methanone. The final component of the structure is the tail, that connects to the bottom of the core and is often an alkyptentyl chain that may or may not be halogenated [64].

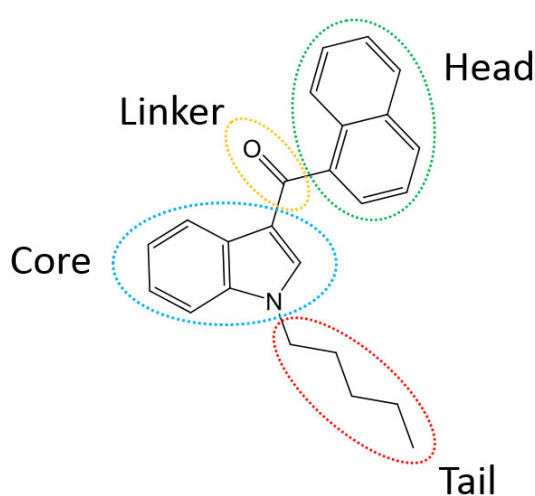


Figure 1.10. Chemical structure of JWH-018 illustrating the head, linker, core and tail components.

Examples of four structurally varying synthetic cannabinoids is shown in Figure 1.11 (PB-22, UR-144, 5F-AKB48 and AB-CHMINACA).

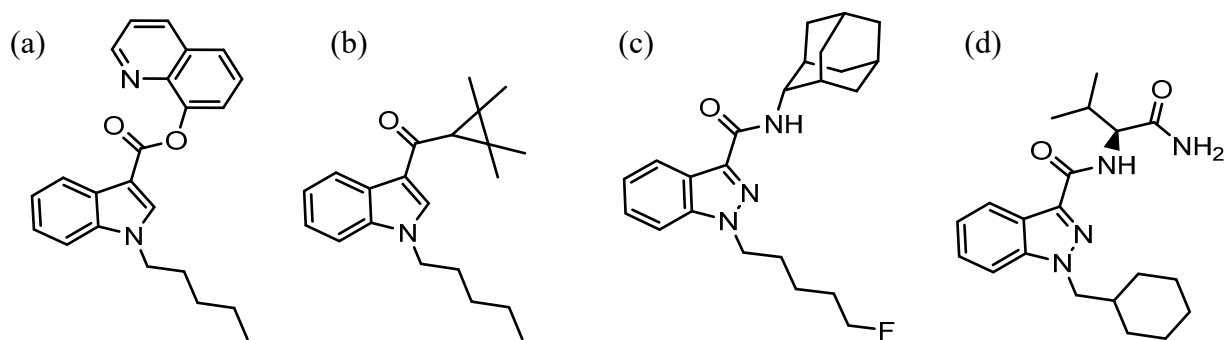


Figure 1.11. Chemical structures of four synthetic cannabinoids: (a) PB-22, (b) XLR-11, (c) 5F-AKB48 and (d) AB-CHMINACA.

PB-22 consists of an indole core with a quinolinyl head connected by a carboxylate linker and an alkyl pentyl chain tail. UR-144 has an indole core with a tetramethylcyclopropyl head linked *via* a methanone and an alkyl pentyl chain tail. 5F-AKB48 consists of an indazole core with an adamantane head linked *via* a carboxamide and a fluorinated pentyl chain tail. AB-CHMINACA has an indazole core with an aminomethyloxobutanyl head linked *via* a carboxamide and a cyclohexylmethyl tail.

1.3.1 Synthetic pathways

With the changes to legislation restricting specific compounds, any minor alteration to the structure was a way for illicit manufactures to circumvent legislation. Popularity of particular synthetic cannabinoids emerged as waves due to the legislation bans [61]. Due to these on-going chemical alterations fuelled by legislation bans there are now hundreds of compounds classified as a synthetic cannabinoid [64, 65]. Synthesis of these compounds depends largely on what series they belong to and according to the United Nations Office on Crimes and Drugs (UNODC) and previously referred to within a British Advisory Council on the Misuse of Drugs (ACMD) report, synthetic cannabinoids can be classified into six categories [66, 67].

1. **Classical cannabinoids** (THC and structurally related derivatives). Examples include HU-210, AM-906, AM-411 and O-1184.
2. **Non-classical cannabinoids** (cyclohexylphenols or 3-arylcyclohexanols). Examples include CP-47,497 and CP-55,244).
3. **Hybrid cannabinoids** (combinations of classical and non-classical). An example is AM-4030.
4. **Aminoalkylindoles** - that is further divided into naphthoylindoles, phenylacetylindoles, naphthylmethylindoles and benzoylindoles.
5. **Eicosanoids** (Endocannabinoids such as anandamide, and their analogs)
6. **Others** – diarylpyrazoles, naphthoylpyrroles, naphthylmethylindines or derivatives of naphthalene-1-yl-(4-pentyloxynaphthalen-1-tyl)methanone.

A generalised synthetic pathway for indole derivatives is presented in Figure 1.12.

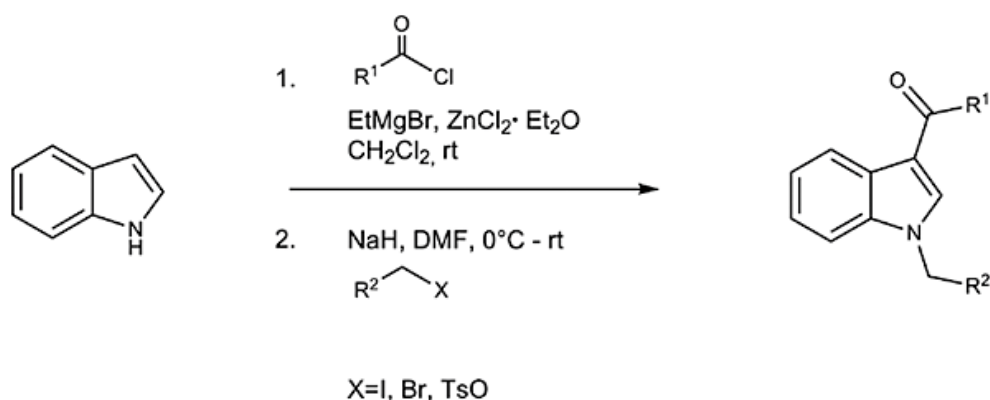


Figure 1.12. Synthetic pathway for indole derivatives of synthetic cannabinoid compounds. Image from reference [68].

An example of a specific synthesis of (1-(5-fluoropentyl)-1*H*-indol-3-yl)(2,2,3,3-tetramethylcyclopropyl)methanone (XLR-11) requires addition of ethylmagnesium bromide, zinc chloride in diethyl ether and 2,2,3,3-tetramethylcyclopropanecarbonyl chloride to a solution of 1*H*-indole to yield (1*H*-indol-3-yl)(2,2,3,3-tetramethylcyclopropyl)methanone [68]. Sodium hydride and 1-bromo-4-fluoropentane in DMF is added resulting in a sodium bromide precipitate, that is filtered off and the resulting product is then separated and concentrated under reduced pressure. The mixture is then purified with 100% DCM and yields an XLR-11 oil that crystallises on standing [68].

According to the Australian Crime Commission Illicit Drug Data Report, China is a major producer and exporter for NPS, including synthetic cannabinoids [28]. To date there has been no local laboratories detected by authorities and as such this highlights the fact that the majority of synthetic cannabinoids are likely to be imported across the Australian border and similar to the amphetamine type stimulants has shown to be most commonly through air cargo and international mail [1, 28].

1.3.2 History and appeal

Abuse of synthetic cannabinoids began in the early 2000s as these substances were sold online or in adult shops as "legal highs". They were promoted as "natural" or "herbal" and contained the words "not for human consumption", typically being sold as an incense or pot pourri [69, 70]. In 2004 there was a spike in popularity due to one brand of herbal substrate called "spice". Once these substrates were tested and the active ingredients were found to be synthetic cannabinoids, primarily JWH-018, the products were then being monitored by the European Monitoring Centre for Drugs and Drug Addiction (EMCDDA) [65]. Following that, individual synthetic cannabinoid structures became illegal however there were legislation loopholes and the number of cases dramatically increased between 2008 and 2012 [57]. Changing the cannabinoid structure slightly was one way to avoid the legislation. This could be as simple as adding a fluorine onto the end of the alkyl pentyl chain tail [71]. Example of this shown in Figure 1.13 with THJ-018 and THJ-2201.

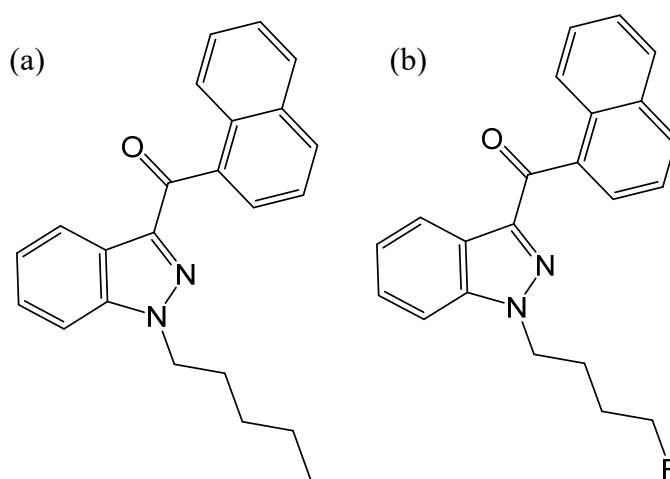


Figure 1.13. Chemical structures of two synthetic cannabinoids that vary only by fluorination of the alkyl pentyl chain. (a) THJ-018 and (b) THJ-2201.

Each state within Australia varies in regards to legislation of these substances and in Victoria, in 2011, eight specific compounds were listed as prohibited substances [72]. Following this, in

2013, a number of individual synthetic cannabinoids were added to the 1981 Act as a schedule eleven drug of dependence and schedule nine poison [73]. The original ban on specific compounds was later superseded by a blanket ban on all synthetic cannabinoids in March 2017. This blanket ban restricts any production, supply, sale or trafficking of these substances to be used for their psychoactive effects. All states and territories within Australia now carry this blanket ban [74].

Many illicit drug surveys including two completed by Vandrey *et al.* and Winstock and Barratt have looked into the reasons as to why people would use synthetic cannabinoids with two main reasons standing out in all surveys - an alternative to cannabis and simple curiosity [59, 61, 75]. As an alternative to cannabis, synthetic cannabinoids became a cheaper, more accessible and "legal" high. There was no deterrence due to the timing of legislation changes as users were often not participating in an illegal activity. Also, with any new synthetic drug, there is always the temptation due to curiosity. Many users wanted to compare naturally grown cannabis to synthetic cannabinoids, but also, some users just wanted to see how it affected them. Most surveys resulted in users preferring natural over synthetic as they found many unwanted side effects from these herbal mixtures [59, 75].

The desired effects wanted by consumers is similar to cannabis that tends to elevate mood, alter perceptions and aid in relaxation [31]. It has also been reported that synthetic cannabinoids are more potent than the THC alternative and include a number of unwanted side effects. This includes nausea, confusion, agitation, increased heart rate and hallucinations. In extreme cases, at very high doses, it can also raise blood pressure that reduces blood supply to the heart and leads to myocardial infarction [76-80]. Figure 1.14 illustrates the media attention synthetic cannabinoids have had in the last two years, with multiple overdoses and deaths globally. The

recent and on-going media attention illustrates the prevalence of these NPS and the need for preventative and detection methods in place.

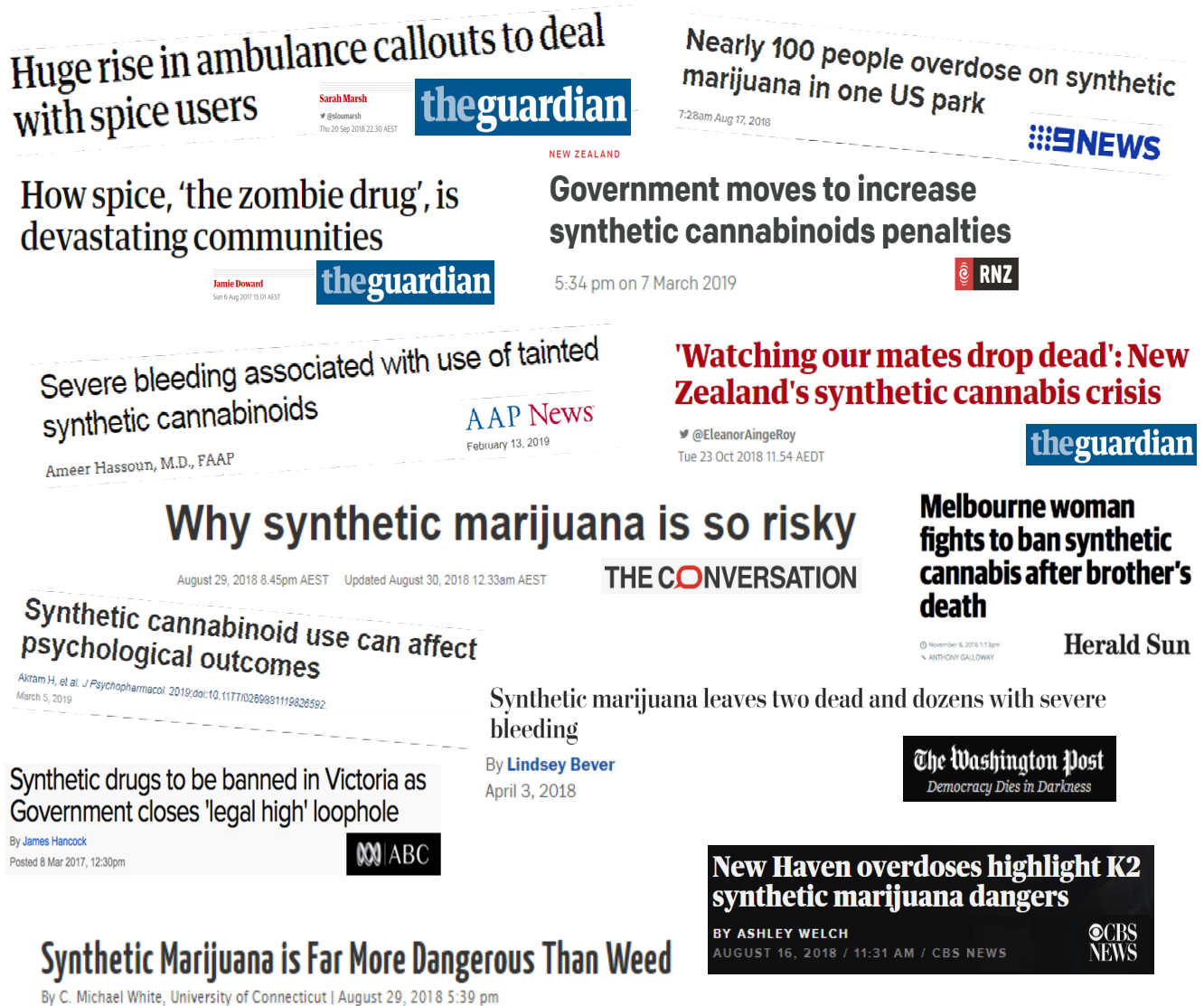


Figure 1.14. Recent media headlines outlining synthetic cannabinoids and the social or health affects involved.

Recent literature also outlines the prevalence and health concerns surrounding these substances with multiple fatalities due to synthetic cannabinoid intoxication [81]. Between July and October 2013 in the US, four deaths were linked to 5F-PB22 intoxication with post-mortem blood samples containing between 1.1 ng/mL to 1.5 ng/mL [82]. In 2014, two deaths in the US were linked to XLR-11 with analysis finding 1.4 ng/mL and 0.6 ng/mL in post-mortem samples [83]. A study surrounding adolescent fatalities within the US summarised eight causes of death

with users aged between 15 and 17 years. Three deaths were sudden, four were intoxication and one was from multiple injuries obtained in a motor vehicle accident associated with synthetic cannabinoids. Concentrations of synthetic cannabinoid in post-mortem blood samples ranged from 1.1 ng/mL to 12.3 ng/mL [84]. This study also illustrated that synthetic cannabinoids are not routinely tested by medical examiners unless prompted to do so by scene investigators or by the individuals' medical history. This lack of routine testing indicates that there is likely to be many synthetic cannabinoid related fatalities that remain unknown [84]. Within Australia, the 2018 annual overdose report highlights that the number of deaths due to cannabinoids continues to increase with 197 deaths in 2016 compared to 77 in 2013 [85].

1.3.3 Current separation and detection methods

With the onset of any new illicit substance being identified in public use there is the need for a rapid and reliable detection method. As these synthetic cannabinoids are relatively new, there is quite a broad range of recent literature that covers various methods of detection.

Preliminary tests such as colourimetric detection has been explored however it is not as effective as it is with other illicit substance groups. The Duquenois-Levine reagent that is commonly employed for THC is negative for the synthetic cannabinoids. The van Urk reagent that detects indole-containing drugs also elicits a negative response. The Marquis reagent elicits a positive response for cyclohexylphenols and the JWH series, however is negative for other series. These screening tests are selective towards cyclohexylphenols and the JWH series, but cannot detect low concentrations or mixtures of synthetic cannabinoids, therefore are not commonly employed [71].

Other preliminary and confirmatory tests presented within the literature involve a range of analytical detection methods. Attenuated total reflectance fourier transform infrared spectroscopy (ATR-FTIR) has been utilised for the identification and quantification of four specific synthetic cannabinoids (RCS-4, JWH-210, UR-144 and JWH-081). Although it provides a rapid technique for identification it requires an extraction to remove the synthetic cannabinoid from the herbal substrate [86]. Penn *et al.* explored a screening method involving two clinical immunoassay techniques as well as a gas chromatography/mass spectrometry (GC-MS) analysis. Due to the non-homogeneous nature of the real world sample preparation, the determination of the synthetic cannabinoid were inconsistent, and as a result extensive care with extraction techniques needs to be considered. Even with a selective technique such as GC-MS, some synthetic cannabinoids were un-detected [87]. Marino *et al.* illustrated the

limitations with chromatographic separations requiring extraction processes and mass spectrometers being unable to discriminate between two isomers. As a result of this, a method was developed utilising ^1H solution-state nuclear magnetic resonance (NMR) spectroscopy to determine the presence of a synthetic indole or indazole cannabinoid [88]. Ultra high performance liquid chromatography with time of flight mass spectrometry (UPLC-TOF-MS) detection provides selective identification however sample extraction combined with longer run times resulted in analysis taking between 20 minutes and 40 minutes for this particular separation [89] Another technique by Uchiyama *et al.* provides a method of identification utilising ultra-high performance liquid chromatography with electrospray ionization mass spectrometry (UPLC-ESI-MS) however sample extraction required 30 minutes of ultrasonication followed by fraction collection after a thin layer chromatography separation. [90]. All of the techniques described rely on extraction of the active ingredient from the herbal substrate that is not ideal for a rapid at-scene detection within a forensic context.

Detection methods highlighted from this research include traditional techniques such as flow injection analysis (FIA), and high performance liquid chromatography (HPLC) coupled with UV absorbance detection. It also explores HPLC coupled with chemiluminescence (CL) detection, electrochemiluminescence (ECL) and solid-state nuclear magnetic resonance (SSNMR) spectroscopy. Electrochemiluminescence and SSNMR identification is favoured as no extraction method is needed for identification of the active ingredients.

1.4 Proposed separation and detection methods

These proposed separation and detection methods provide alternative options for law enforcement agencies to utilise when approaching amphetamine type stimulants or synthetic cannabinoid substances. The detection methods afford little to no sample preparation that can provide a rapid at-scene mode for forensic investigators.

1.4.1 Flow injection analysis (FIA)

Flow injection analysis (FIA) is a continuous-flow method that involves injecting a specific volume of a solution into a carrier stream. It was developed in the mid-1970s by Stewart *et al.* [91] and Ruzicka and Hansen [92].

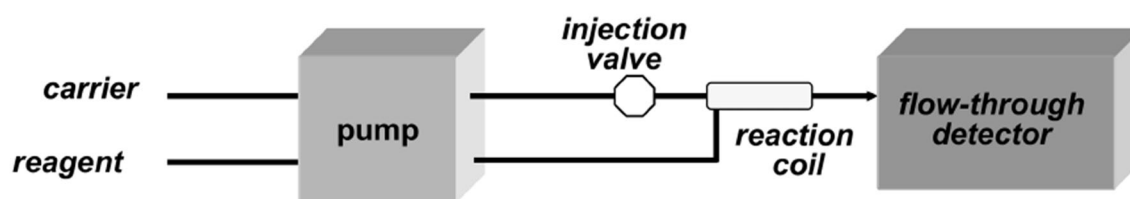


Figure 1.15. Schematic manifold of an FIA system. Image from [93].

The sample that is added to the carrier stream *via* an injection valve merges with a reagent at a confluence point (reaction coil) where the reaction takes place. The confluence point is located near the inlet of the flow cell, where the emitted light is detected, traditionally *via* a photomultiplier tube (PMT) as displayed in Figure 1.15 [94]. System design, including reaction kinetics, geometry of flow cell, flow rate and volumes need to be optimised to detect maximum emission signals [95-98]. The reaction that takes place involves chemiluminescence emissions that are described in more detail in section 1.4.3. [99] This technique affords a rapid quantitative screening and has proven to be viable within environmental, food and beverage testing, and previous forensically relevant experiments at Deakin University. The potential for

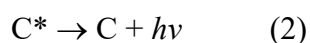
portable devices such as lab-on-valve or lab-on-chip systems with miniaturised FIA is particularly important for an at-scene drug screening by forensic personnel [93, 100].

1.4.2 High performance liquid chromatography (HPLC)

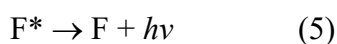
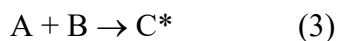
High performance liquid chromatography (HPLC) is a widely utilised separation technique that pumps a sample mixture in a solvent (mobile phase) through a column with specific packing material (stationary phase). The analytes in the sample mixture will interact with the stationary phase within the column and separate based on their competitive interactions between the mobile and stationary phases [101, 102]. For both amphetamine type stimulants and synthetic cannabinoid compounds, reverse phase techniques are routinely utilised. This involves a hydrophobic (or non-polar) stationary phase (typically C₁₈) where the polar analytes will pass through the column at a faster rate and analytes will be separated through differences in polarities [101, 102]. Traditional HPLC separations are coupled with UV absorbance detection through a diode array detector [51, 55, 56, 103]. For this research, UV absorbance will be explored alongside post-column chemiluminescence detection that is described in more detail in section 1.4.3.

1.4.3 Chemiluminescence (CL) detection

Chemiluminescence (CL) is a light producing reaction that involves creating a product in its excited state which emits a photon upon relaxation back to the ground state [99, 104, 105]. The intensity of the light emitted is indicative of the concentration of the reductant (or analyte) [104, 106]. Direct CL involves two species reacting to produce one CL emitting product (equations 1-2).

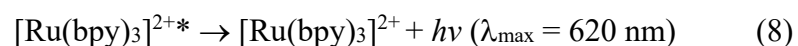
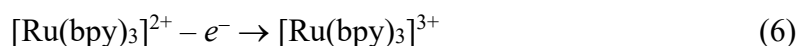


Indirect CL involves transferring the energy from the excited product to a fluorophore, which then emits light once relaxed back to the ground state (equations 3-5) [106, 107].



Chemiluminescence has many advantages over other analytical detection techniques as it requires simple instrumentation (a transparent flow cell mounted against a photosensitive device), has increased sensitivity and selectivity, and improved signal-to-noise ratios due to the absence of excitation sources and monochromators [104, 108, 109]. There is a wider analytical working range that offers lower detection limits compared to other techniques [104, 106, 110]. This is particularly important for detection of forensically important compounds as they are often in low concentrations that may be undetectable *via* other analytical methods. There are a number of common reagents in the literature for CL detections, including acidic potassium permanganate, luminol, acridirium, esters, dioxetanes, hypohalites, diaryloxalates and tris(2,2'-bipyridine)ruthenium(II) [106].

Tris(2,2'-bipyridine)ruthenium(II) ($[\text{Ru}(\text{bpy})_3]^{2+}$) CL requires chemically oxidising the reagent from the $[\text{Ru}(\text{bpy})_3]^{2+}$ species into the $[\text{Ru}(\text{bpy})_3]^{3+}$. This $[\text{Ru}(\text{bpy})_3]^{3+}$ species is then reduced to form an excited $[\text{Ru}(\text{bpy})_3]^{2+*}$, which emits light upon relaxation (equations 6-8) [111-115].



This specific reagent was first published in 1966 and is widely used for species containing an amine moiety [111, 116, 117]. This includes amino acids, tetracycline antibiotics, the oxalate ion, some alkaloids and aliphatic amines. Generally, tertiary substituted amines give the greatest emission, followed by secondary and then primary amines [100, 114]. Commercial $[\text{Ru}(\text{bpy})_3]^{2+}$ is typically purchased as a hexafluorophosphate (PF_6) salt that limits reagent use due to poor stability once chemically oxidised. A stable $[\text{Ru}(\text{bpy})_3]^{2+}$ has been developed that involves preparing $[\text{Ru}(\text{bpy})_3](\text{ClO}_4)_2$ in acetonitrile containing HClO_4 . This is then oxidised with solid lead dioxide which is filtered off prior to entering the analytical system [113, 117, 118]. The stable $[\text{Ru}(\text{bpy})_3]^{2+}$ will be used for all chemiluminescence detections within this thesis.

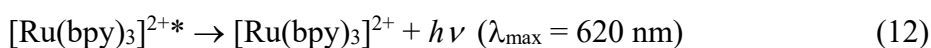
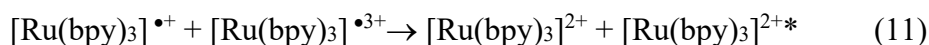
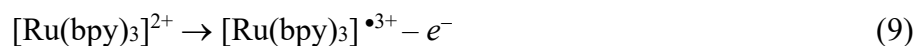
1.4.4 Electrochemiluminescence (ECL) detection

Electrochemiluminescence (ECL) is similar to chemiluminescence (CL) detection as it results in an emission of light due to electron transfer reactions. In ECL however, the species is electrochemically oxidised or reduced at the surface of an electrode, rather than by chemical oxidation [119, 120]. These experiments involve the application of potentials great enough to oxidise or reduce reagents and are paired with a light detecting instrument. This includes a photomultiplier tube (PMT), charge coupled device (CCD) spectrometer or a digital camera [111, 121-123]. The PMT and CCD detectors are the two most commonly used optical detectors for ECL and have their own advantages. The PMT's can be optimised to detect specific responses from different coloured luminophores whilst CCD spectrometers provide spectral information at expense of the sensitivity [124]. A digital camera can be used to visualise emission colours and have proven to be a sensitive technique for ECL emissions [123, 125, 126].

The literature surrounding ECL dates back until the 1920s [127] however the first comprehensive investigation was performed in the 1960s by Hercules and Bard [128-130]. Electrochemiluminescence has many advantages when comparing to CL detection systems. This includes the possibility of species regenerations that as a result takes place in the reaction more than once [131], the exclusions of potentially harmful chemical oxidants (such as lead dioxide) and control of electrochemical potentials to improve sensitivity and selectivity of target analytes [124]. In recent years, ECL has established itself as a major focus area of research in both fundamental studies and analytical applications [132-137].

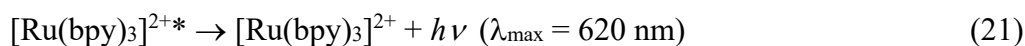
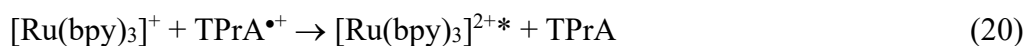
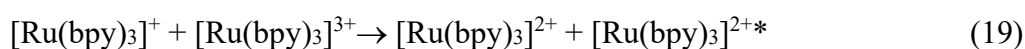
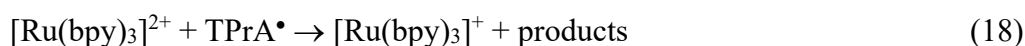
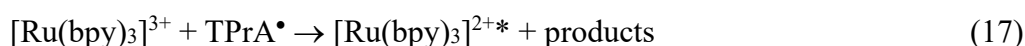
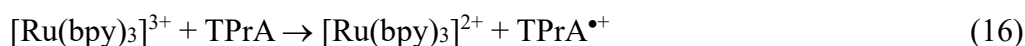
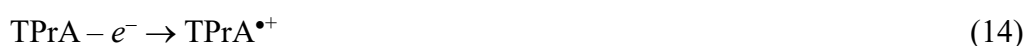
There are two reaction pathways for ECL emissions, annihilation and co-reactant [138]. This chapter will describe both pathways in relation to the $[\text{Ru}(\text{bpy})_3]^{2+}$ metal chelate as it is the most commonly used reagent and the only commercially available ECL diagnostic tool [139-141]. The same principles apply to all metal chelates.

Annihilation ECL alternates the applied voltage between oxidation and reduction potentials that results in the formation of both an oxidised and reduced species at the surface of the working electrode [119]. The oxidised species annihilates with the reduced species where one will produce an excited state and emit a photon upon relaxation back to the ground state (equations 9-12) [119].



In aqueous environments, the electrochemical window is not large enough to facilitate both oxidation and reduction of most luminophores. As a result of this, annihilation pathways are limited to organic solvents where a wider applied potential range is possible [121].

Co-reactant pathways can generate an ECL response from application of a single potential with the addition of a reagent. The co-reactant is oxidised (or reduced) at the surface of the working electrode alongside the metal luminophore [142]. The co-reactant species or electrochemically produced products (such as the spontaneously formed radical cation) then reacts with the luminophore to form an excited state species that can emit a response upon relaxation [122, 138]. Tri-*n*-propylamine (TPrA) is the most studied co-reactant and the reaction with $[\text{Ru}(\text{bpy})_3]^{2+}$ is shown in equations 13-21 [142].



Two common electrochemical methods for ECL emission involves cyclic voltammetry (CV) and chronoamperometry. Cyclic voltammetry applies potentials as a scan from one starting point to an end potential (forward sweep), then reversed to a final end point (reverse sweep). It

is utilised to gain information about the redox processes within a system that helps to facilitate and understand ECL responses [143-145]. An example CV for $[\text{Ru}(\text{bpy})_3]^{2+}$ is shown in Figure 1.16, that illustrates the reversible oxidation process and multiple reversible processes, plus one irreversible reduced redox event at very negative potentials.

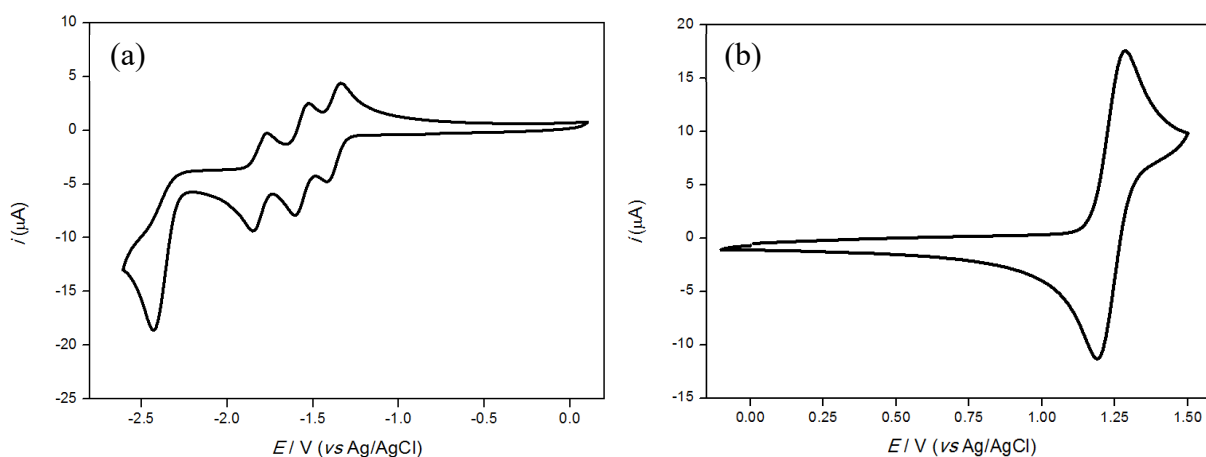


Figure 1.16. Cyclic voltammetry showing oxidation and reduction potentials for 1 mM $[\text{Ru}(\text{bpy})_3]^{2+}$ (vs Ag/AgCl) with 0.1 M TBAPF_6 as the supporting electrolyte in freshly distilled acetonitrile. Reverse sweep (a) and forward sweep (b).

In chronoamperometry experiments rather than applying a scan of potentials, one specific potential is applied as a pulse or a series of potentials applied as steps [146].

The transition metal complexes can exhibit many electron transfer processes that may result in an ECL response. Figure 1.17 illustrates a schematic diagram of the energy transitions and molecular orbitals for a typical octahedral metal complex, such as $[\text{Ru}(\text{bpy})_3]^{2+}$ [111, 121].

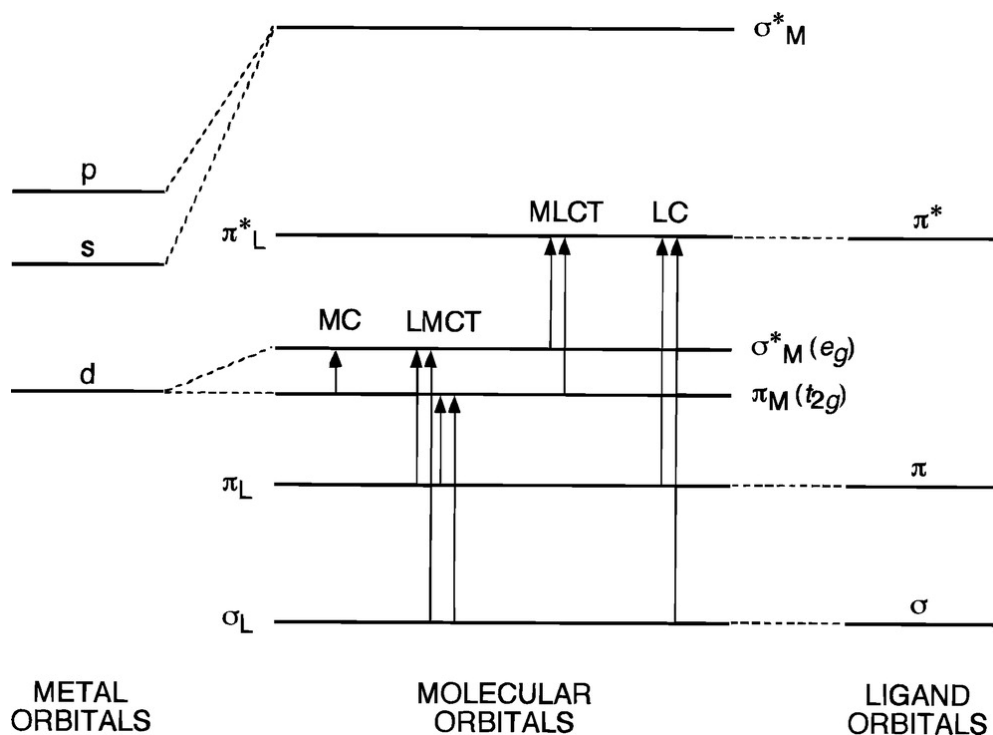


Figure 1.17. Schematic representation of the energy transitions and molecular orbitals within an octahedral metal complex. Image from reference [147].

Each molecular orbital (MO) is labelled as the metal (M) or ligand (L), depending on the principal location. The electronic transitions that produce an ECL response are illustrated as MC, LMCT, MLCT and LC. MC refers to transitions between different MOs within the metal centre. LMCT and MLCT are two charge transfer transitions from the ligand to the metal based orbital (LMCT) or *vice versa* (MLCT), and LC relates to transitions between different MOs of the ligands [147]. For metal complexes the most common electronic transition that produces an ECL response is the metal to ligand charge transfer (MLCT) [147]. The energy difference between the highest occupied molecular orbital (HOMO, π_M) and the lowest unoccupied molecular orbital (LUMO, π^*) is proportional to the emission energy and varies between individual complexes [121, 147]. The higher the HOMO-LUMO gap, the higher the energy wavelength emissions [121]. The oxidation potential of a complex is the energy required to remove an electron from the HOMO and the reduction potential corresponds to the energy

required to add an electron into the LUMO. Therefore the HOMO and LUMO of each complex is directly related to its oxidation and reduction potentials [121].

Multi-coloured ECL has been explored previously with Bruce and Richter successfully exhibiting dual emission with $[\text{Ru}(\text{bpy})_3]^{2+}$ and $\text{Ir}(\text{ppy})_3$ in a co-reactant system with TPrA [148]. Figure 1.18. A illustrates the dual emission system where both emission wavelengths are distinguishable in order to get separate signals in a co-reactant system with both complexes present [148].

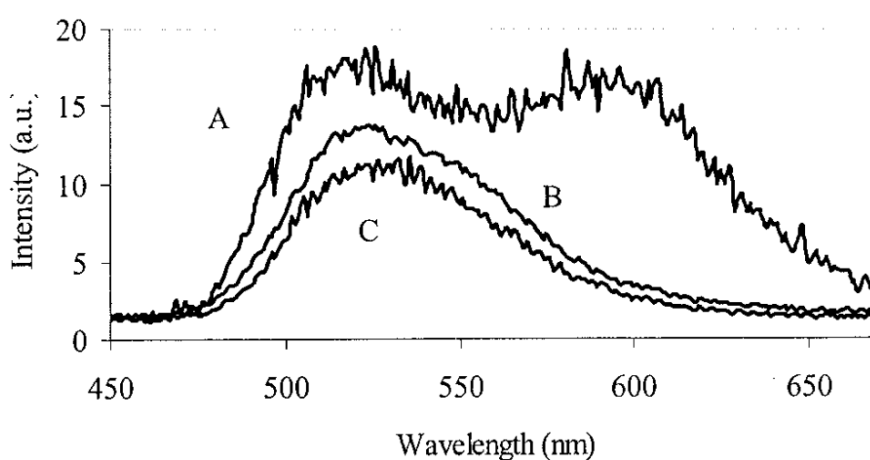


Figure 1.18. ECL spectra of (A) a $10\ \mu\text{M}$ $\text{Ir}(\text{ppy})_3$ and $10\ \mu\text{M}$ $[\text{Ru}(\text{bpy})_3]^{2+}$ solution in CH_3CN containing $0.05\ \text{M}$ TPrA ($0.1\ \text{M}$ Bu_4NPF_6 as electrolyte), (B) $10\ \mu\text{M}$ $\text{Ir}(\text{ppy})_3$ ($0.05\ \text{M}$ TPrA) in CH_3CN ($0.1\ \text{M}$ Bu_4NPF_6), and (C) $10\ \mu\text{M}$ $\text{Ir}(\text{ppy})_3$ ($0.05\ \text{M}$ TPrA) in $\text{CH}_3\text{CN}/\text{H}_2\text{O}$ ($50:50$ (v/v), $0.1\ \text{M}$ KH_2PO_4). Image from reference [148].

Soulsby *et al.* has also observed dual emission with these two luminophores in annihilation reactions *via* emission at both the working and counter electrode simultaneously. Location of emission was visualised using a digital camera to photograph ECL responses [149]. Applying positive potentials resulted in an anodic emission at the working electrode while the corresponding negative potential at the counter electrode exhibited a cathodic response, and *vice versa*. Utilising more than one reagent allows for luminophore selectivity that could potentially play an important role in forensic applications, as described in chapter 5. Specific

anodic or cathodic reaction pathways are also important in understanding luminophore potential emissions that aids with selectivity.

1.4.5 Solid-state nuclear magnetic resonance (SSNMR) spectroscopy detection

The principles of nuclear magnetic resonance (NMR) spectroscopy involves the measurement of energy when a magnetic field is applied to nuclei [150]. The first measurement of nuclear magnetic moments dates back to 1939 where Rabi *et al.* developed a molecular beam resonance method of three nuclei - ${}^6\text{Li}$, ${}^7\text{Li}$ and ${}^{19}\text{F}$ [151]. In 1946, Bloch *et al.* and Purcell *et al.* illustrated the nuclear magnetic resonance for water and paraffin, respectively, that measured the radiofrequency energy of protons [152]. From this, the basic principles and applications of NMR were explored and by the mid-1950s commercial instruments for ${}^1\text{H}$ NMR spectroscopy were available [153]. Today, NMR is an extensively utilised tool for the analysis and structural determination of molecular structure and is important in chemistry, biochemistry and medical fields [154, 155]. Additionally, the NMR peak area is proportional to the number of nuclei providing quantitative information without the need for a standard calibration as in other analytical techniques [156]. The majority of NMR experiments are performed within deuterated solvents as solution-state however solid-state NMR has emerged for analysis of organic and inorganic complexes, zeolites, catalysts, polymers and resins [157-159].

Compared to solution-state, solid-state NMR is not as commonly used as the spectra is generally represented by broad resonances that are relatively featureless. The resolution of solid-state spectra has improved as significant advancements have been made in recent years. This resolution is comparable to solution-state providing specific methods are employed, including cross polarisation (CP) and magic angle spinning (MAS) [150]. In CP experiments there is an overlap of the ${}^1\text{H}$ and ${}^{13}\text{C}$ energies allowing the polarisation to transfer from ${}^1\text{H}$

nuclei that are abundant, to ^{13}C that is dilute. Magic angle spinning requires rotating the sample along an axis within the magnetic field. The SSNMR experiments explored in chapter 5 are CP MAS, that involves CP techniques to increase signal to noise ratio and continuous MAS to remove chemical shift anisotropy [150]. Direct polarisation of nuclei is also explored with MAS experiments to identify ^1H , ^{13}C and ^{19}F nuclei within forensically important compounds. The advantages of utilising SSNMR is that it is non-destructive and requires little sample preparation, with no extraction necessary, that is important for illicit substances and offers the opportunity for further testing if needed.

1.5 Project aims

This project aims to develop novel methods of detection for illicit substances - namely amphetamine type stimulants and synthetic cannabinoids. The ideal goal is to provide a quick, on-the-spot test that could identify specific structures rather than focusing on classes of compounds. This is particularly important for law enforcement agencies to aid in prosecutions within acceptable timeframes and adhering to legislations.

A rapid separation for complex amphetamine type stimulant samples will be developed with a novel and selective method of detection to be explored. This detection method will utilise tris(2,2'-bipyridine)ruthenium(II) $[\text{Ru}(\text{bpy})_3]^{2+}$ chemiluminescence (CL) that is known to be selective towards compounds with an amine moiety. Real amphetamine seizure samples, with known concentrations of MDMA, will be exploited to test the viability of CL for quantification. This method development will extend onto synthetic cannabinoid mixtures and a different CL reagent will be explored to increase selectivity.

Previous work at Deakin University explored the detection of synthetic cannabinoids. This project aims to expand on this preliminary data and explore the viability of ECL detections for specific synthetic cannabinoid compounds. This will be performed by utilising multiple metal chelate complexes and exploring co-reactant reaction mechanisms.

Tri-*n*-propylamine (TPrA) is a widely explored co-reactant in ECL experiments and this work will continue to use TPrA to better understand the reaction mechanisms of common metal chelates. Dual emission on both the counter and working electrodes will be investigated by introducing two reagents into one system. By exploring dual emission, it is possible to develop bi-detection systems for the identification of two compounds simultaneously. This method development will focus on using TPrA to better understand the anodic and cathodic pathways

of individual metal complexes to then be applied to synthetic cannabinoid compounds. The ECL emission interference from the synthetic cannabinoid herbal substrates will be explored in order to develop a method that requires little to no sample preparation. Coinciding with the ECL experiments, a collaborative project involving SSNMR will also be explored as a technique that provides spectral information whilst maintaining sample integrity.

CHAPTER TWO:

CHEMILUMINESCENCE DETECTION OF ILLICIT
SUBSTANCES

Chapter overview

This chapter explores the viability for tris(2,2'-bipyridine)ruthenium(II) chemiluminescence detection of amphetamine type stimulants and synthetic cannabinoids. Methylenedioxy substituted amphetamines (MDA, MDEA and MDMA) were investigated alongside a number of related compounds in street drug samples. Optimisation of reaction conditions was completed using flow injection analysis (FIA) and then applied to post-column high performance liquid chromatography (HPLC). A separation of six compounds was performed (MDA, MDEA, MDMA, ephedrine, pseudoephedrine and caffeine) with both UV absorbance and CL detection. Limits of detection were calculated for the six analytes and were sufficient for the analysis of typical street drug samples. The amount of MDMA present was quantified using both UV absorbance and CL detection. These values were then compared to known concentrations and were found to be in good agreement.

Three commonly seized synthetic cannabinoids (AM-2201, PB-22, and 5F-AKB48) were separated and detected using post column UV absorbance and CL. The traditional stable tris(2,2'-bipyridine ruthenium(II) CL reagent was modified to improve selectivity of the three compounds. This modified reagent was then subjected to stability studies to compare with the traditional reagent and determine the viability of a new, more selective ruthenium metal chelate reagent.

2.1 Introduction

Both amphetamine type stimulants and synthetic cannabinoids are important classes of compounds for illicit drug research. Amphetamines have a long history with a pharmaceutical background before being exploited for illicit highs [12]. Despite the long history, they continue to remain one of the ongoing trends and a growing concern worldwide [160]. According to the 2018 world drug report, 'ecstasy' continues to have a large market within Oceania and use is among the highest in the world [1]. Synthetic cannabinoids however, are relatively new in the illicit drug market therefore little research is available on these substances. Synthetic cannabinoids make up the largest category of the new psychoactive substances (NPS) worldwide [1]. Within Australia, amphetamines and synthetic cannabinoids are a popular choice for drug users as they are relatively cheap and readily available compared to other illicit substances [161-164].

2.1.1 Amphetamine type stimulants

Amphetamine type stimulants are commonly abused as party drugs due to their euphoric effect and ease of availability [28, 29, 165]. The street drug 'ecstasy' typically contains 3,4-methylenedioxymethamphetamine (MDMA) as the active ingredient, that affects both the central nervous system (by increasing the levels of serotonin, dopamine and noradrenaline in the brain) and the sympathetic nervous system [32]. However, depending on the source, 'ecstasy' samples may also contain combinations of related amphetamines such as 3,4-methylenedioxyamphetamine (MDA) or 3,4-methylenedioxyethylamphetamine (MDEA), and/or other drugs [28, 32, 165, 166]. According to recent surveys, ecstasy is the second-most popular illicit drug after cannabis and is largely used among people aged between 20 and 29 years [165]. Illicit amphetamines are produced in clandestine laboratories, usually in either

powder or tablet form, with cutting agents such as sugars, caffeine and paracetamol added to increase sample bulk [28, 37, 39]. Street drug samples also often contain traces of precursors such as ephedrine and pseudoephedrine that can remain following incomplete reaction synthesis [28]. In addition, the levels of MDMA present in samples can vary significantly depending on the source [166, 167].

Legally, on a global scale, it is essential that the active component of seized drug samples can be quickly identified. Preliminary 'at-scene' identification of the drug class can be performed using colorimetric spot tests (such as the Marquis reagent) [5, 38], but further testing is necessary to indisputably confirm the presence of individual amphetamines within a sample, and to enable quantification [38]. Street drug samples are often quite complex containing a mixture of active components and/or numerous adulterants. Due to the complex mixtures of compounds that are found within street drug samples, analytical separations, such as gas chromatography or high performance liquid chromatography (HPLC), are necessary to detect individual components [5, 38, 50]. Therefore, forensic laboratories would benefit from the development of more rapid and selective analysis techniques targeted towards specific illicit substances.

Tris(2,2'-bipyridine)ruthenium(II) chemiluminescence has been used for the highly sensitive determination of numerous illicit compounds, including heroin and other opioid substances [109]. The approach can be reasonably selective, due to the limited number of reactions that produce light, plus the absence of an excitation source results in improved signal to noise ratios and hence detection limits [168]. MDMA and related compounds have previously been determined in hair using a peroxyoxalate reagent following derivatization [169], however direct chemiluminescence from these compounds has not previously been observed. The tris(2,2'-bipyridine)ruthenium(III) reagent is known to produce intense chemiluminescence

emissions (from the electronically excited tris(2,2'-bipyridine)ruthenium(II) product of its reduction) with analytes containing an amine [109, 170]. In general, tertiary substituted amines provide the greatest intensity, followed by secondary and then primary amines [109, 170]; however, the selectivity of this reagent is highly dependent on the reaction conditions. The chemical structure of MDMA contains a secondary amine, and related amphetamine derivatives MDEA and MDA contain a secondary and primary amine group respectively (Figure 2.1).

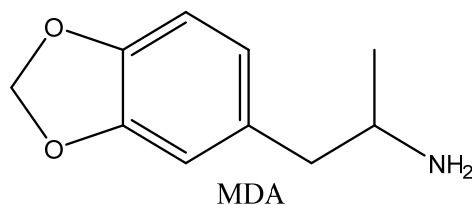
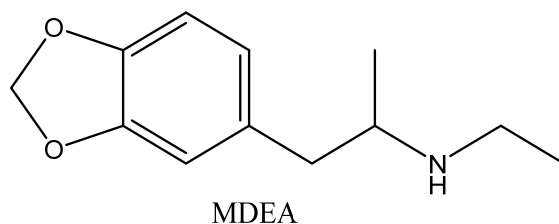
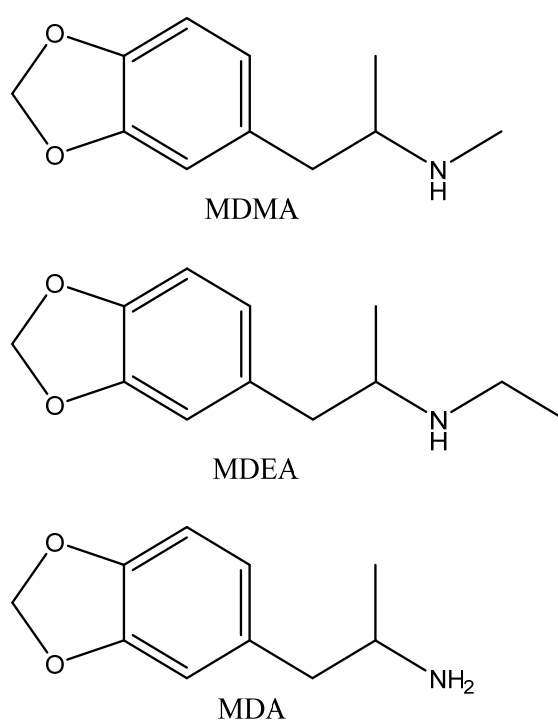


Figure 2.1. Chemical structures of the three amphetamine derivatives: 3,4-methylenedioxyamphetamine (MDMA), 3,4-methylenedioxyethylamphetamine (MDEA) and 3,4-methylenedioxyamphetamine (MDA)

Herein, the use of tris(2,2'-bipyridine)ruthenium(II) chemiluminescence as a novel method for the targeted determination of MDMA is examined. Reaction conditions were optimized for analytes containing a secondary amine, eliminating signals from several common interferents and the approach was then successfully applied to the post-column detection of MDMA in five street drug samples using HPLC.

2.1.2 Synthetic cannabinoids

Synthetic cannabinoids are a relatively new illicit drug and have grown in popularity since the early 2000s [171]. The substances are dissolved in an appropriate solvent and sprayed onto an herbal substrate. Administration of the herbal substrate is similar to that of cannabis, primarily through inhalation [31]. Less commonly, synthetic cannabinoids are made into food or herbal teas [172]. Due to the number of compounds and changes in legislation, synthetic cannabinoid products will have one or more analytes present and it is unlikely that buying the same brand twice means getting the same synthetic cannabinoid(s) [172].

Here, a mixture of three commonly found synthetic cannabinoids (AM-2201, PB-22 and 5F-AKB48) for separation using HPLC methodologies and detection *via* tris(2,2'-bipyridine)ruthenium(II) chemiluminescence are examined. AM-2201 has one tertiary amine, PB-22 has one tertiary and one secondary amine, while 5F-AKB48 has two tertiary and one secondary amine (Figure 2.2). Therefore it is proposed that all three synthetic cannabinoids should be good candidates to elicit a response with tris(2,2'-bipyridine)ruthenium(II).

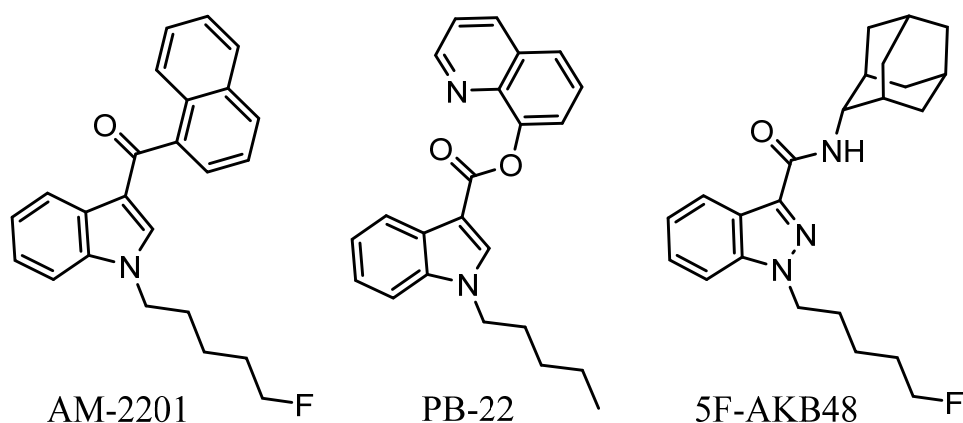


Figure 2.2. Chemical structures of the three synthetic cannabinoid derivatives: AM-2201, PB-22 and 5F-AKB48.

Reaction conditions were based on preliminary data collected at Deakin University [62] and optimised further for these three analytes. The tris(2,2'-bipyridine)ruthenium(II) metal complex was modified to bis(acetonitrile)bis(2,2'-bipyridine)ruthenium(II) [173] to explore and potentially increase selectivity of these particular compounds. The bis(acetonitrile)bis(2,2'-bipyridine)ruthenium(II) reagent has limited prior research therefore the stability of this new chemiluminescence reagent is explored.

2.2 Experimental

2.2.1 Chemicals

Reagents used were of analytical grade standard unless otherwise stated. Acetylsalicylic acid, acetaminophen, caffeine, D-sorbitol, lactose, lead dioxide, mannitol, sodium tetraborate and sodium perchlorate were obtained from Sigma-Aldrich (Castle Hill, New South Wales, Australia). 3,4-methylenedioxymethamphetamine (MDMA), PB-22, AM-2201, 5F-AKB48, ephedrine and pseudoephedrine were obtained from National Measurement Institute (Melbourne, Victoria, Australia). 3,4-methylenedioxyethylamphetamine (MDEA) and 3,4-methylenedioxyamphetamine (MDA) were obtained from the Victoria Police Forensic Sciences Department (Macleod, Victoria, Australia). Acetonitrile was obtained from Scharlau (Sentmenat, Barcelona, Spain). Perchloric acid (70%) was obtained from Ajax Fine Chemicals (Sydney, New South Wales, Australia). Methanol and sulfuric acid were obtained from Merck (Kilsyth, Victoria, Australia). Orthophosphoric acid (85%) was obtained from Chem-Supply (Port Adelaide, South Australia, Australia). Tris(2,2'-bipyridine)ruthenium(II) dichloride hexahydrate was obtained from Strem Chemicals (Newburyport, Massachusetts, USA).

To prepare the chemiluminescence reagent, tris(2,2'-bipyridine)ruthenium(II) dichloride hexahydrate (0.4 g) was dissolved in water (6 mL) before adding solid sodium perchlorate (0.2 g) and mixing thoroughly. The tris(2,2'-bipyridine)ruthenium(II) perchlorate precipitate was filtered, washed and dried over phosphorus pentoxide for a 24 hour period (92% yield). The tris(2,2'-bipyridine)ruthenium(II) perchlorate was dissolved in acetonitrile containing perchloric acid (0.02 M). The tris (2,2'-bipyridine)ruthenium(II) species was oxidised into tris(2,2'-bipyridine)ruthenium(III) by addition of lead dioxide (0.2 g per 100 mL), which was filtered prior to entering the analytical system [113].

Stock solutions of amphetamine street drug samples (powder form) were prepared by dissolving 5 mg of solid material in 50 mL of acetonitrile. Prior to analysis, stock solutions were diluted 50-fold in deionized water.

Bis(acetonitrile)bis(2,2'-bipyridine)ruthenium(II) was prepared by exposing tris(2,2'-bipyridine)ruthenium(II) to a 10 W 180 lm 455 nm LED module run from a constant current power supply for 40 hours until one bipyridine ligand was displaced by two acetonitrile molecules. This product was confirmed using UV-Vis absorption spectroscopy [173]. Bis(acetonitrile)bis(2,2'-bipyridine)ruthenium(II) was prepared without perchloric acid present and then was added to solution prior to chemical oxidation with lead dioxide as described above.

2.2.2 Instrumentation

2.2.2.1 Amphetamine type stimulants

A three-line flow injection analysis manifold was constructed as previously described [168], and a schematic is shown in Figure 2.3. Reagent, buffer and carrier solutions were pumped at 4.0 mL/min using a Gilson Minipuls 3 peristaltic pump.

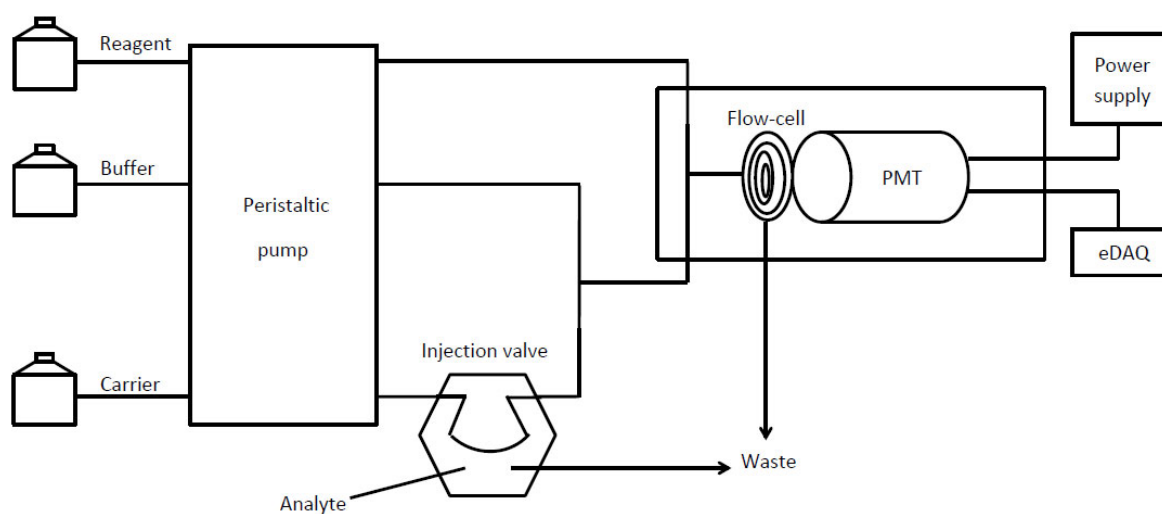


Figure 2.3. Schematic of a FIA manifold.

Analytes were injected (70 μL) into the carrier stream that merged with the buffer solution (0.1 M sodium tetraborate) at a T-piece located prior to a 15 cm mixing coil. The reagent (5×10^{-5} M in acetonitrile with 0.02 M perchloric acid) merged with the carrier at a second confluence point, just prior to the entrance of the flow cell, that consisted of a coil of transparent PTFE-PFA tubing. The flow cell was mounted against a photomultiplier tube (Electron Tubes model 9828SB, ETP; Ermington, NSW, Australia) within a light-tight housing. The output signal was recorded using an e-corder 410 data acquisition system (eDAQ Denistone East, NSW, Australia). All data was exported from eDAQ into csv files for use in Microsoft excel or OriginPro.

Chromatographic separations were carried out on an Agilent Technologies 1260 series HPLC, equipped with a quaternary pump, solvent degasser system and autosampler (Agilent Technologies, Mulgrave, Victoria, Australia), using a Phenomenex Gemini-C18 (150 × 4.6 × 150 μm) reverse phase column at 35°C, with an injection volume of 20 μL and a flow rate of 1 mL/min. Isocratic elution was performed using 90% solvent A: deionized water adjusted to pH 2.2 with orthophosphoric acid and 10% solvent B: acetonitrile. Post-column UV absorbance (210 nm) detection was carried out using a 1260 series variable wavelength detector (Agilent Technologies, Mulgrave, Victoria, Australia).

Post-column chemiluminescence detection was employed using the manifold shown in Figure 2.4, by merging the column eluent with the tetraborate buffer stream (0.075 M; pH 9) before merging with the tris(2,2'-bipyridine)ruthenium(III) reagent (2.5×10^{-4} M in acetonitrile with 0.02 M perchloric acid). A Dual Piston Pump (Series 12 × 6, model D05PFD01; Scientific Systems, State College, PA, USA) set at 1.0 mL/min was used for the reagent, whilst a secondary quaternary pump was used for the buffer stream. The buffer stream (1 mL/min) was switched to a water stream (2 mL/min) for 12 min every hour to prevent precipitation build-up in the flow cell, followed by 10 min of equilibration once the buffer was re-introduced. UV absorbance and chemiluminescence detections were recorded and processed within Agilent Technologies software. Data was exported into csv files for Microsoft excel or OriginPro.

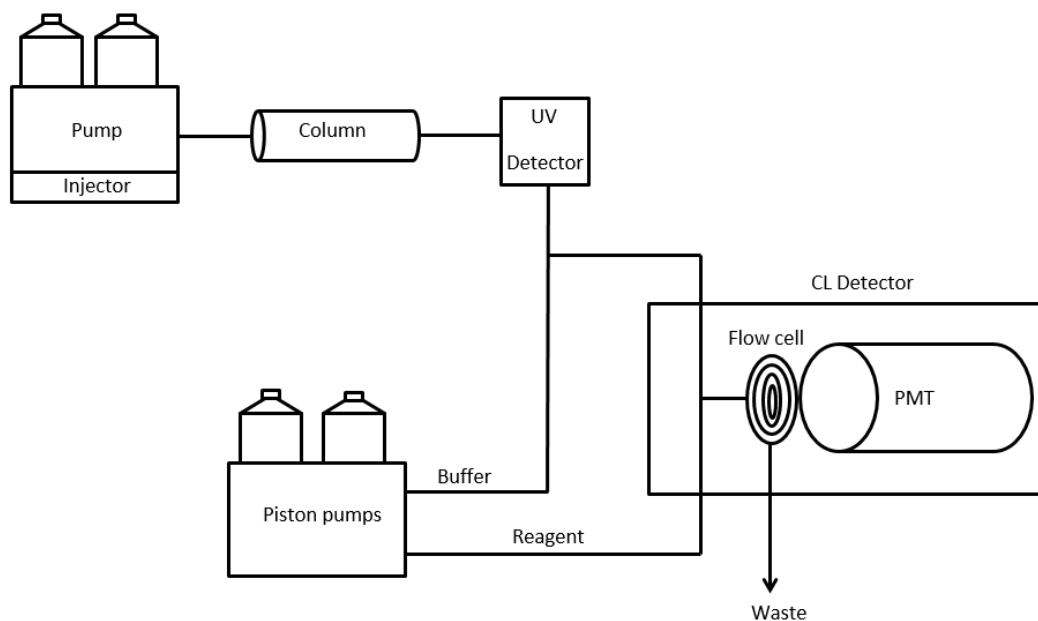


Figure 2.4. Schematic of a 3-line HPLC manifold.

2.2.2.2 Synthetic cannabinoids

Chromatographic separations were carried out on an Agilent Technologies 1260 series HPLC, equipped with a quaternary pump, solvent degasser system and autosampler (Agilent Technologies, Mulgrave, Victoria, Australia), using an Agilent Eclipse XDB-C18 ($150 \times 4.6 \times 150 \mu\text{m}$) reverse phase column at 25°C , with an injection volume of $20 \mu\text{L}$ and a flow rate of 1 mL/min . Solvent A comprised of deionised water with 0.1% formic acid and solvent B comprised of methanol with 0.1% formic acid. A gradient elution was performed at 70% solvent B increasing to 100% solvent B over 14 minutes. Post-column UV absorbance (254 nm) detection was carried out using a 1260 series variable wavelength detector (Agilent Technologies, Mulgrave, Victoria, Australia).

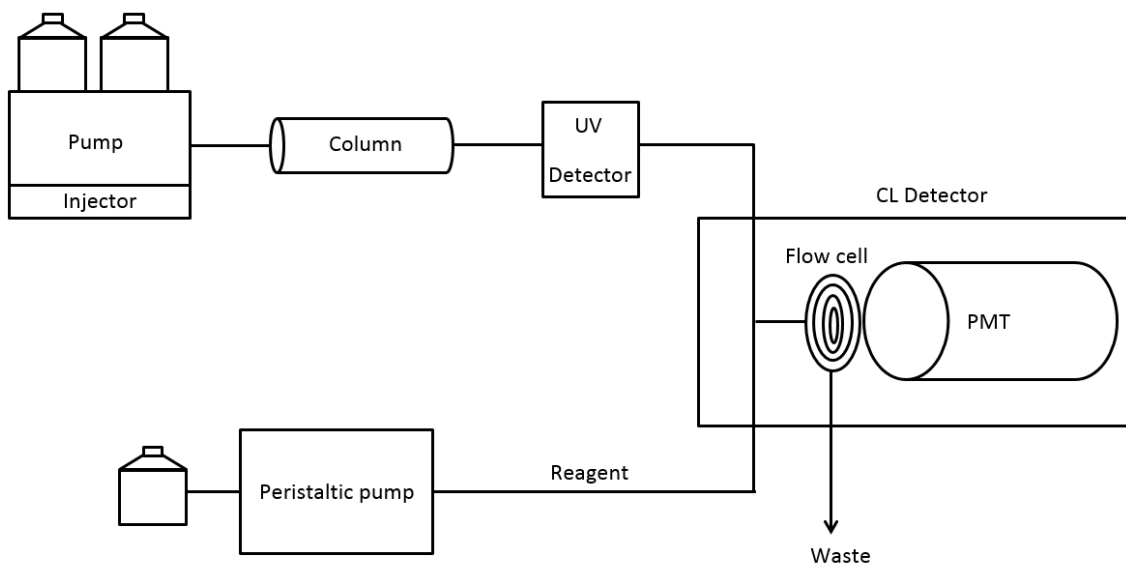


Figure 2.5. Schematic of a 2-line HPLC manifold.

Post-column chemiluminescence detection was employed using the manifold shown in Figure 2.5, by merging the column eluent with the tris(2,2'-bipyridine)ruthenium(III) reagent (5×10^{-4} M in acetonitrile with 0.05 M perchloric acid). A Gilson Minipuls 3 peristaltic pump was used for the reagent that merged with the column eluent at a confluence point just prior to the entrance of the flow cell, that consisted of a coil of transparent PTFE-PFA tubing. The flow cell was mounted against a photomultiplier tube (Electron Tubes model 9828SB, ETP; Ermington, NSW, Australia) within a light-tight housing. UV absorbance and chemiluminescence detections were recorded and processed within Agilent Technologies software. Data was exported into csv files for Microsoft excel or OriginPro.

2.3 Results and discussion

2.3.1 Amphetamine type stimulants

Initial optimisation of the chemiluminescence reaction conditions was conducted using flow injection analysis with five analytes of interest (MDMA, MDA, MDEA, ephedrine and pseudoephedrine). The tris(2,2'-bipyridine)ruthenium(III) reagent is commonly used in acidic conditions [111]; however, several studies have indicated that compounds containing secondary amines may elicit greater responses in a basic reaction environment [174, 175]. To alter the pH, a sodium tetraborate buffer (0.1 M) was introduced *via* a third line that merged with the analyte stream prior to mixing with the reagent. Generally, chemiluminescence intensities for these analytes were superior at higher pH. Despite an increase in the blank response under these conditions, signal to noise ratios were also improved. The secondary amines MDEA and MDMA, both gave similar responses and produced the greatest signals at pH 8 (Figure 2.6 (a)). The primary amine MDA, elicited only weak responses, with an optimum pH of 10. Ephedrine and pseudoephedrine are precursors in the synthesis of methamphetamine and are commonly found within street drug samples (See chapter 1 for specific reaction pathways of amphetamine type stimulants) [28, 39]. The optimum pH condition for these enantiomeric compounds was pH 10. As the optimum pH for the five analytes ranged from 8 to 10, a pH of 9 was used for all subsequent analyses.

In order to determine the possibility of interferences from six commonly used cutting agents, they were tested at the optimal pH using the FIA manifold described above. These included sugars such as lactose, mannitol and sorbitol, as well as caffeine, aspirin and paracetamol - and produced no chemiluminescence response with this reagent (Figure 2.6 (b)). Therefore, it was concluded that these expedients would not cause a false positive response during sample

analysis. This result demonstrates the inherent selectivity of chemiluminescence detection, as only compounds containing specific functionalities will elicit light.

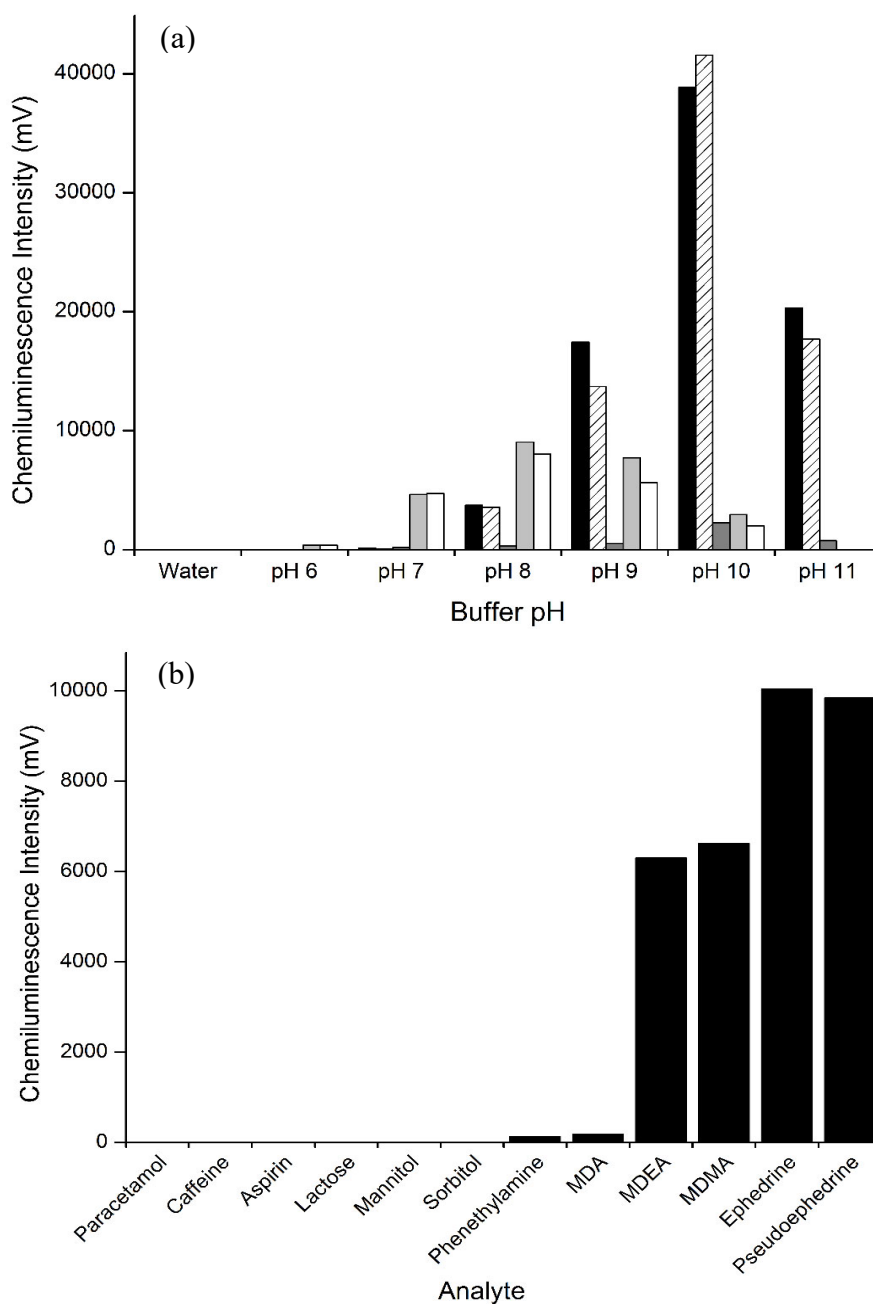


Figure 2.6. (a) Chemiluminescence intensities of five analytes (1×10^{-5} M): ephedrine (black bars), pseudoephedrine (striped bars), MDA (dark grey bars), MDEA (light grey bars) and MDMA (white bars) with tris(2,2'-bipyridine)ruthenium(III) (5×10^{-5} M) with increasing buffer pH. (b) Chemiluminescence intensities of MDMA and potentially interfering compounds (1×10^{-5} M) with tris(2,2' bipyridine)ruthenium(III) (5×10^{-5} M) at a pH of 9 using flow injection analysis.

Five street drug samples (known to contain MDMA) were obtained, and their overall chemiluminescence response with the tris(2,2'-bipyridine)ruthenium(III) reagent was examined. Each sample exhibited an intense response, indicating the presence of secondary amine species such as MDMA. The approximate MDMA concentration of each sample (calculated using the total chemiluminescence response of the sample and a MDMA standard calibration) was determined to range between 21% and 43% (m/m) (Table 2.2).

Although the tris(2,2'-bipyridine)ruthenium(III) reagent afforded no measurable response with several common cutting agents, street drug samples typically contain a complex mixture of adulterants and/or contaminants [176] that may still interfere with the analysis. Consequently, a separation technique is usually required to confirm the presence of MDMA and obtain more accurate quantitative data. Therefore, the chemiluminescence conditions employed in flow analysis were subsequently transferred to HPLC post-column detection. The concentration of the reagent and buffer were adjusted to reduce the baseline chemiluminescence intensity and avoid precipitation of the buffer in the mixed solvent conditions. A mobile phase consisting of 90% deionised water adjusted to pH 2.2 with orthophosphoric acid and 10% acetonitrile was used to analyse a mixture of six compounds (MDMA, MDA, MDEA, ephedrine, pseudoephedrine and caffeine) in under 10 mins.

As can be seen in Figure 2.7 (b), when the analyte mixture was injected, three peaks were observed. Ephedrine and pseudoephedrine could not be resolved under these conditions as they are an enantiomeric pair, and they therefore eluted as a single peak at 2.3 min. A second peak at 3.5 min corresponded to MDMA whilst the third at 4.4 min corresponded to MDEA. As described previously, the remaining analytes did not elicit a chemiluminescence response. When the same analyte mix was examined using UV absorbance detection (210 nm), MDA and caffeine were also detected. However, MDA co-eluted with ephedrine and

pseudoephedrine in the first peak (Figure 2.7 (a)). The increased selectivity of detection with tris(2,2'-bipyridine)ruthenium(III) removes the need for a more complex separation method, as less interfering species are detected.

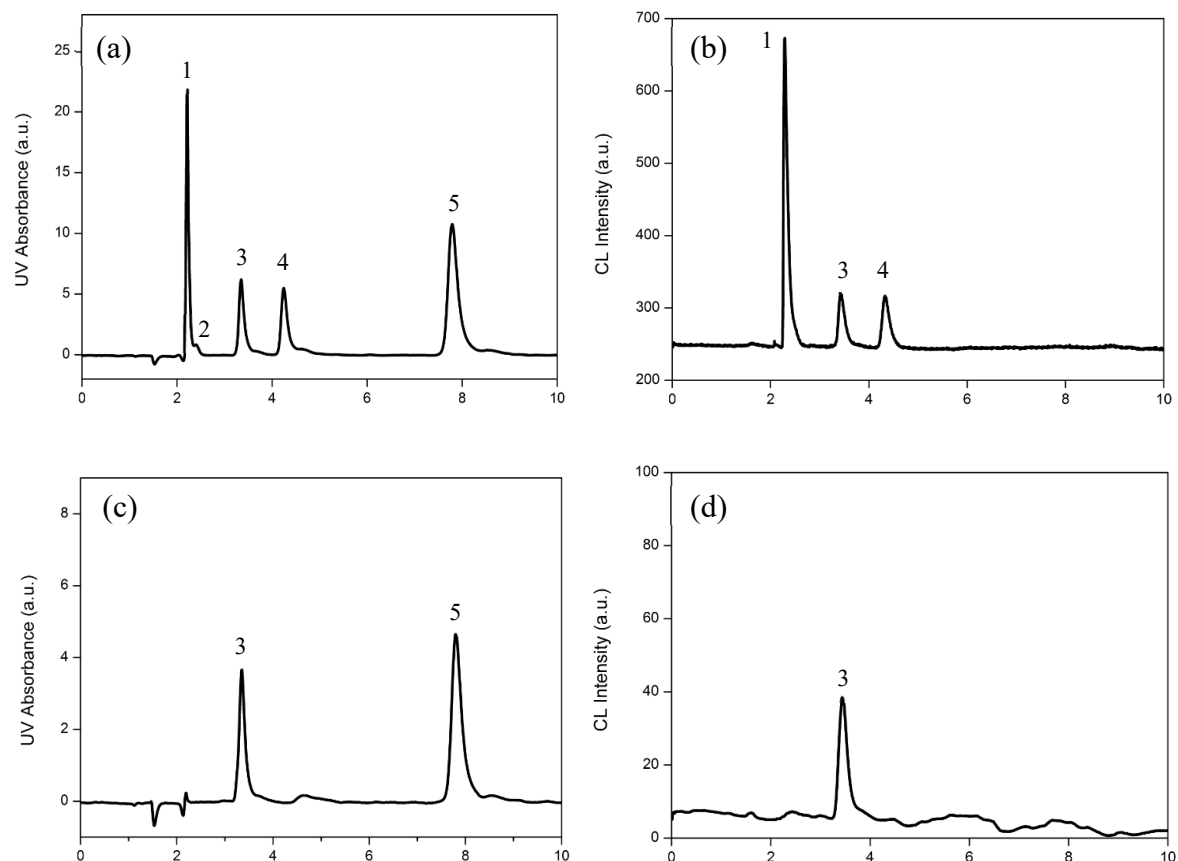


Figure 2.7. HPLC separations of six standards (7×10^{-6} M) using: (a) UV absorbance detection at 210 nm and (b) tris(2,2' bipyridine)ruthenium(II) chemiluminescence detection (2.5×10^{-4} M); and typical chromatograms obtained for the analysis of a street drug sample (5 mg dissolved in 50 mL acetonitrile, diluted 1/50 in deionized water) using (c) UV absorbance and (d) chemiluminescence detection (smoothed). Peaks: 1:

ephedrine/pseudoephedrine, 2: MDA, 3: MDMA, 4: MDEA, 5: caffeine

Calibration curves were constructed for the six analytes in order to determine analytical figures of merit. The relationship between signal (peak area) and concentration approximated linearity ($R^2 \geq 0.999$) for all analytes. The limits of detection (defined as blank + 3SD) ranged from

0.18 μM to 0.48 μM (Table 2.1). Most importantly, the detection limit for MDMA (0.48 μM) is sufficient for the analysis of typical street drug samples [166, 177].

Table 2.1. Analytical figures of merit obtained using tris(2,2'-bipyridine)ruthenium(III) ($2.5 \times 10^{-4}\text{M}$) chemiluminescence detection post-column.

Analyte	Retention		R^2	Linear	%RSD ^b	LOD (μM)
	Time (min)	%RSD ^b		range (μM)		
Peak 1 ^a	2.30	0.71	0.999	0.5-7.0	6.69	0.18
MDMA	3.51	1.70	0.999	0.7-7.0	3.89	0.48
MDEA	4.44	2.01	0.999	0.7-7.0	4.71	0.48

^a Peak 1 contains ephedrine and pseudoephedrine in a 1:1 ratio. ^b n = 5.

The HPLC method was then applied to the five street drug samples, with both chemiluminescence and UV absorbance detection. The chromatograms obtained for each of the five samples using chemiluminescence detection contained a single peak corresponding to MDMA (Figure 2.7 (d)). This again demonstrates the greater selectivity of the chemiluminescence detection method. In the UV absorbance chromatograms, numerous small unidentified peaks were also observed in several samples, and sample 5 contained a significant component that was not completely resolved from the MDMA peak and was not observed using chemiluminescence detection. Two of the samples (3 and 4) contained peaks corresponding to the known retention time for caffeine (7.8 min). As illicit substances are often mixtures of active ingredients and adulterants, the selectivity of the CL detection compared to the UV absorbance is important for accurate quantification. It is likely that multiple substances

will co-elute within UV detections as it is less selective and the combined peaks cannot be used for quantification calculations.

Table 2.2. Concentration (g/g of sample) of MDMA in street drug samples.

Method of Analysis	1	2	3	4	5
FIA-CL	0.31	0.33	0.21	0.43	0.30
HPLC-CL	0.26	0.30	0.20	0.38	0.23
HPLC-UV	0.25	0.30	0.18	0.38	0.29
HPLC-UV ^a	0.27	0.27	0.17	0.38	N/A

^a Analysis performed in an external laboratory.

The amount of MDMA present in each sample was quantified using both detection methods. The values obtained using HPLC with both chemiluminescence and UV absorption were consistent. Tris(2,2'-bipyridine)ruthenium(II) chemiluminescence detection resulted in MDMA concentrations ranging from 20% to 38% (m/m), whilst UV absorbance afforded a similar range of 18% to 38% (m/m) MDMA (Table 2.2). Sample 5 showed the most variation between methods (26% difference), as quantification was hindered by the presence of a co-eluting peak in the UV absorbance. The calculated proportion of MDMA in four of the street drug samples was also compared to values obtained using a second HPLC-UV method performed in an external laboratory (Table 2.2), and were also found to be in good agreement. Street seizure drug samples have quite a large range in the concentration of active component [11, 166, 178]. This research has developed a rapid method of quantifying the amount of active MDMA without the presence of interferences. Using chemiluminescence as a sensitive technique, it is possible to detect lower concentrations that can be present in seizure samples.

Not only is this research sensitive and selective towards the amine moieties, it has developed a rapid separation of the active components from potential adulterants or interferences.

2.3.2 Synthetic cannabinoids

Initial HPLC reaction conditions were based on preliminary work completed at Deakin University by Niki Burns [62] and was further optimised for these particular analytes of interest. Three synthetic cannabinoids (AM-2201, PB-22 and 5F-AKB48) were screened for a rapid separation and viability of the tris(2,2'-bipyridine)ruthenium(II) chemiluminescence. A mobile phase gradient consisting of deionised water and varying ratios of methanol, both with 0.1% formic acid, was used to analyse this mixture in 12 minutes. Figure 2.8 displays the separation of these three analytes with both UV absorbance (254 nm) and chemiluminescence detection. In the UV absorbance detection (Figure 2.8 (a)), the peak at 6.9 min corresponded to AM-2201, the second peak at 8.0 min corresponded to PB-22 and the third peak at 10.9 min corresponded to 5F-AKB48. As can be seen in Figure 2.8 (b) only two of the three analytes were detected using chemiluminescence. The small peak at 7.1 min corresponded to AM-2201 whilst the larger peak at 8.2 min corresponded to PB-22 and 5F-AKB48 did not elicit a chemiluminescence response. The larger peak for PB-22 displays a greater emission signal and preferred selectivity with the tris(2,2'-bipyridine)ruthenium(II) reagent compared to AM-2201. In an effort to improve selectivity, a bis(acetonitrile)bis(2,2'-bipyridine)ruthenium(II) chemiluminescence reagent was explored by displacing one of the bipyridine ligands on the metal complex with two acetonitrile groups [173]. This was confirmed through a UV-Vis spectrometer where the maximum absorbance peak shifts from approximately 450 nm for the tris(2,2'-bipyridine)ruthenium(II) to approximately 425 nm for bis(acetonitrile)bis(2,2'-bipyridine)ruthenium(II) (Figure 2.9). This aligns with previous literature by Yoshikawa *et al.* who illustrated an absorption of 251 nm and 426 nm for the tris(2,2'-bipyridine)ruthenium(II) and bis(acetonitrile)bis(2,2'-bipyridine)ruthenium(II) complexes, respectively [173].

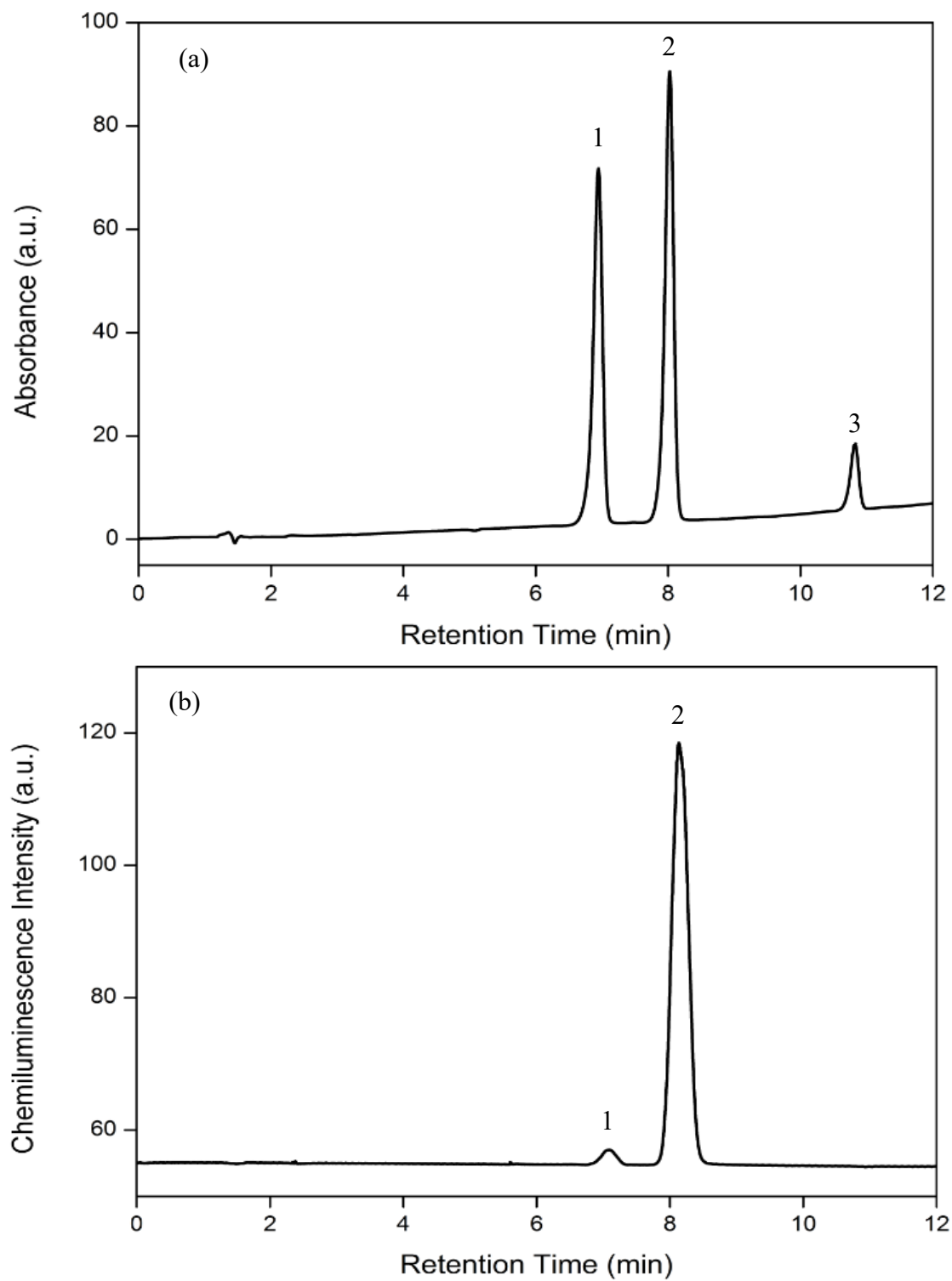


Figure 2.8. HPLC separations of three standards (5×10^{-5} M) using: (a) UV absorbance detection at 254 nm and (b) tris(2,2' bipyridine)ruthenium(II) chemiluminescence detection (2.5×10^{-4} M); Peaks: 1: AM-2201, 2: PB-22 and 3: 5F-AKB48.

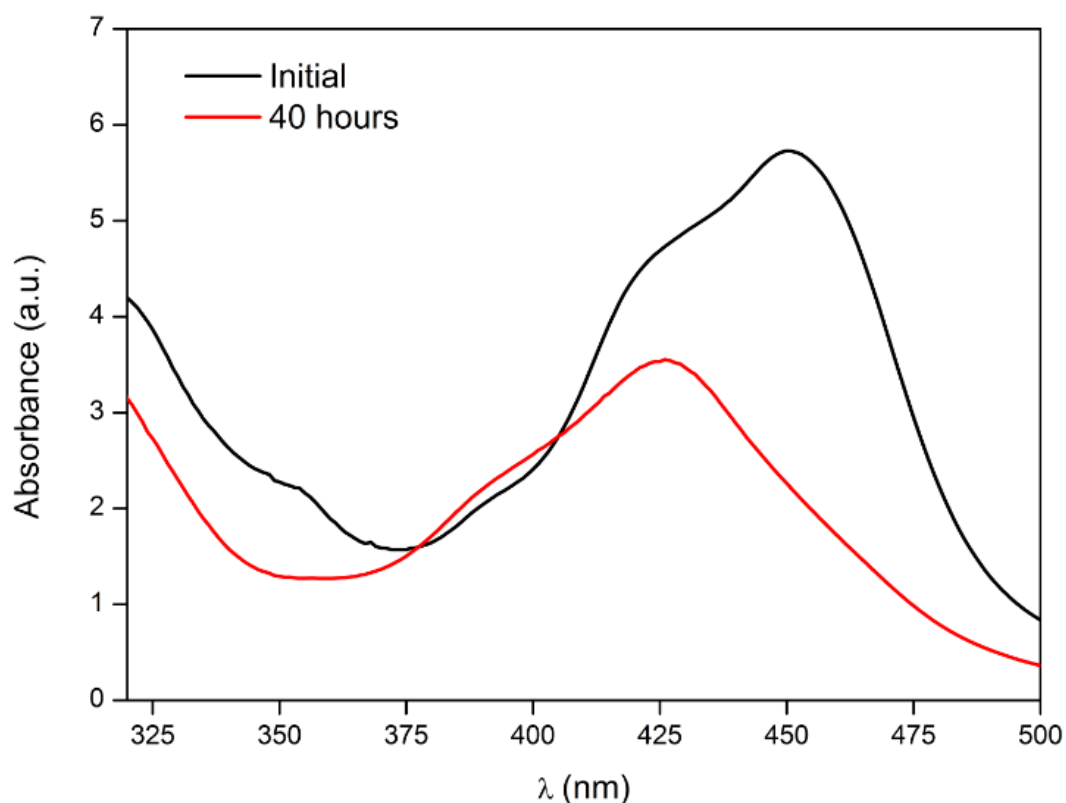


Figure 2.9. UV-Vis absorbance spectra of tris(2,2'-bipyridine)ruthenium(II) (2.5×10^{-4} M) (black line) and bis(acetonitrile)bis(2,2'-bipyridine)ruthenium(II) (2.5×10^{-4} M) (red line).

The acetonitrile complex was unlikely to be stable once chemically oxidised with lead dioxide, therefore varying ratios of bis(acetonitrile)bis(2,2'-bipyridine)ruthenium(II) and tris(2,2'-bipyridine)ruthenium(II) were explored for optimum emissions and stability. The optimal ratios for emissions were determined to be 10% bis(acetonitrile)bis(2,2'-bipyridine)ruthenium(II) and 90% tris(2,2'-bipyridine)ruthenium(II). The same HPLC conditions as in previous experiments were employed and the results can be shown in Figure 2.10. The UV absorbance detection (Figure 2.10 (a)) yields the same response as above, with all three analytes present. With the 10% acetonitrile complex, the CL detection (Figure 2.10 (b)) has greater selectivity compared to 100% tris(2,2'-bipyridine)ruthenium(II). With this reagent, AM-2201 has a greater emission with increased sensitivity, PB-22 has a smaller emission with decreased sensitivity, and 5F-AKB48 elicits a response, unlike previous

results. This difference in CL emission can be visualised in Figure 2.11 where the two chromatograms are overlaid.

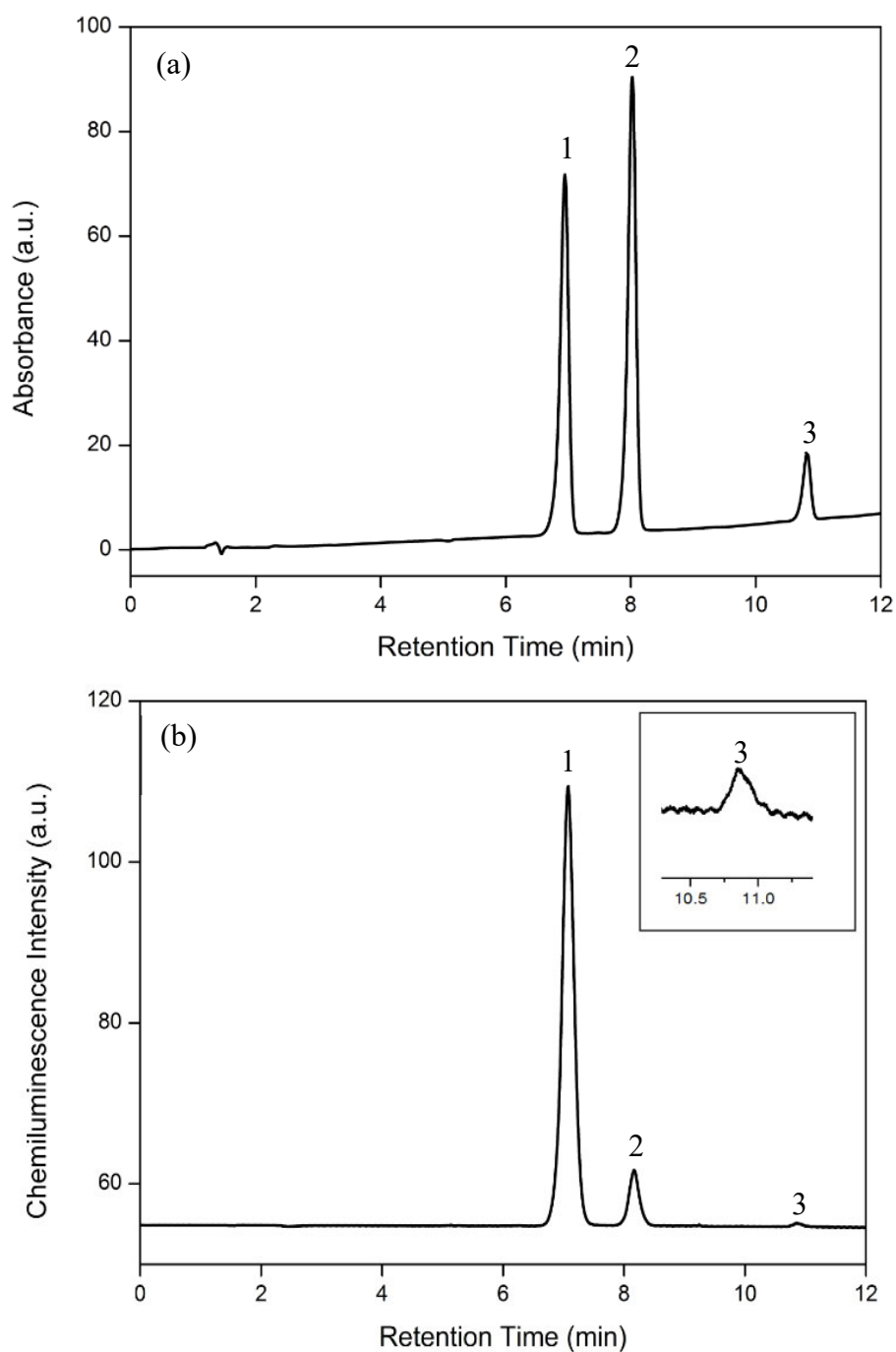


Figure 2.10. HPLC separations of three standards (5×10^{-5} M) using: (a) UV absorbance detection at 254 nm and (b) 10% bis(acetonitrile)bis(2,2' bipyridine)ruthenium(II) and 90% tris(2,2' bipyridine)ruthenium(II) chemiluminescence detection (2.5×10^{-4} M); Peaks: 1: AM-2201, 2: PB-22 and 3: 5F-AKB48.

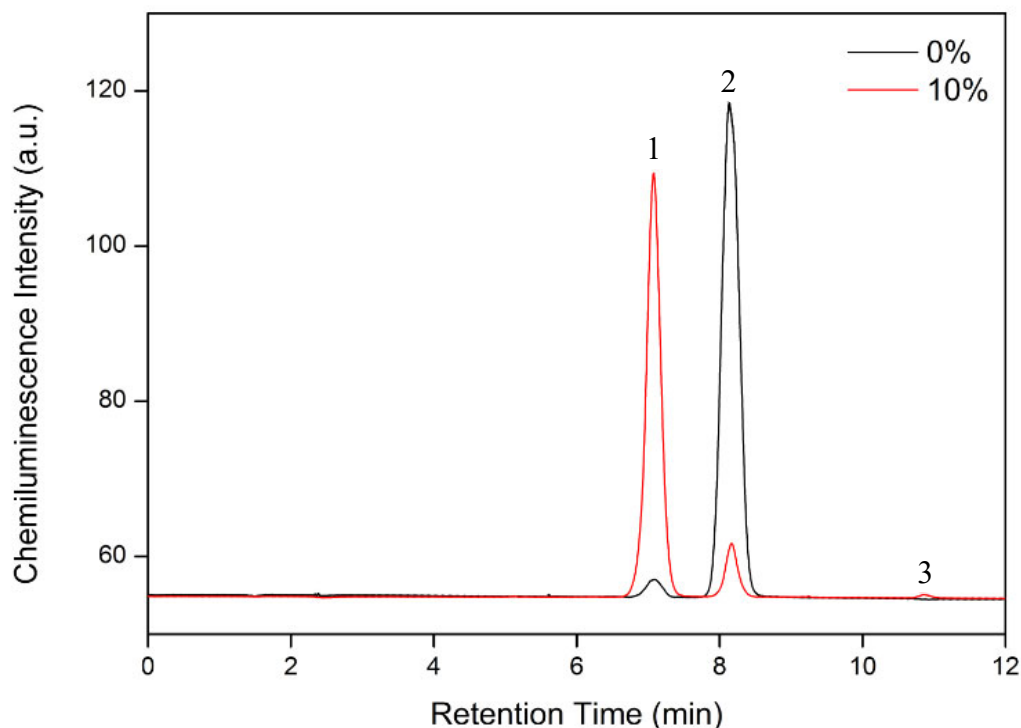


Figure 2.11. The two chemiluminescence chromatograms from Figures 2.8 and 2.10 overlaid. Black line represents a 100% tris(2,2'-bipyridine)ruthenium(II) (0% bis(acetonitrile)bis(2,2'-bipyridine)ruthenium(II) (2.5×10^{-4} M)) reagent while the red line represents a 10% bis(acetonitrile)bis(2,2'-bipyridine)ruthenium(II) reagent (2.5×10^{-4} M). Peaks: 1: AM-2201, 2: PB-22 and 3: 5F-AKB48.

Rather than trying to optimise the above system to increase signal emissions, it was important to explore how stable the 10% acetonitrile complex was once chemically oxidised with lead dioxide. The traditional tris(2,2'-bipyridine)ruthenium(II) reagent is known to be stable once oxidised and it will remain in the 3^+ state for as long as the analysis is required [113]. One of the many advantages of using tris(2,2'-bipyridine)ruthenium(II) over other CL reagents was the stability of the oxidised solution [113]. For forensically important compounds, the stability of the CL reagent affords the opportunity to increase the number of samples processed in a quicker time frame as the need for excessive reagent preparation is limited. This is important as accurate detection of illicit substances in the field relies upon a robust methodology and the stability of the system is critical.

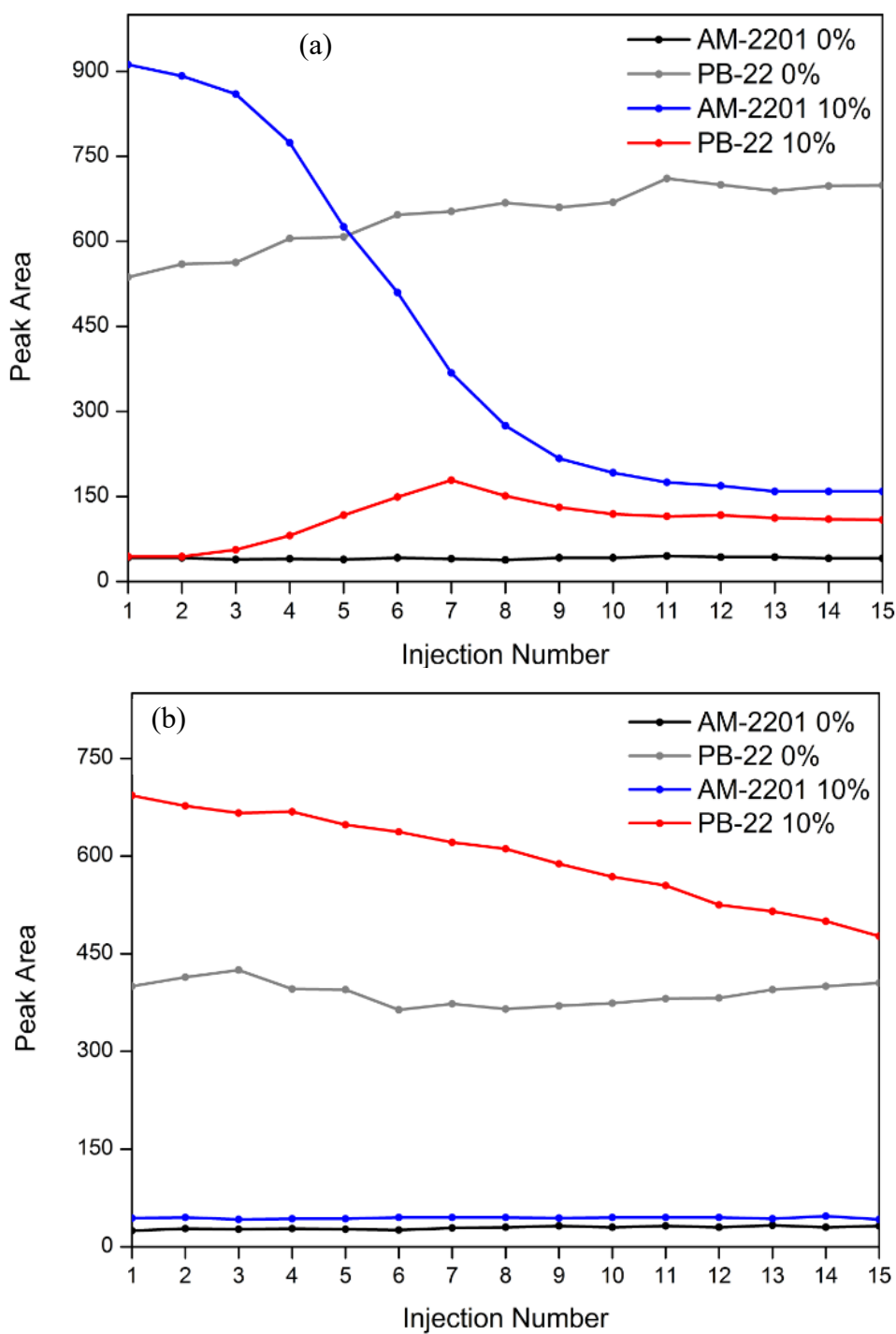


Figure 2.12. Peak areas of chemiluminescence detection post-column HPLC. (a) 0% and 10% bis(acetonitrile)bis(2,2'-bipyridine)ruthenium(II) (2.5×10^{-4} M) prepared in regular acetonitrile and (b) 0% and 10% bis(acetonitrile)bis(2,2'-bipyridine)ruthenium(II) (2.5×10^{-4} M) prepared in dry acetonitrile. Colours - Black: AM-2201 with 0%, Grey: PB-22 with 0%, Blue: AM-2201 with 10% and Red: PB-22 with 10%.

The stability of the oxidised acetonitrile complex was explored with both HPLC-CL detection and as well UV-Vis absorption spectroscopy. A sequence of 15 injections was run giving the total experimental time to be approximately 4.5 hours and the CL peak areas were measured to determine stability. Figure 2.12 (a) shows the peak areas for both AM-2201 and PB-22 with 0% and 10% bis(acetonitrile)bis(2,2'-bipyridine)ruthenium(II). For the tris(2,2'-bipyridine)ruthenium(II) (0%) peak areas for both analytes varied slightly but overall they were quite stable, as expected. The 10% bis(acetonitrile)bis(2,2'-bipyridine)ruthenium(II) emissions however varied considerably. The signal response for AM-2201 drops rapidly after approximately 1 hour (3 injections) while PB-22 increases slightly before plateauing after approximately 2.5 hours (7 injections).

To overcome this stability issue, using dry acetonitrile to prepare both reagents was explored. Figure 2.12 (b) shows the peak areas of the signal response for both AM-2201 and PB-22 with 0% and 10% bis(acetonitrile)bis(2,2'-bipyridine)ruthenium(II) prepared in dry acetonitrile. The stability of the peak areas for the 10% solution improved considerably however it is important to note that the selectivity was similar to that of the traditional tris(2,2'-bipyridine)ruthenium(II) reagent. AM-2201 no longer has the greater emission, PB-22 had a larger signal and 5F-AKB48 did not elicit a CL response with this reagent prepared in dry acetonitrile.

The stability of the two reagents once oxidised was confirmed using UV-Vis spectroscopy. Tris(2,2'-bipyridine)ruthenium(II) was stable over a 2 hour period (Figure 2.13 (a)), while 10% bis(acetonitrile)bis(2,2'-bipyridine)ruthenium(II) absorbance increased, decreasing emission potential (Figure 2.13 (b)). Figure 2.13 (c) illustrates the absorbance of a 10% bis(acetonitrile)bis(2,2'-bipyridine)ruthenium(II) solution prepared in dry acetonitrile, that

supports HPLC-CL data suggesting that dry acetonitrile is more stable once oxidised however due to the selectivity issues, this research was not further explored.

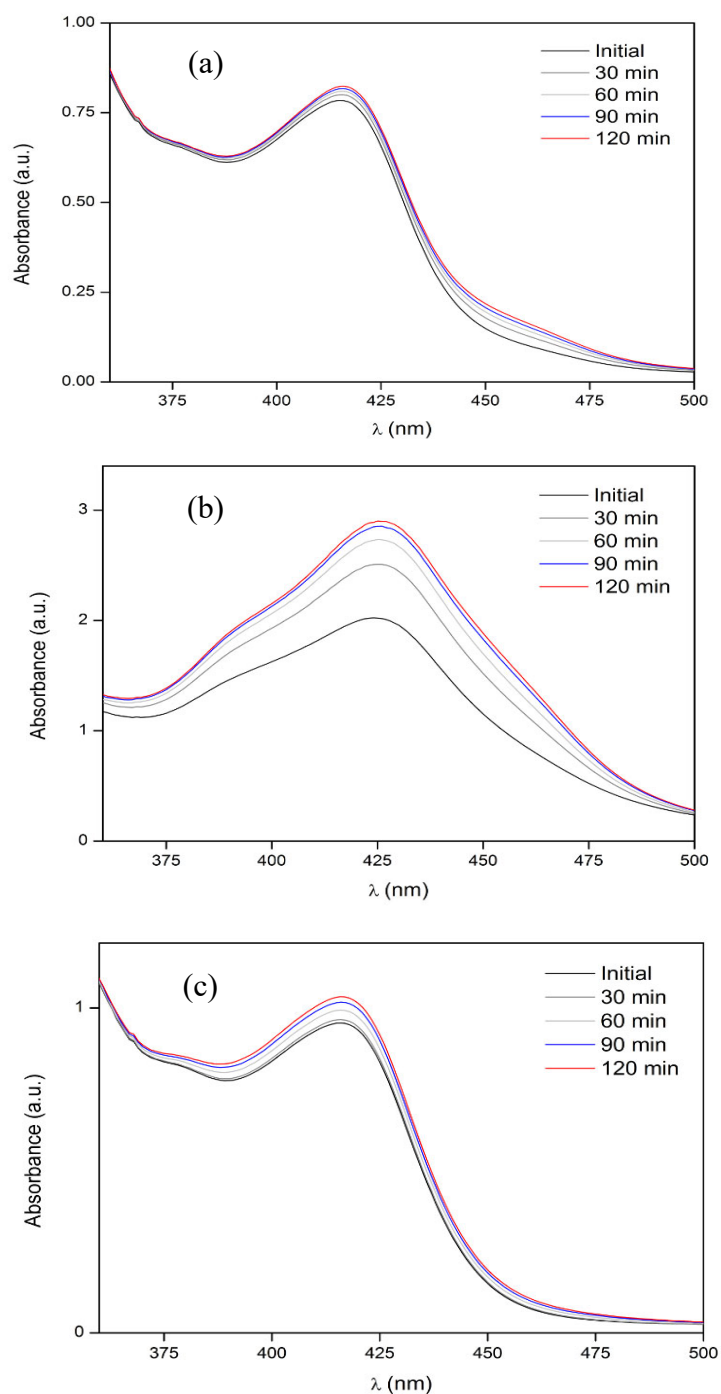


Figure 2.13. UV-Vis spectra over a two hour period once reagents were chemically oxidised.

- (a) Tris(2,2'-bipyridine)ruthenium(II) in regular acetonitrile (2.5×10^{-4} M),
- (b) 10% bis(acetonitrile)bis(2,2'-bipyridine)ruthenium(II) in regular acetonitrile (2.5×10^{-4} M) and
- (c) 10% bis(acetonitrile)bis(2,2'-bipyridine)ruthenium(II) in dry acetonitrile (2.5×10^{-4} M).

This research on synthetic cannabinoids is particularly important for a selective determination of target compounds. As there are hundreds of known derivatives [64], having a generalised method for these substances will not align with the needs of the law enforcement agencies. As well as the selectivity improvements it also affords a rapid separation of mixtures that corresponds to real world samples. There are many avenues to where this research can expand on and future work for chemiluminescence detection of synthetic cannabinoids is discussed in greater detail in chapter 6.

2.4 Conclusions

2.4.1 Amphetamine type stimulants

A new method of detecting MDMA using tris(2,2'-bipyridine)ruthenium(II) chemiluminescence in a basic reaction environment was optimised. Under these conditions, considerable selectivity towards compounds containing a secondary amine was observed, with no significant signal obtained for several common interferents. The sensitivity was found to be sufficient for the determination of MDMA in typical street drug samples, with a detection limit of 0.48 μM .

In conjunction with chromatographic separation, chemiluminescence detection was applied to street drug samples known to contain MDMA. The results were consistent with those of two separate HPLC procedures with UV absorbance detection, suggesting that the chemiluminescence approach is a viable and accurate technique. As chemiluminescence is more selective than conventional UV absorbance detection, there is considerable scope to decrease separation times, and thus dramatically increase sample throughput.

2.4.2 Synthetic cannabinoids

Previous HPLC conditions were optimised for a rapid separation of three forensically important synthetic cannabinoids. The tris(2,2'-bipyridine)ruthenium(II) chemiluminescence reagent was explored for viability of detection for these analytes. Under optimised HPLC conditions, the CL was selective towards two of the three analytes. By modifying the tris(2,2'-bipyridine)ruthenium(II) reagent to provide bis(acetonitrile)bis(2,2'-bipyridine)ruthenium(II) the selectivity increased at expense of the reagent stability. Dry acetonitrile was used to explore the effect on reagent stability and through both HPLC-CL and UV-Vis spectroscopy it showed promising increases in the stability of the reagent once chemically oxidised.

CHAPTER THREE:

ELECTROCHEMILUMINESCENCE DETECTION IN AQUEOUS
ENVIRONMENTS

Chapter overview

This chapter outlines the use of TPrA to better understand the reaction mechanisms in a phosphate buffered system of $[\text{Ru}(\text{bpy})_3]^{2+}$ for electrochemiluminescence (ECL). Previous research suggests that applying negative potentials results in a reductive-oxidation (or cathodic) emission at the working electrode however location of ECL emission has never been visually explored.

Herein, previous research methods are explored to determine the location of ECL emissions by utilising a Canon EOS 6D DSLR digital camera as the photodetector. This research also explores the possibility of a secondary emission source at the counter electrode, to be utilised for a bi-detection system.

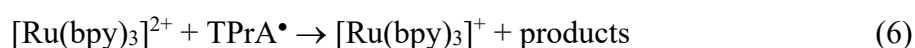
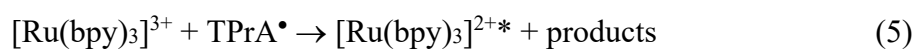
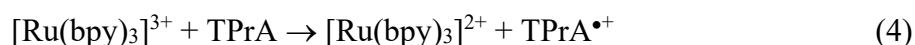
Cyclic voltammetric experiments were conducted in order to establish similar PMT responses to reported literature, and then replaced with camera images. The nature of the ECL emission species was confirmed by a CCD spectrometer in comparison with the luminescence spectra of the $[\text{Ru}(\text{bpy})_3]^{2+}$ complex.

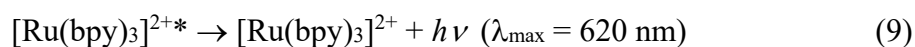
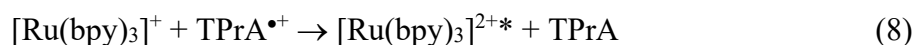
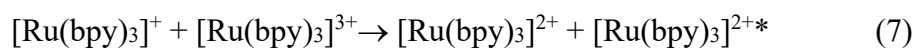
Surface areas and materials (glassy carbon or platinum) of the counter electrode were also trialled in order to observe any differences in ECL responses.

3.1 Introduction

Electrochemiluminescence (ECL) continues to be exploited in a diverse range of analytical applications [179-183], as the emission of light from the excited products of electrogenerated species against a dark background, and the ability to repeatedly excite reversible electrochemiluminophores in the presence ‘co-reactants’, provides an exceedingly sensitive mode of detection. Moreover, the temporal and spatial control of the electrochemical excitation process creates opportunities for multiplexing and imaging approaches [123, 184-186].

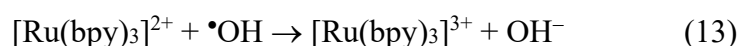
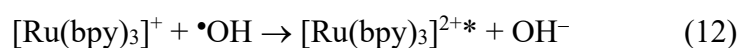
The majority of analytical applications of ECL have been based on tris(2,2'-bipyridine)ruthenium(II) ($[\text{Ru}(\text{bpy})_3]^{2+}$) with various secondary or tertiary alkylamine co-reactants such as tri-*n*-propylamine (TPrA). The mechanisms of these ‘oxidative-reduction’ (or anodic) co-reactant systems have been widely explored [142, 187, 188]. The ECL of $[\text{Ru}(\text{bpy})_3]^{2+}$ with TPrA, for example, proceeds *via* Equations 1 to 9, where one or both species are oxidised at the electrode surface followed by homogeneous electron transfer reactions involving the aminium cation ($\text{TPrA}^{\bullet+}$) and α -amino alkyl (TPrA^\bullet) radicals [142]. In applications in which this ECL system is used to detect the amine co-reactant with relatively high concentrations of $[\text{Ru}(\text{bpy})_3]^{2+}$, the predominant reaction pathways are depicted by Equations 1-5 and 9.





Electrochemiluminescence can also be generated through analogous ‘reductive-oxidation’ (or cathodic) pathways, using co-reactants such as persulfate [189-191] and benzoyl peroxide [192, 193], where the reactants are reduced at the working electrode before homogeneous electron transfers generate the electronically excited product.

Cathodic ECL has relatively few analytical applications, but Cao *et al.* [194] reported that many compounds that traditionally served as oxidative-reduction co-reactants (including TPrA) could also be sensitively detected with $[\text{Ru}(\text{bpy})_3]^{2+}$ in aqueous phosphate buffer solution when applying a low cathodic potential (between -0.40 V and -0.80 V vs Ag/AgCl). The ECL was attributed to the reduction of dissolved oxygen, leading to the formation of $\bullet\text{OH}$, capable of oxidising $[\text{Ru}(\text{bpy})_3]^{2+}$. Choi and Bard [127] subsequently reported the ECL of $[\text{Ru}(\text{bpy})_3]^{2+}$ with hydrogen peroxide as a co-reactant in phosphate buffer solution when applying cathodic potentials (between -1.30 V and -1.50 V vs Ag/AgCl) and proposed a mechanism involving the $\bullet\text{OH}$ radical (Equations 10-13, 7 and 9).



Choi and Bard measured a weak background ECL in the absence of hydrogen peroxide, when scanning the electrode potential in the negative direction [127]. In contrast to Cao and

co-workers' observations [194], Choi and Bard reported that the intensity of the background emission increased upon the removal of oxygen. Moreover, the emission was no longer detected when the counter electrode was isolated from the catholyte using a glass capillary with porous frit, suggesting the background emission that they observed, and by extension the ECL reported by Cao *et al.* [194], may actually arise from anodic processes at the counter electrode, but Choi and Bard did not examine the reaction with TPrA [127]. In a related study, Yuan *et al.* [195] reported 'cathodic' ECL from $[\text{Ru}(\text{bpy})_3]^{2+}$ in acetonitrile containing acetic acid, sodium acetate and tetrabutylammonium perchlorate. The emission was enhanced by TPrA and inhibited by H_2O_2 . These authors also stated that no emission was observed when the counter electrode was isolated in a glass capillary with a porous frit.

In conventional ECL experiments, the light is generally assumed to emanate from solution near the working electrode surface, but contributions from simultaneous reactions at the counter electrode may be more common than previously recognised [149, 196]. Further, the advancement towards multi-luminophore and potential-resolved ECL approaches [182, 197-199], that require wider ranges of electrode potentials, has placed new importance in understanding ECL reactions at the counter electrode. With this in mind, the nature of the ECL reaction reported by Cao *et al.* [194] was explored by monitoring and measuring the potential at both the working and the counter electrode, and visualizing the source of light using a digital camera positioned under the electrochemical cell and synchronised with the potentiostat. As in the previous studies a glassy carbon working, platinum counter and Ag/AgCl reference electrode were used for all experiments [127, 194]. As Cao *et al.* did not give details of the Pt counter electrode, experiments were conducted using a Pt wire, that is more commonly employed, and then with a Pt disk electrode, which provided clearer visualization of its entire active surface.

These experiments will not only provide a mechanistic understanding of the counter electrode processes, it illustrates a spatial resolution for clearer identification of emission source. The fundamental studies exploring source of ECL emission is important in order to determine reaction pathways that can be exploited for application of forensically important compounds. Exploring a potential secondary emission source allows for bi-detection systems that can be utilised for seizure samples that contain two active ingredients. Understanding fundamental ECL with a model compound may have the potential to significantly reduce the screening time for real world samples, by exploiting two responses in one reaction vessel.

3.2 Experimental

3.2.1 Chemicals

Reagents used were of analytical grade standard unless otherwise stated. Sodium phosphate monobasic monohydrate, sodium phosphate dibasic heptahydrate and tri-*n*-propylamine were obtained from Sigma-Aldrich (Castle Hill, New South Wales, Australia). Tris(2,2'-bipyridine)ruthenium(II) dichloride hexahydrate was obtained from Strem Chemicals (Newburyport, Massachusetts, USA). Sodium hydroxide was obtained from Ajax Fine Chemicals (Seven Hills, New South Wales, Australia). Each experiment was conducted in freshly prepared 0.1 M phosphate buffer (pH 6.8) with 50 mM tri-*n*-propylamine and 1 mM tris(2,2'-bipyridine)ruthenium(II).

3.2.2 Instrumentation

All cyclic voltammetry experiments were conducted using an Autolab PGSTA12 potentiostat (Metrohm Autolab, B.V, Netherlands) and chronoamperometry using an Autolab PGSTAT128N potentiostat (Metrohm Autolab, B.V, Netherlands). The electrochemical cell comprised a cylindrical glass vessel with a flat base and custom-built Teflon lid with appropriate sized holes to fit the relevant electrodes. A 3 mm glassy carbon working electrode (CH instruments), leak free Ag/AgCl reference electrode (model KZT-5, 5 mm diameter, 3.4 M KCl filling; Innovative Instruments, USA) and either a 2 mm platinum disk or platinum wire counter electrode (CH instruments) was utilised for all experiments (Figure 3.1). The Ag/AgCl reference electrode was utilised as it minimised any potential shifting over the course of the experiments which was seen when using a silver wire. The design of the leak free electrode also eliminated any liquid-junction potentials. Prior to each experiment, each electrode was cleaned/polished. Glassy carbon and platinum disk electrodes were polished using 0.05 mm

alumina powder on a felt pad with deionized water. All electrodes were rinsed with acetone and dried with either nitrogen or argon. For all experiments, the electrochemical cell was housed in a custom-built light-tight Faraday cage.

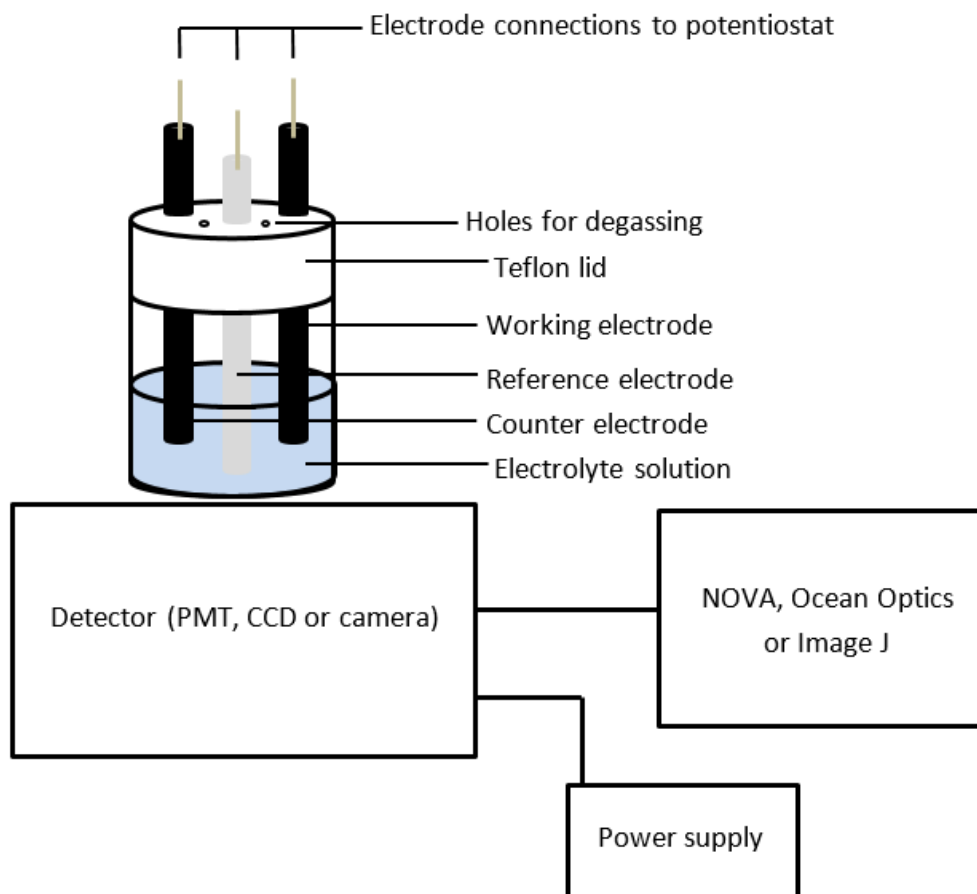


Figure 3.1. Schematic of electrochemical cell set-up for ECL experiments.

For cyclic voltammetry experiments the ECL emission was monitored with an extended-range trialkali S20 photomultiplier tube (PMT; ET Enterprises model 9828B) positioned under the cell. For chronoamperometry experiments, the potentiostat was outfitted with a pX1000 module. This module was configured to measure the potential difference between the counter and reference electrode, alongside measurement of the current and the applied working electrode potential. The ECL at the working and counter electrodes was photographed using a Canon EOS 6D DSLR camera (Canon, Japan) fitted with a Tonika AT-X PRO MACRO 100 mm f/2.8 D lens (Kenko Tonika Co., Japan), that was controlled by the potentiostat using a

digital output pin interfaced with the camera remote shutter release. The camera was positioned directly under the base of the electrochemical cell (within the light tight faraday cage) and focused manually on the surface of the electrodes. An ISO value of 8000 and aperture of F2.8 was used for all images. The camera was replaced with an Ocean Optics QEPro CCD spectrometer interfaced with the cell *via* optical fibre and collimating lens for all emission and photoluminescence spectra.

3.3 Results and discussion

Initial experiments were to interrogate the electrochemical behaviour using cyclic voltammetry while monitoring the ECL emission with an extended-range trialkali S20 photomultiplier tube (PMT; ET Enterprises model 9828B) positioned under the cell.

Figure 3.1 shows the cathodic cyclic voltammogram (CV) and associated ECL response for 1 mM $[\text{Ru}(\text{bpy})_3]^{2+}$ and 50 mM TPrA in 0.1 M phosphate buffer solution (pH 6.8). The CV exhibits two reduction waves with the first starting at approximately -0.50 V, that is attributed to the reduction of dissolved oxygen while the second begins at -1.20 V. In agreement with Cao *et al.* [194], ECL was observed when these negative potentials were applied to the working electrode, after the onset of the O_2 reduction.

The PMT was then replaced with a DSLR camera (Canon, Japan) fitted with a Tonika AT-X PRO MACRO 100 mm f/2.8 D lens (Kenko Tonika, Japan), and added to the potentiostat a pX1000 module (Metrohm Autolab B.V, Netherlands) configured to measure the potential occurring at the counter electrode. Using a camera as the photodetector enables direct visualisation of the location of the emission [198, 200]. As shown in Figure 3.1 (d), under these conditions, the ECL was observed at the Pt disk counter electrode, while no emission was seen at the working electrode.

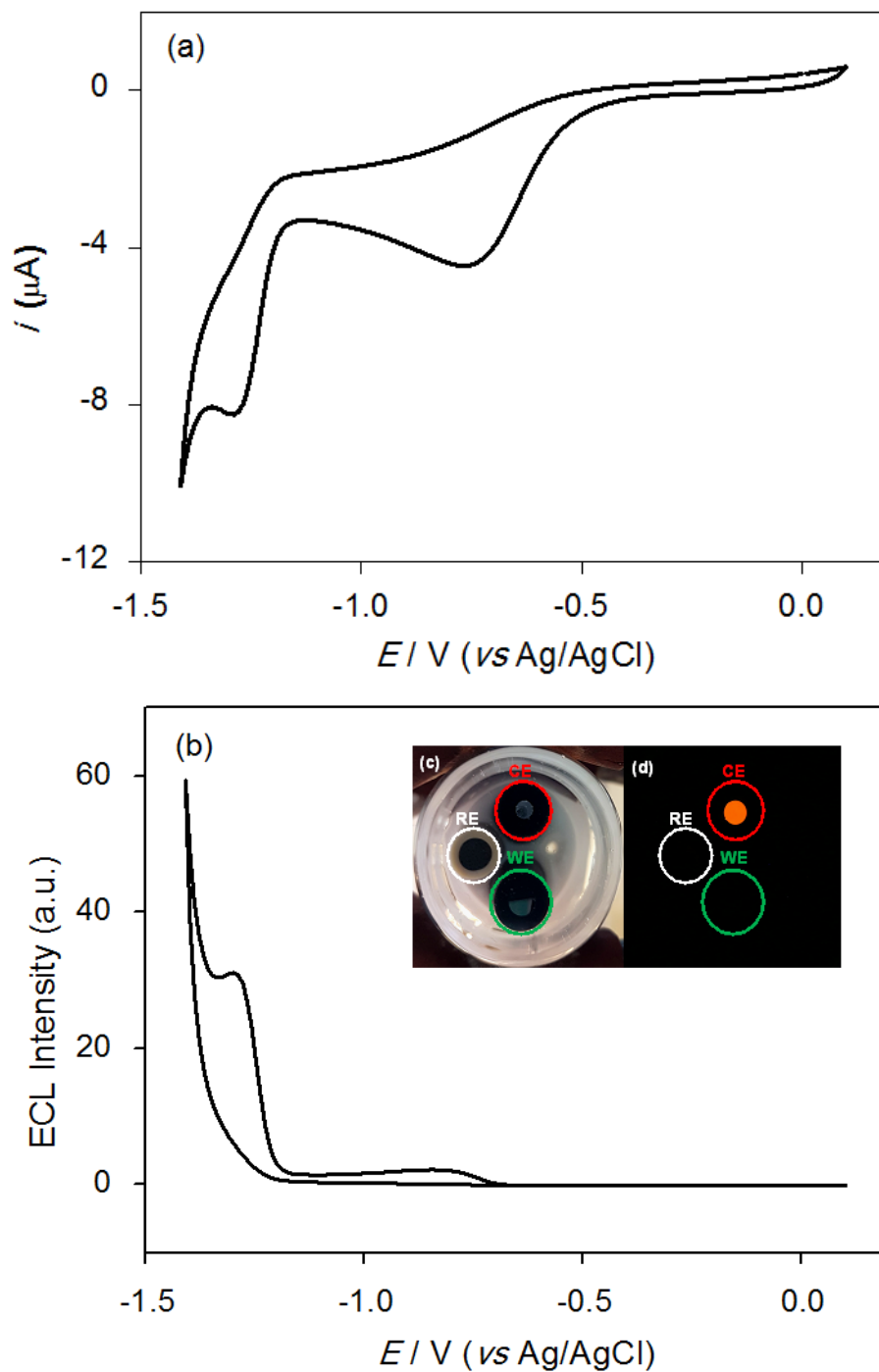


Figure 3.1. (a) Cyclic voltammogram of 1 mM $[\text{Ru}(\text{bpy})_3]^{2+}$ with 50 mM TPrA in 0.1 M phosphate buffer (pH 6.8) at a scan rate of 100 mV s^{-1} over the potential range -1.60 V to 0.20 V vs Ag/AgCl. (b) ECL signals recorded simultaneously with the traces from (a). (c) Inset shows the three-electrode configuration of GC working electrode (WE, green line), Pt disk counter electrode (CE, red line) and Ag/AgCl reference electrode (RE, white line). (d) ECL emission recorded for electrode set up in (c) recorded on a Canon EOS 6D DSLR camera.

Table 3.1. Potentials applied at the GC working electrode and measured at the Pt wire or Pt disk counter electrode, and photographs of the ECL at the Pt disk counter electrode upon application of each working electrode potential.

Electrode	Electrode Potential (<i>E</i>) / V vs Ag/AgCl											
	-0.40	-0.50	-0.60	-0.70	-0.80	-0.90	-1.00	-1.10	-1.20	-1.30	-1.40	-1.50
GC working												
Pt wire counter	0.62	0.69	0.76	0.76	0.77	0.77	0.75	0.75	0.83*	0.85*	0.88*	0.93*
Pt disk counter	0.72	0.85	0.90*	0.91*	0.91*	0.90*	0.90*	0.89*	0.91*	0.92*	0.93*	0.94*
Photographs of Pt disk emission ^a												

*Potentials at which ECL was observed at the counter electrode. ^aPhotographs recorded on a Canon EOS 6D DSLR camera (Canon, Japan) fitted with a Tonika AT-X PRO MACRO 100 mm f/2.8 D lens (Kenko Tonika Co., Japan) of ECL at the Pt disk counter electrode. A 40 s exposure time was used for each image with an ISO value of 8000 and an aperture of F2.8. Conditions: 0.1 M phosphate buffer solution (pH = 6.8) containing 1 mM [Ru(bpy)₃]²⁺ and 50 mM TPrA.

Using a series of chronoamperometric experiments in which potentials from -0.40 V to -1.50 V vs Ag/AgCl were applied at the working electrode (Table 3.1), the corresponding potentials measured at the counter electrode ranged from 0.72 V to 0.94 V for the Pt disk and 0.62 V to 0.93 V for the Pt wire. Images obtained for the Pt wire electrode are shown in Table 3.2. The greater potentials at the disk electrode were ascribed to its lower effective surface area, resulting in higher current densities and higher resistance at the electrode surface. Consequently, ECL was observed at the Pt disk counter electrode when lower cathodic potentials were applied at the working electrode (-0.60 V, compared to -1.20 V for the Pt wire).

Table 3.2. Potentials applied at the GC working electrode and measured at the Pt wire counter electrode, and photographs of the ECL at the Pt wire counter electrode upon application of each working electrode potential. Two configurations of the Pt wire: straight (top) and circular (bottom).

Electrode	Electrode Potential (E) / V vs Ag/AgCl			
GC working	-1.20	-1.30	-1.40	-1.50
Pt wire counter	0.83	0.85	0.88	0.93
Photographs of Pt wire emission ^a				
Pt wire counter	0.80	0.83	0.86	0.93
Photographs of Pt wire emission ^a				

^aInstrumentation set-up and conditions same as Table 3.1.

As shown in Table 3.1, ECL was observed at the counter electrode when the potential at that electrode was approximately 0.85 V (vs Ag/AgCl) or above, that is consistent with the oxidative-reduction (anodic) co-reactant pathway of $[\text{Ru}(\text{bpy})_3]^{2+}$ with TPrA (Figure 3.2).

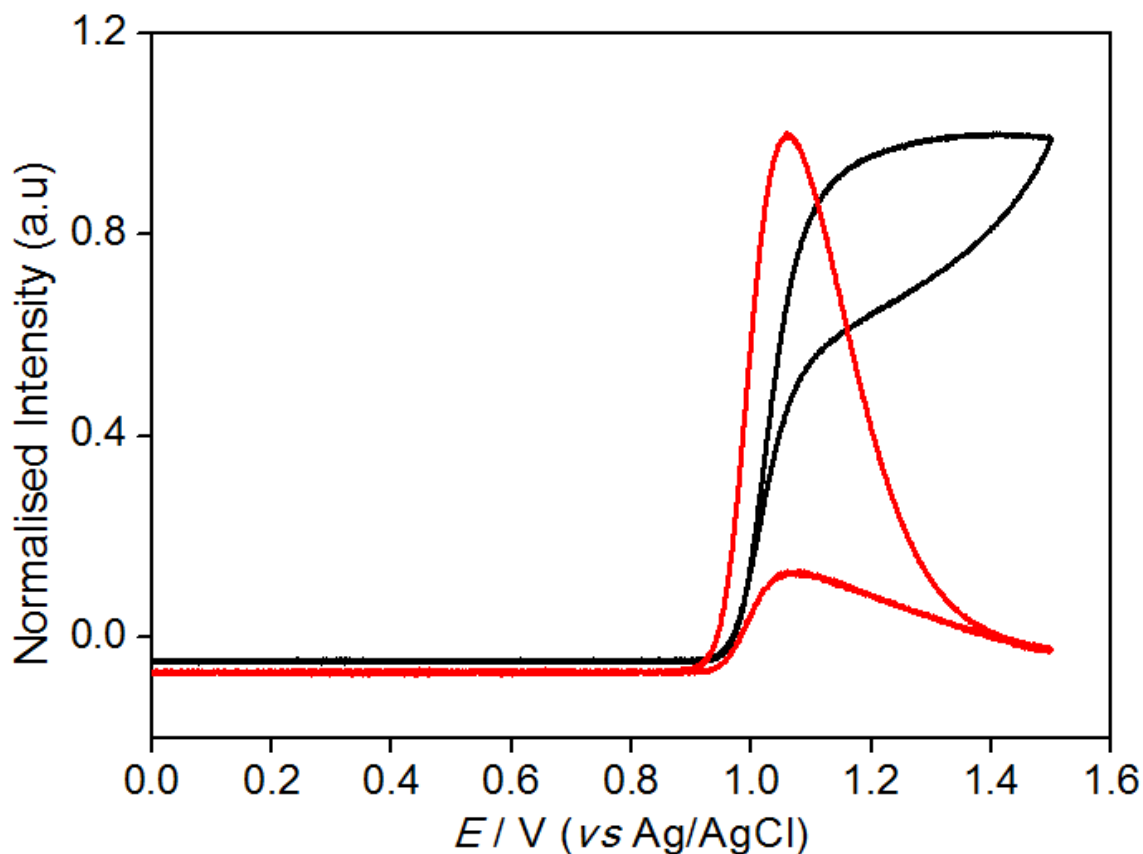


Figure 3.2. Typical ECL response for 1 mM $[\text{Ru}(\text{bpy})_3]^{2+}$ with 50 mM TPrA in 0.1 M phosphate buffer (pH = 6.8) when scanning from 0 V to 1.50 V vs Ag/AgCl and then back to 0 V, at a scan rate of 100 mV s^{-1} , when using a GC working electrode and Pt counter electrode (black line) or a Pt disk working electrode and GC counter electrode (red line).

The onset of anodic ECL is similar for GC and Pt working electrodes, represented by an ECL-CV trace shown in Figure 3.3. To confirm that the orange emission observed at the counter electrode (Table 3.1) was the characteristic luminescence from the $^3\text{MLCT}$ excited state of $[\text{Ru}(\text{bpy})_3]^{2+}$ [201, 202], the camera was replaced with an Ocean Optics QEPro CCD spectrometer interfaced with the cell *via* optical fiber and collimating lens. The maximum ECL emission was $\sim 620 \text{ nm}$, matching that of the ECL observed at the working electrode when anodic potentials were applied, and the photoluminescence of the same complex (Figure 3.3).

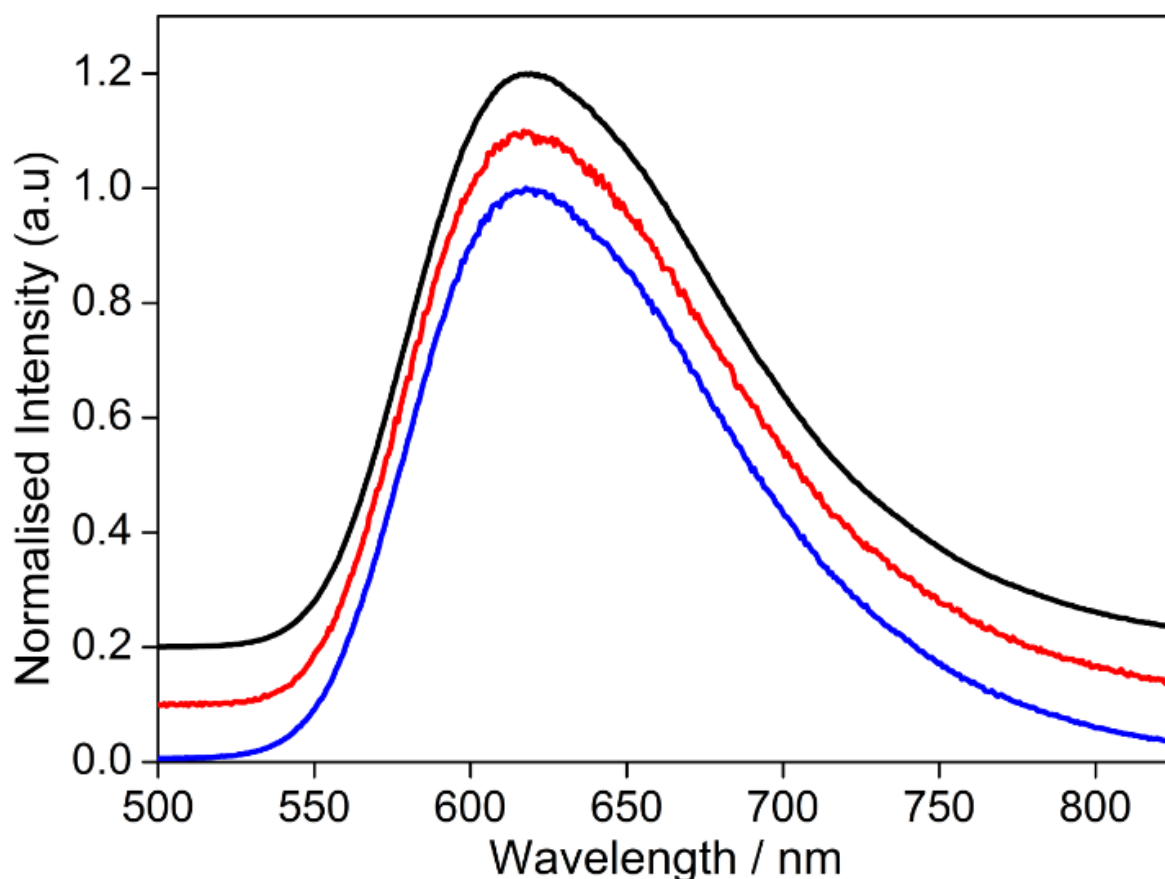


Figure 3.3. Emission spectra (stacked for easier visualisation) for ECL at the counter electrode (blue line) upon application of cathodic potentials at the working electrode, as shown in Fig. 3.1; and ECL at the working electrode (red line) upon application of anodic potentials, as shown in Fig. 3.2, for 1 mM $[\text{Ru}(\text{bpy})_3]^{2+}$ with 50 mM TPrA in 0.1 M phosphate buffer (pH = 6.8) solution; and the photoluminescence (black line) for the same solution upon excitation with UV light (370 nm LED).

Contrary to the previous proposal that the ECL of $[\text{Ru}(\text{bpy})_3]^{2+}$ and TPrA when applying cathodic potentials arises from the generation of a reactive oxygen species capable of oxidising the metal complex, the data presented here shows that the emission from the $^3\text{MLCT}$ excited state of $[\text{Ru}(\text{bpy})_3]^{2+}$ occurs predominantly at the counter electrode through an oxidative-reduction co-reactant pathways (Equations 1-5 and 9) [142]. This finding is congruent with Choi and Bard's [127] account of removing the weak background ECL from

$[\text{Ru}(\text{bpy})_3]^{2+}$ under cathodic potentials by isolating the counter electrode in a capillary with a porous frit.

The operation of both ECL pathways proposed in the previous studies was conceivable, if the light from the counter electrode was unintentionally obscured from the photodetector in the work of Cao *et al.* [194], and the absence of TPrA in Choi and Bard's study rendered the intensity of the cathodic ECL far lower than the weak emission attributed to electron transfers at the counter electrode. The conflicting observations of the two groups on the influence of dissolved oxygen on their respective reactions provides some support for this notion. In our examination of the conditions described by Cao *et al.*, however, we did not observe a decrease in ECL intensity when deaerating the solution. Moreover, we found that the onset of ECL when scanning cathodic potentials was dependent on the configuration (effective surface area) or the counter electrode, and more negative than the reduction potential of oxygen. Most convincingly, the absence of any observable emission from the working electrode in our study when cathodic potentials were applied, considering Cao and co-workers' claim that the cathodic ECL was similar in intensity to conventional anodic ECL of $[\text{Ru}(\text{bpy})_3]^{2+}$ and TPrA, leads us to rule out any analytically useful ECL from this purported cathodic ECL pathway.

3.4 Conclusions

This work highlights the importance of considering electrochemical processes occurring at the counter electrode in the elucidation of ECL reaction mechanisms and outlines a convenient instrumental approach to ascertain the source of emission, both the emitting species and its spatial distribution within the electrochemical cell. Not surprisingly, the processes that were observed to occur at the counter electrode were dependent on the configuration of the electrochemical cell, as (i) the voltage at the counter electrode is adjusted by the potentiostat to account for any change within the system to maintain the desired potential at the working electrode, and (ii) the position and geometry of the counter electrode will determine the portion of emitted light that is measured by the photodetector. Beyond the implications for investigation into ECL reaction mechanism, the recognition of processes at the counter electrode resulting in intense ECL and the development of our instrumental approach to distinguish the source of the emission creates exciting possibilities for analytical applications involving a dual ECL response at the working and counter electrode.

CHAPTER FOUR:

ELECTROCHEMILUMINESCENCE DETECTION IN ORGANIC ENVIRONMENTS

Chapter overview

This chapter focuses on anhydrous organic environments utilising tri-*n*-propylamine (TPrA) as a model compound to better understand the reaction mechanisms of three metal chelates for electrochemiluminescence (ECL) detections - tris(2-phenylpyridine- C^2,N)iridium(III) ($Ir(ppy)_3$), bis[3,5-difluoro-2-(2-pyridinyl- κN)phenyl- κC][2-[1-(phenylmethyl)-1H-1,2,3-triazol-4-yl- $\kappa N3$]pyridine- κN]iridium(III) ($[Ir(df-ppy)_2(ptb)]^+$) and tris(2,2'-bipyridine)ruthenium(II) ($[Ru(bpy)_3]^{2+}$).

A recent study has successfully reported multi-coloured detection systems with dual emission at the working and counter electrodes simultaneously, by annihilation ECL with a multi-complex system of $Ir(ppy)_3$ and $[Ru(bpy)_3]^{2+}$ [149]. Herein two multi-complex systems ($[Ir(df-ppy)_2(ptb)]^+$ with $[Ru(bpy)_3]^{2+}$ and $Ir(ppy)_3$ with $[Ru(bpy)_3]^{2+}$) for potential dual emission using TPrA co-reactant ECL are examined.

Acetonitrile was used as the solvent for all experiments. The anhydrous organic environment provides a wider electroactive window and the solvent is suitable for the forensic application described in the following chapter. Similar to in chapter 3, a counter electrode with a lower effective surface area was employed in order for higher current densities and higher resistance at the electrode surface and provided a wider range of potentials at the counter electrode.

Initial experiments were completed using chronoamperometry techniques with a camera to determine the location and relative intensity of the ECL response. Spectra were acquired using a CCD spectrometer to determine wavelengths and distribution of emission in mixtures, while images were analysed for their corresponding RGB values to determine emission from multiple luminophores. Once anodic and cathodic ECL emissions were established, cyclic voltammetric sweeps was explored using a PMT detector to measure the emission. Dual emission within

multi-complex systems was established through camera photography once individual anodic and cathodic potentials were determined.

4.1 Introduction

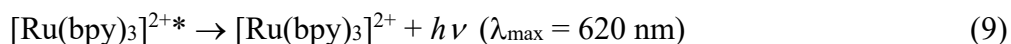
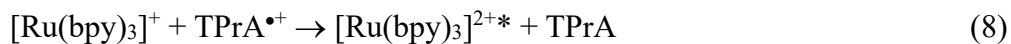
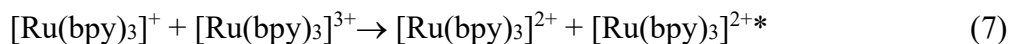
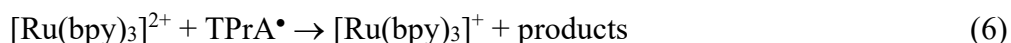
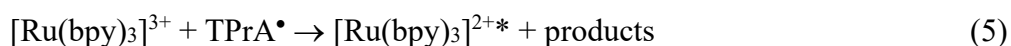
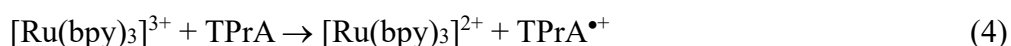
Recent interest in the application of bipolar electrochemistry in ECL as an alternative to the traditional three-electrode cell has directed focus on both anodic and cathodic reactions at the two electrode poles [181, 203]. Providing the two zones are spatially resolved it is possible for dual emission of different wavelengths and therefore there is potential for multiple detections in one experiment [181, 203]. Li *et al.* explored multi-coloured ECL emission from $[\text{Ru}(\text{bpy})_3]^{2+}$ and $\text{Ir}(\text{ppy})_3$ in solution with TPrA using a bipolar object [180]. In traditional ECL experiments using a conventional three-electrode cell configuration, possible emission at the counter electrode has been dismissed as an unwanted interference [149, 196]. It has only recently been discovered that counter electrode ECL could be exploited for multiplexed detection systems. Soulsby *et al.* explored mixed-metal complexes using the same two luminophores *via* annihilation ECL and demonstrated a multi-coloured detection system [149]. As described in chapter 3, some previous ECL systems attributed to cathodic processes may actually involve anodic reactions at the counter electrode, and the instrumental approaches described in this thesis enable clearer interpretation of these systems.

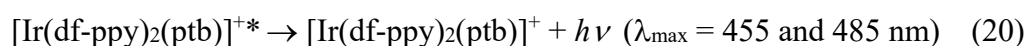
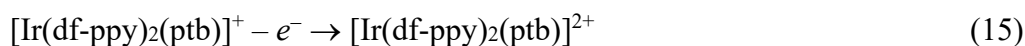
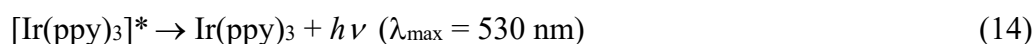
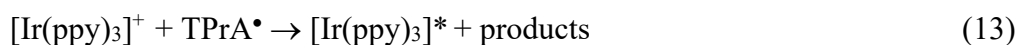
Herein, emission of anodic and cathodic reactions at the working and counter electrodes of a traditional three-electrode cell is explored with $\text{Ir}(\text{ppy})_3$, $[\text{Ir}(\text{df-ppy})_2(\text{ptb})]^+$ and/or $[\text{Ru}(\text{bpy})_3]^{2+}$ (Figure 4.1) with TPrA as a model co-reactant in acetonitrile. These systems provide information towards the co-reactant pathways that can be exploited for screening of forensically important compounds, as described in chapter 5, in that luminophore selectivity towards specific illicit substances and their potential for an ECL response is explored.

In a single-complex system of either $[\text{Ru}(\text{bpy})_3]^{2+}$, $\text{Ir}(\text{ppy})_3$, or $[\text{Ir}(\text{df-ppy})_2(\text{ptb})]^+$ with TPrA, when a positive potential is applied, oxidative-reduction ECL occurs at the working electrode

following equations 1-9, 10-14 or 15-20, respectively [141, 142]. One advantage the $[\text{Ru}(\text{bpy})_3]^{2+}$ has over the iridium(III) complexes is that it can emit an ECL response at lower potentials to its direct oxidation by a reaction of $[\text{Ru}(\text{bpy})_3]^{2+}$ with TPrA^\bullet (equation 6) that is followed by a reaction between $[\text{Ru}(\text{bpy})_3]^+$ and $\text{TPrA}^{\bullet+}$ (equation 8), resulting in an excited state product. The oxidised species can also generate an excited species *via* annihilation with the reduced product (equation 7) [142, 204].

The oxidised species of $\text{Ir}(\text{ppy})_3$ is not reduced with TPrA as with the other two complexes (equations 4 and 18). Instead, $[\text{Ir}(\text{ppy})_3]^+$ is reduced to the excited state by a reaction with TPrA^\bullet (equation 13), due to the similar oxidation potentials between $\text{Ir}(\text{ppy})_3$ and TPrA [141, 142].





In the traditional three-electrode cell where a 3 mm glassy carbon (GC) disk is used as the working electrode and a platinum wire is used at the counter, the surface area of the wire is greater than that of the GC disk. This ensures that there is a smaller difference between what is applied at the working and the corresponding opposite charge on the counter. The small difference is traditionally preferred because it decreases the likelihood for an emission to occur at the counter electrode as interference. If we exploit the difference in working and counter electrodes by changing the surface areas, there is potential to use the counter electrode as a secondary emission source. In this case, we have utilised a 2 mm platinum disk as the counter electrode that has a smaller surface area than the 3 mm GC working electrode. This will enable a greater difference between applied and opposing potentials to exploit a wider range simultaneously.

Previous research in chapter 3 of this thesis, has demonstrated the counter electrode as a source of emission for co-reactant ECL in aqueous solutions. With the intention of exploring the ECL

detection of synthetic cannabinoids (chapter 5), many of which are insoluble in aqueous solution, there is the need to examine co-reactant ECL at the working and counter electrodes in an anhydrous organic environment with the correct supporting electrolyte. This also enables common ECL luminophores that are insoluble in water, such as iridium(III) complexes, to be evaluated. Moreover, many energetic species require potentials outside the aqueous electrochemical window in order for efficient oxidation and reduction processes to occur [121]. By expanding the window one is able to facilitate both anodic and cathodic reaction pathways [205]. As the applied positive potential increases, there is a higher negative potential on the counter electrode, and *vice versa*. This research focuses on using anhydrous acetonitrile, with tetrabutylammonium hexafluorophosphate (TBAPF₆) as the supporting electrolyte, resulting in a potential window of approximately -2.90 V to +1.90 V. Tri-*n*-propylamine (TPrA) is the model co-reactant of choice as reaction mechanisms are well known and it provides the optimum ECL response, particularly with [Ru(bpy)₃]²⁺ [206, 207].

Three metal chelates are explored individually and in mixtures to gain insight into anodic and cathodic emissions at both the counter and working electrodes. Tris(2,2'-bipyridine)ruthenium(II) ([Ru(bpy)₃]²⁺: a red emitter) and tris(2-phenylpyridinato)iridium(III) (Ir(ppy)₃; a green emitter) were chosen because they are commonly used metal complexes and easy to distinguish through their emission spectra. There is also a considerable difference in their oxidation and reduction potentials that is important for selectivity and offers greater electrochemical control.

Bis[3,5-difluoro-2-(2-pyridinyl-κN)phenyl-κC][2-[1-(phenylmethyl)-1H-1,2,3-triazol-4-yl-κN3]pyridine-κN]iridium(III) ([Ir(df-ppy)₂(ptb)]⁺) was chosen as a third complex, that emits a distinguishable blue colour. A mixture of [Ir(df-ppy)₂(ptb)]⁺ and [Ru(bpy)₃]²⁺ is trialled as a second dual emission system.

In both mixed-complex systems a higher concentration of the iridium complex was used compared to $[\text{Ru}(\text{bpy})_3]^{2+}$ to compensate for quenching of the iridium based luminophores as previously reported [149]. These investigations using TPrA as a model co-reactant, examining the emission at both working and counter electrodes, provides a fundamental basis for the application of ECL with these three luminophores for forensically important analytes in chapter 5.

4.2 Experimental

4.2.1 Chemicals

Reagents used were of analytical grade standard unless otherwise stated. Acetonitrile was obtained from Scharlau (Sentmenat, Barcelona, Spain) and distilled over anhydrous calcium hydride. Tetrabutylammonium hexafluorophosphate was purchased from Sigma-Aldrich (Castle Hill, New South Wales, Australia). Tris(2-phenylpyridine- κ C,N)iridium(III) was obtained from Rubipy Scientific Inc. (Ottawa, Ontario, Canada). Bis[3,5-difluoro-2-(2-pyridinyl- κ N)phenyl- κ C][2-[1-(phenylmethyl)-1H-1,2,3-triazol-4-yl- κ N3]pyridine- κ N]iridium(III) was synthesised and characterised as previously described [170]. Each experiment was conducted in freshly distilled acetonitrile with 10 mM tri-*n*-propylamine and varying concentrations of the metal complexes as required. Refer to chapter 3 experimental for chemical information regarding tri-*n*-propylamine and tris(2,2'-bipyridine)ruthenium(II). The chemical structures of the three metal complexes utilised within this chapter is illustrated in Figure 4.1.

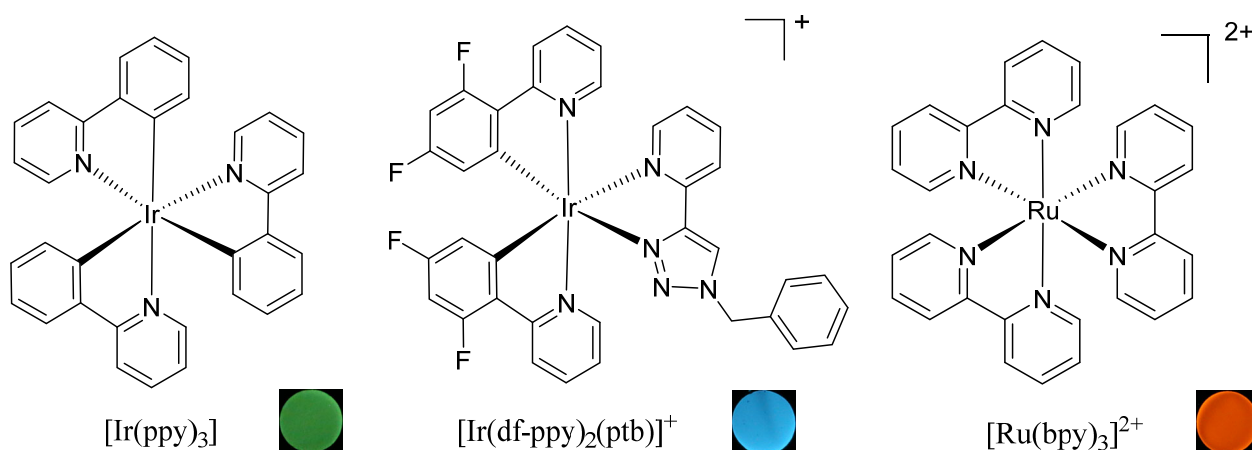


Figure 4.1. Chemical structures of the three metal centred complexes. Ir(ppy)₃, [Ir(df-ppy)₂(ptb)]⁺ and [Ru(bpy)₃]²⁺ with their respective emission images.

4.2.2 Instrumentation

Refer to chapter 3 for experimental conditions and a schematic manifold of the ECL set-up. Each solution was prepared in freshly distilled acetonitrile with 0.1 M TBAPF₆ as the supporting electrolyte. Oxygen from the atmosphere is removed from the system by aerating with either argon or nitrogen gas before and during experiments. This ensures that the oxidation or reduction of oxygen within the system does not interfere with ECL emissions from the co-reactant.

Oxidation and reduction potentials were determined *via* cyclic voltammetry at a scan rate of 0.1 Vs⁻¹ and referenced to Ag/AgCl. An ISO value of 8000 was used for all images and aperture was adjusted as required. RGB values were exported as an average value of the coloured area on the surface of the electrode, using Image J software (<https://imagej.nih.gov/ij/>).

4.3 Results and discussion

Initial cyclic voltammetry experiments were completed to understand the specific redox processes with each metal luminophore as well as TPrA, and required forward and reverse sweeps to illustrate both oxidation and reduction potentials. Any ECL response from a single complex system with TPrA as a co-reactant was explored utilising chronoamperometry experiments paired with a DSLR digital camera as the photodetector. This was then expanded onto mixed-complex systems and dual emission was explored.

Cyclic voltammetric scans show the oxidation and reduction peaks for Ir(ppy)₃, [Ir(df-ppy)₂(ptb)]⁺ and [Ru(bpy)₃]²⁺. It also illustrates the oxidation peak of TPrA and no reduction peaks from sweeping below zero as shown in Figure 4.2 and summarised in Table 4.1. A cathodic peak for TPrA is only possible if a forward scan is performed first, followed by the negative sweep, as reported in Zhou *et al.* [208].

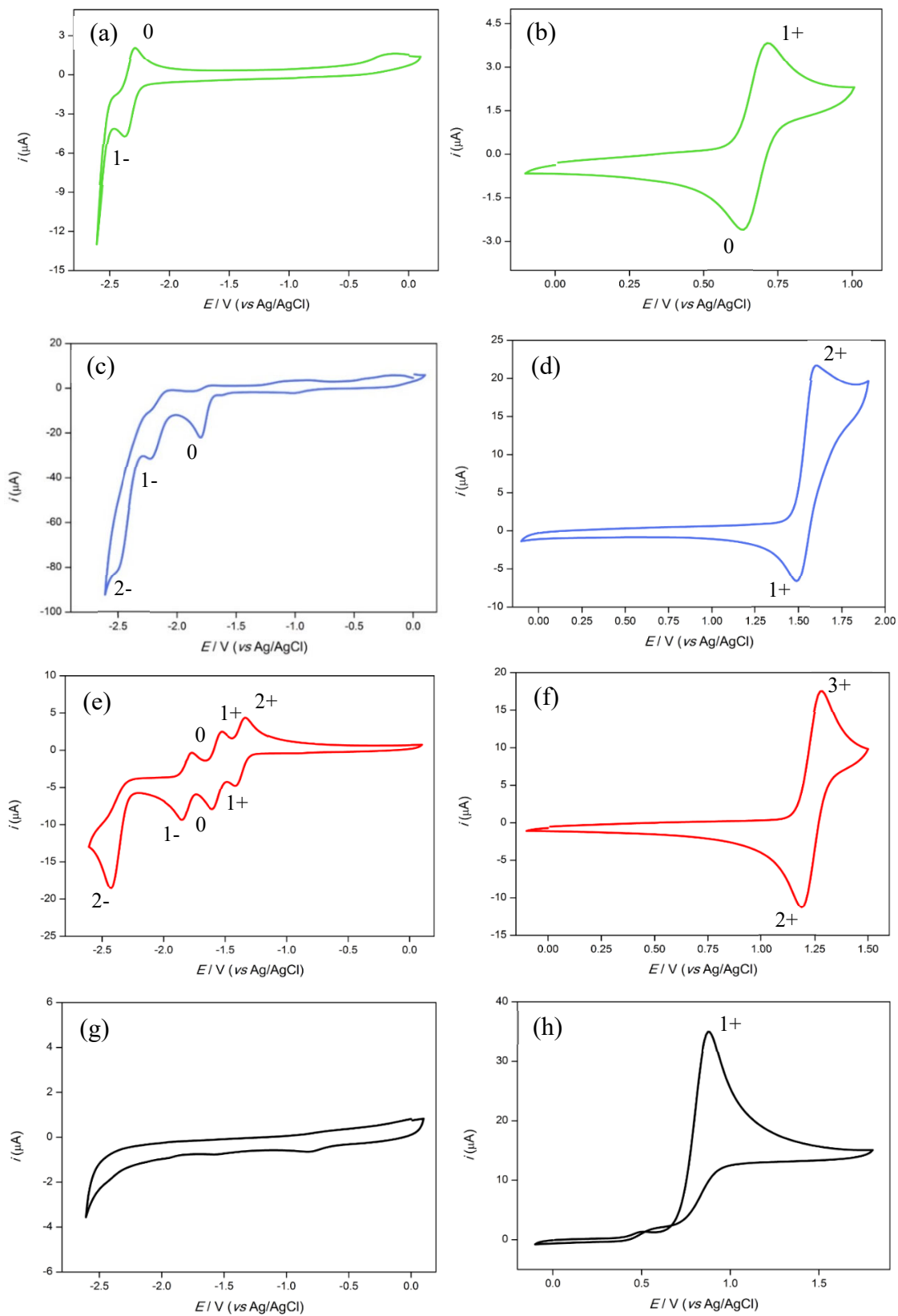


Figure 4.2. Cyclic voltammetry showing reduction and oxidation potentials for 0.2 mM Ir(ppy)₃ ((a) and (b)), 1 mM [Ir(df-ppy)₂(ptb)]⁺ ((c) and (d)), 1 mM [Ru(bpy)₃]²⁺ ((e) and (f)) and 1 mM TPrA ((g) and (h)).

Table 4.1. Summaries of oxidation and reduction potentials for Ir(ppy)₃, [Ir(df-ppy)₂(ptb)]⁺, [Ru(bpy)₃]²⁺ and TPrA.

	E_{ox}/V vs Ag/AgCl	E_{red}/V vs Ag/AgCl
Ir(ppy) ₃	0.68	-2.32
[Ir(df-ppy) ₂ (ptb)] ⁺	1.56	-1.80, -2.23, -2.51
[Ru(bpy) ₃] ²⁺	1.25	-1.37, -1.56, -1.82, -2.45
TPrA	0.89	

These oxidation and reduction potentials result in the characteristic electron-transfer processes of the metal chelates and TPrA. When positive potentials are applied, Ir(ppy)₃ has a reversible oxidation to form [Ir(ppy)₃]⁺ and negative potentials results in the reversible reduction product [Ir(ppy)₃]⁻. The [Ir(df-ppy)₂(ptb)]⁺ species is reversibly oxidised to form [Ir(df-ppy)₂(ptb)]²⁺ and has three irreversible reduction peaks forming [Ir(df-ppy)₂(ptb)]⁰, [Ir(df-ppy)₂(ptb)]⁻ and [Ir(df-ppy)₂(ptb)]²⁻. The ruthenium complex [Ru(bpy)₃]²⁺ has a reversible oxidation to [Ru(bpy)₃]³⁺ and three reversible reductions forming [Ru(bpy)₃]⁺, [Ru(bpy)₃]⁰, and [Ru(bpy)₃]⁻ and one irreversible reduction product [Ru(bpy)₃]²⁻. TPrA has one irreversible oxidation potential forming [TPrA]⁺ and no reduction potentials under typical conditions.

All three metal chelates were reacted with TPrA and ECL emission was photographed using a Canon EOS 6D DSLR camera fitted with a Tonika AT-X PRO MACRO 100 mm f/2.8 D lens. Images of the single complex system reaction emissions are shown in Tables 4.2-4.7.


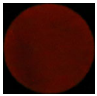
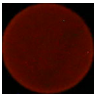
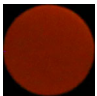
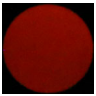



It is important to note that all single complex systems gave only oxidative-reduction ECL emission, observed at the working electrode when positive potentials were applied or at the counter electrode when negative potentials were applied. No ECL is observed at cathodic

potentials for any of the single complexes, illustrating a mechanism limited to anodic pathways with this particular co-reactant.

In a single complex system containing $[\text{Ru}(\text{bpy})_3]^{2+}$ and TPrA, applying positive potentials using a series of chronoamperometry experiments results in oxidative-reduction ECL emission at the surface of the working electrode from approximately 0.70 V until the edge of the electrochemical window of 1.90 V (Table 4.2). This emission is visualised as the characteristic orange/red colour previously described for $[\text{Ru}(\text{bpy})_3]^{2+}$ [201, 202].

Table 4.2. Oxidative-reduction ECL emission at the working electrode when positive potentials applied to a system containing 5 μM $[\text{Ru}(\text{bpy})_3]^{2+}$ and 10 mM TPrA. Images recorded with ISO 8000 and an aperture value

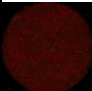
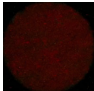
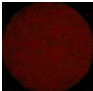
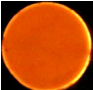
F5.

Electrode	Electrode Potential (E) / V vs Ag/AgCl							
	0.70	0.80	0.90	1.10	1.30	1.50	1.70	1.90
GC working	0.70	0.80	0.90	1.10	1.30	1.50	1.70	1.90
Pt disk counter	-1.75	-1.80	-1.80	-1.95	-1.95	-1.95	-2.00	-2.00
Photographs of GC emission								

Applying very high negative potentials (-2.60 V to the edge of the electrochemical window of -2.90 V) results in oxidative-reduction ECL emission at the surface of the Pt disk counter electrode once it reaches approximately 0.60 V and greater (Table 4.3).

Table 4.3. Oxidative-reduction ECL emission at the counter electrode when negative potentials applied to a system containing 5 μM $[\text{Ru}(\text{bpy})_3]^{2+}$ and 10 mM TPrA. Images recorded with ISO 8000 and an aperture value


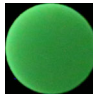
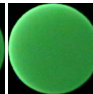
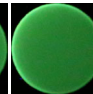
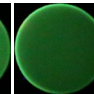
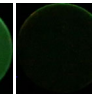
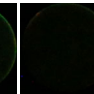
F2.8.

Electrode	Electrode Potential (E) / V vs Ag/AgCl			
GC working	-2.60	-2.70	-2.80	-2.90
Pt disk counter	0.60	0.61	0.68	2.70
Photographs of Pt disk emission				

In the single complex system containing $\text{Ir}(\text{ppy})_3$ and TPrA, applying positive potentials, the ECL emission begins at a lower potential compared to the $[\text{Ru}(\text{bpy})_3]^{2+}$. An oxidative-reduction green emission is observed from approximately 0.50 V until 0.80 V where emission has 'switched off' [204] (Table 4.4). Doeven *et al.* illustrated the 'switch off' mechanism for the $\text{Ir}(\text{ppy})_3$ metal complex as a quenching of the excited $[\text{Ir}(\text{ppy})_3]^*$ state by the $\text{TPrA}^{\bullet+}$ radical due to the similarities between their redox potentials. This 'switch off' phenomenon is reversible and occurs immediately, independently of any secondary complex within the system. It is also dependant on the concentration of the TPrA co-reactant and would not be observed at lower TPrA concentrations [204].

Table 4.4. Oxidative-reduction ECL emission at the working electrode when positive potentials applied to a system containing 0.2 mM Ir(ppy)₃ and 10 mM TPrA. Images recorded with ISO 8000 and an aperture value

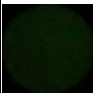
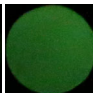
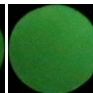
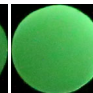
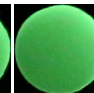
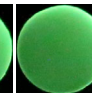
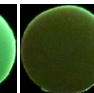
F2.8.

Electrode	Electrode Potential (<i>E</i>) / V vs Ag/AgCl						
GC working	0.50	0.55	0.60	0.65	0.70	0.75	0.80
Pt disk counter	-1.65	-1.77	-1.87	-1.95	-1.99	-2.33	-2.33
Photographs of GC emission							

Applying high negative potentials (−2.30 V to −2.90 V) results in oxidative-reduction ECL emission at the surface of the Pt disk counter electrode from approximately 0.47 V until 0.74 V (Table 4.5).



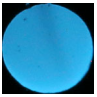
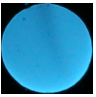
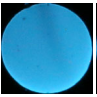
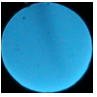
Table 4.5. Oxidative-reduction ECL emission at the counter electrode when negative potentials applied to a system containing 0.2 mM Ir(ppy)₃ and 10 mM TPrA. Images recorded with ISO 8000 and an aperture value

F3.5.

Electrode	Electrode Potential (<i>E</i>) / V vs Ag/AgCl						
GC working	-2.30	-2.40	-2.50	-2.60	-2.70	-2.80	-2.90
Pt disk counter	0.47	0.49	0.51	0.54	0.56	0.60	0.74
Photographs of Pt disk emission							


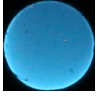

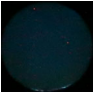
In the single complex system containing [Ir(df-ppy)₂(ptb)]⁺ and TPrA, applying positive potentials, the ECL emission begins at much higher potentials compared to that of [Ru(bpy)₃]²⁺. At approximately 1.40 V an oxidative-reduction ECL emission, of the characteristic blue colour for [Ir(df-ppy)₂(ptb)]⁺, at the working electrode is observed (Table 4.6).

Table 4.6. Oxidative-reduction ECL emission at the working electrode when positive potentials applied to a system containing 1 mM $[\text{Ir}(\text{df-ppy})_2(\text{ptb})]^+$ and 10 mM TPrA. Images recorded with ISO 8000 and an aperture value F22.

Electrode	Electrode Potential (E) / V vs Ag/AgCl					
	1.40	1.50	1.60	1.70	1.80	1.90
GC working	1.40	1.50	1.60	1.70	1.80	1.90
Pt disk counter	-1.95	-2.00	-2.05	-2.00	-2.00	-2.00
Photographs of GC emission						

Applying negative potentials to this system results in an oxidative-reduction ECL emission at the surface of the Pt disk counter electrode when applied potentials are between -2.20 V and -2.50 V. Between this range the counter electrode potentials is monitored to be between 0.90 V and 2.60 V (Table 4.7).


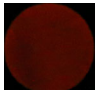



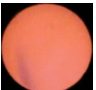
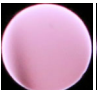



Table 4.7. Oxidative-reduction ECL emission at the counter electrode when negative potentials applied to a system containing 1 mM $[\text{Ir}(\text{df-ppy})_2(\text{ptb})]^+$ and 10 mM TPrA. Images recorded with ISO 8000 and an aperture value F22.

Electrode	Electrode Potential (E) / V vs Ag/AgCl			
	-2.20	-2.30	-2.40	-2.50
GC working	-2.20	-2.30	-2.40	-2.50
Pt disk counter	0.90	1.50	2.50	2.60
Photographs of Pt disk emission				

Although only anodic (oxidative-reduction) ECL was observed in these single complex systems, when high cathodic potentials were applied at the working electrode, ECL was observed due to anodic processes at the counter electrode.

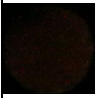
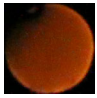

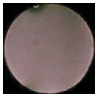
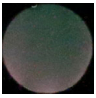
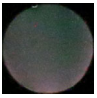
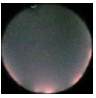
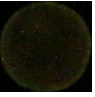
In a multi-complex system containing $[\text{Ru}(\text{bpy})_3]^{2+}$ and $[\text{Ir}(\text{df-ppy})_2(\text{ptb})]^+$ with TPrA, the red oxidative-reduction ECL emission begins at 1.00 V, while the blue emission starts at approximately 1.40 V (Table 4.8). The images obtained at potentials above 1.50 V show a pink/purple colour that is the combination of both red and blue colours. The $[\text{Ru}(\text{bpy})_3]^{2+}$ complex emits at lower potentials than its direct oxidation due to equations 6 – 8, and as described in the introduction of this chapter.

Table 4.8. Oxidative-reduction ECL emission at the working electrode when positive potentials applied to a system containing 1 mM $[\text{Ir}(\text{df-ppy})_2(\text{ptb})]^+$, 5 μM $[\text{Ru}(\text{bpy})_3]^{2+}$ and 10 mM TPrA. Images recorded with ISO 8000 and an aperture value F10.

Electrode	Electrode Potential (E) / V vs Ag/AgCl									
	1.00	1.10	1.20	1.30	1.40	1.50	1.60	1.70	1.80	1.90
GC working	1.00	1.10	1.20	1.30	1.40	1.50	1.60	1.70	1.80	1.90
Pt disk counter	-1.73	-1.75	-1.85	-1.90	-1.90	-1.98	-2.20	-2.35	-2.33	-2.40
Photographs of GC emission										

Applying negative potentials an oxidative-reduction ECL emission at the counter electrode is visualised when between -1.90 V and -2.60 V is applied to the working electrode. This results in potentials ranging from 0.70 V to 2.66 V on the counter electrode and no higher negative potentials were applied due to the counter being outside the electrochemical window where reaction mechanisms are not well understood [205]. The red emission begins at counter potential of 0.70 V and remains until 2.66 V. Blue emission occurs from 1.73 V until 2.30 V and is visualised as a combination pink/purple colour (Table 4.9).

Table 4.9. Oxidative-reduction ECL emission at the counter electrode when negative potentials applied to a system containing 1 mM $[\text{Ir}(\text{df-ppy})_2(\text{ptb})]^+$, 5 μM $[\text{Ru}(\text{bpy})_3]^{2+}$ and 10 mM TPrA. Images recorded with ISO 8000 and an aperture value F2.8.


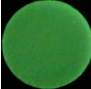
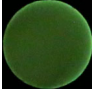
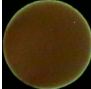
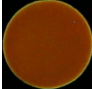
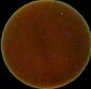





Electrode	Electrode Potential (E) / V vs Ag/AgCl							
GC working	-1.90	-2.00	-2.10	-2.20	-2.30	-2.40	-2.50	-2.60
Pt disk counter	0.70	0.75	1.73	2.20	2.25	2.30	2.30	2.66
Photographs of Pt disk emission								

No emission was visualised in this multi-complex system at cathodic potentials, either at the counter electrode when positive potentials were applied or the working electrode when negative potentials were applied.

Replacing the blue emitter ($[\text{Ir}(\text{df-ppy})_2(\text{ptb})]^+$) with the green emitter ($\text{Ir}(\text{ppy})_3$) there was greater scope to distinguish the two luminophores because the ‘switch off’ of $\text{Ir}(\text{ppy})_3$ ECL (Table 4.4) provides the opportunity to visualise each individual luminophore at different applied potentials [204]. Dual emission with these two complexes has also been reported before in both annihilation [149] and co-reactant ECL experiments [148].



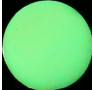







Photographs of oxidative-reduction ECL reactions in the multi-complex system of $\text{Ir}(\text{ppy})_3$, $[\text{Ru}(\text{bpy})_3]^{2+}$ and TPrA are shown in Table 4.10 and Table 4.11. Applying positive potentials, the oxidative-reduction ECL emission occurring at the working electrode begins at 0.55 V and continues until 1.90 V (Table 4.10). Only up to 1.50 V is shown in Table 4.10 as above this potential, emission at both the working and counter electrodes was observed, that is discussed later (Table 4.13). Between 0.55 V and 0.80 V, green emission occurs from the $\text{Ir}(\text{ppy})_3$ complex while $[\text{Ru}(\text{bpy})_3]^{2+}$ emission begins at approximately 0.70 V and continues to emit until 1.90 V. Between 0.70 V and 0.80 V the images illustrate a combination of both orange and green emission.

Table 4.10. Oxidative-reduction ECL emission at the working electrode when positive potentials applied to a system containing 0.1 mM Ir(ppy)₃, 5 μM [Ru(bpy)₃]²⁺ and 10 mM TPrA. Images recorded with ISO 8000 and an aperture value F5.

Electrode	Electrode Potential (<i>E</i>) / V vs Ag/AgCl										
GC working	0.55	0.60	0.65	0.70	0.75	0.80	0.85	0.95	1.10	1.30	1.50
Pt disk counter	-1.70	-1.83	-1.92	-1.96	-2.00	-2.10	-2.10	-2.10	-2.30	-2.25	-2.20
Photographs of GC emission											

Applying negative potentials to the working electrode an oxidative-reduction ECL emission occurs at the counter electrode from -2.00 V until -2.90 V (Table 4.11). Green emission occurs between applied potentials of -2.00 V and -2.80 V where counter potentials ranged from 0.55 V until 0.65 V. Orange/red emission is only visualised when high negative potentials are applied (-2.80 V to -2.90 V) where the counter potential ranges from 0.65 V to 2.60 V. These high negative applied potentials also produced ECL at both the working and counter electrodes, that is discussed later (Table 4.14).

Table 4.11. Oxidative-reduction ECL emission at the counter electrode when negative potentials applied to a system containing 0.1 mM Ir(ppy)₃, 5 μM [Ru(bpy)₃]²⁺ and 10 mM TPrA. Images recorded with ISO 8000 and an aperture value F3.5.

Electrode	Electrode Potential (<i>E</i>) / V vs Ag/AgCl									
GC working	-2.00	-2.20	-2.40	-2.55	-2.65	-2.75	-2.80	-2.85	-2.90	
Pt disk counter	0.55	0.57	0.60	0.59	0.61	0.63	0.65	1.00	2.60	
Photographs of Pt disk emission										

As both anodic and cathodic emission was visualised and there is greater potential separation for this mixed-complex system, compared to $[\text{Ru}(\text{bpy})_3]^{2+}$ and $[\text{Ir}(\text{df-ppy})_2(\text{ptb})]^+$, all further experiments were focused towards the $\text{Ir}(\text{ppy})_3$ and $[\text{Ru}(\text{bpy})_3]^{2+}$ system.

The red, green and blue (RGB) values were exported from each image in this oxidative-reduction ECL emission from the $\text{Ir}(\text{ppy})_3$ and $[\text{Ru}(\text{bpy})_3]^{2+}$ multi-complex system to better understand the colour distribution seen in the photographs of the ECL emission. This is shown in Figure 4.3 and part (a) illustrates the application of positive potentials and the corresponding images from the emission. Using the RGB values it confirms the green emission being predominant between 0.55 V and 0.70 V while the orange/red emission is predominant from 0.85 V. Between 0.75 V and 0.85 V there is varying amounts of both green and red that is exhibited in both the images and the average RGB values. Figure 4.3 part (b) illustrates the RGB values from the counter electrode images when negative potentials were applied. Between -2.00 V and -2.75 V, green was predominant and red was greatest at the very high negatives of -2.80 V to -2.90 V. Potentials -2.75 V and -2.80 V had similar ratios of green and red emission that is exhibited in both the images and RGB values.

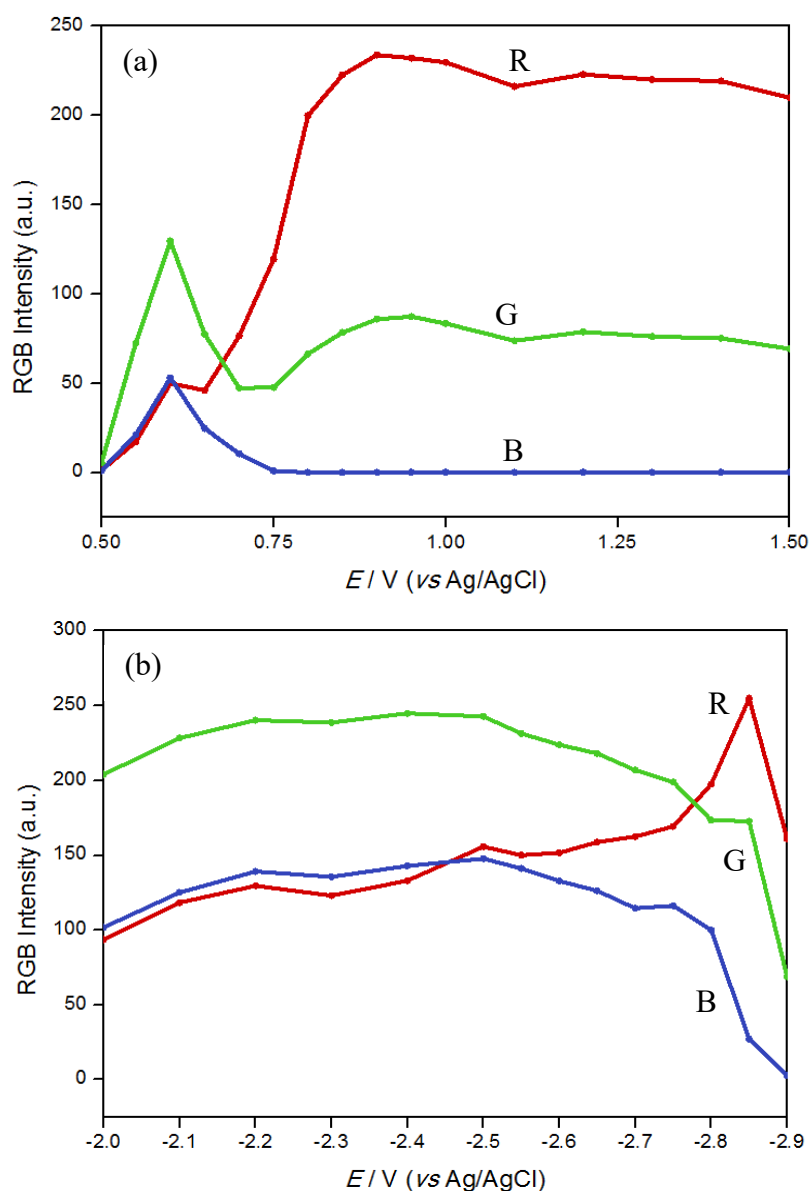


Figure 4.3. RGB values from oxidative-reduction ECL emission images in chronoamperometry experiments for (a) forward potential scan and (b) negative potential scan. RGB values exported using Image J software.

A CCD spectrometer was utilised to determine specific wavelengths of the green, red and combination emissions. Figure 4.4 illustrates three anodic emission spectra when specific potentials were applied to this multi-complex system. The green peak represents the emission spectra at the working electrode when 0.60 V is applied and corresponds to a wavelength of 530 nm. The orange peak represents the emission spectra at the working electrode when 1.00 V is applied and corresponds to a wavelength of 622 nm. The brown spectra illustrates the

combination of emission colours when 0.70 V is applied and two distinct peaks were observed at 530 nm and 622 nm.

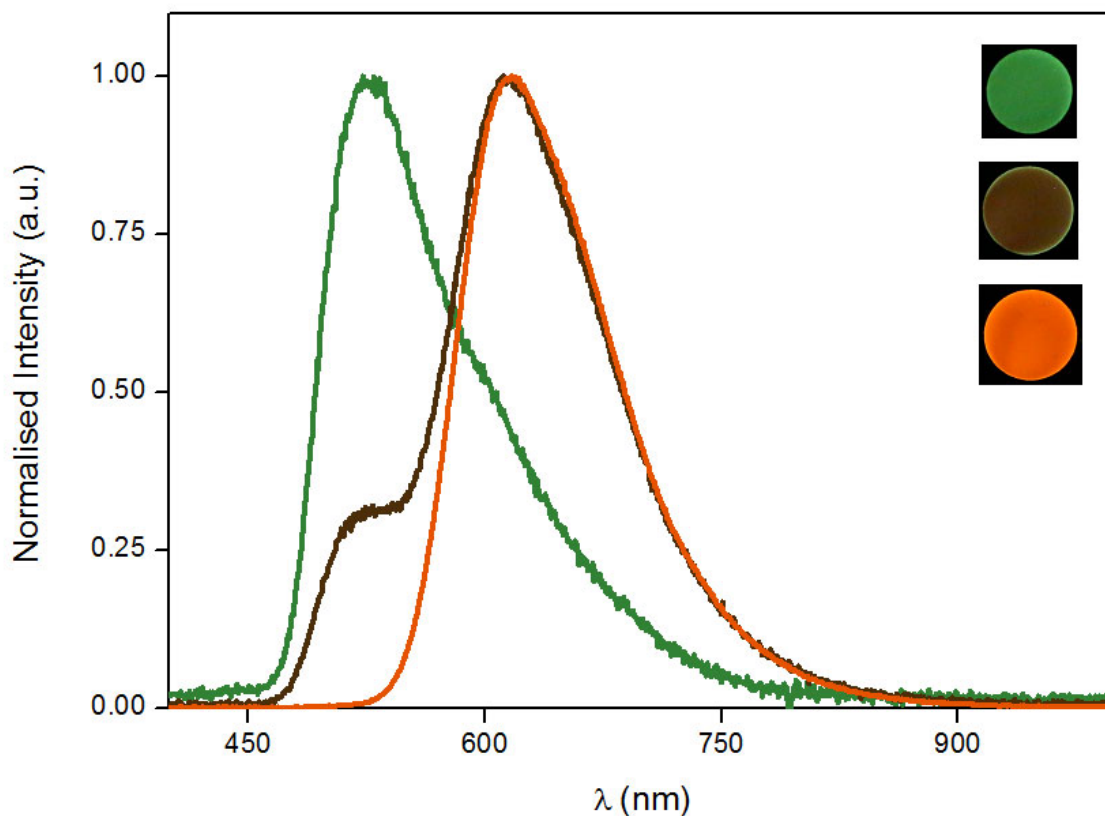


Figure 4.4. CCD spectra of three emitting potentials in a system of 0.1 mM Ir(ppy)₃, 5 μM [Ru(bpy)₃]²⁺ and 10 mM TPrA. Working electrode emission when 0.60 V applied (green peak at 530 nm), 0.70 V applied (two brown peaks at 530 nm and 622 nm) and 1.00 V applied (orange peak at 622 nm).

The presence of two peaks suggests that two separate reactions are occurring within the space surrounding the surface of the working electrode. This is a promising result when exploring potential dual emission as it illustrates the possibility of two emitting species in one reaction vessel simultaneously.

The single complex (Ir(ppy)₃ or [Ru(bpy)₃]²⁺) and multi-complex systems were examined with cyclic voltammetric experiments utilising a PMT as the ECL emission detector. As can be seen

in Figure 4.5, 4.6 and 4.7, all three systems gave both a forward and negative sweep emission signal.

Figure 4.5 (a) illustrates the ECL emission with a single complex system of Ir(ppy)₃ with TPrA. In the forward sweep, an emission occurs from 0.50 V until 0.85 V with the highest intensity being at 0.67 V. Figure 4.5 (b) illustrates the ECL emission of Ir(ppy)₃ with TPrA in a negative or reductive sweep. ECL emission occurs from -2.20 V until -2.70 V with greater intensities towards the higher negative values.

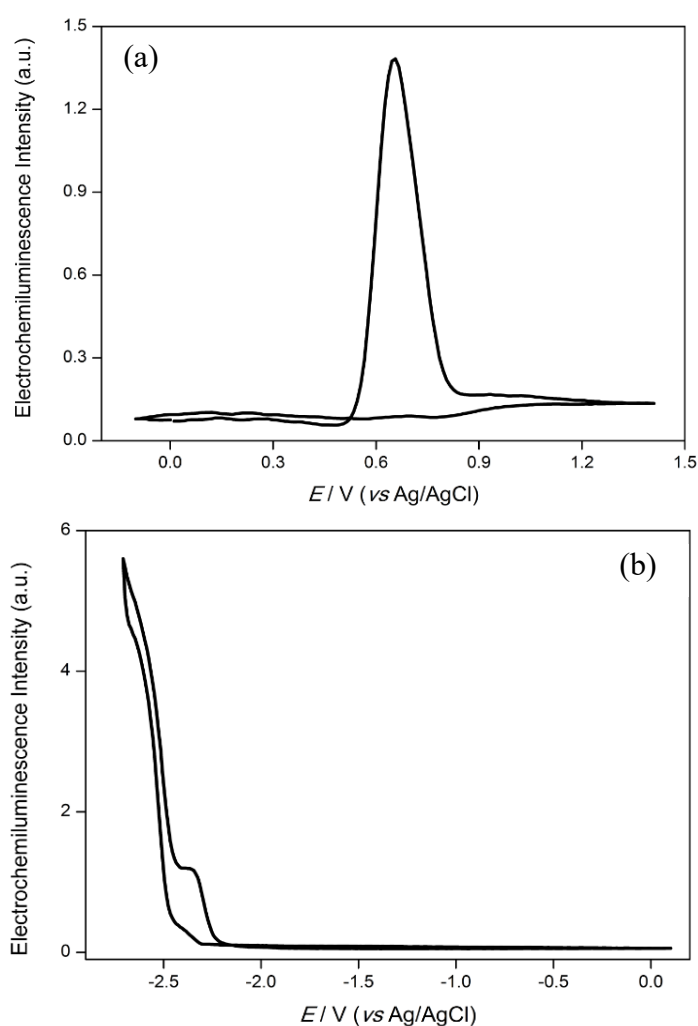


Figure 4.5. Cyclic voltammetric experiments illustrating ECL emission of 0.2 mM Ir(ppy)₃ with 10 mM TPrA using PMT detection. Forward scan of positive potentials (a) and reverse scan of negative potentials (b).

In the $[\text{Ru}(\text{bpy})_3]^{2+}$ with TPrA system the forward sweep resulted in an ECL response from approximately 0.65 V until the edge of the electrochemical window at 1.90 V (Figure 4.6 (a)). The negative sweep only gave an ECL emission at very high negatives of -2.80 V and -2.90 V (Figure 4.6 (b)).

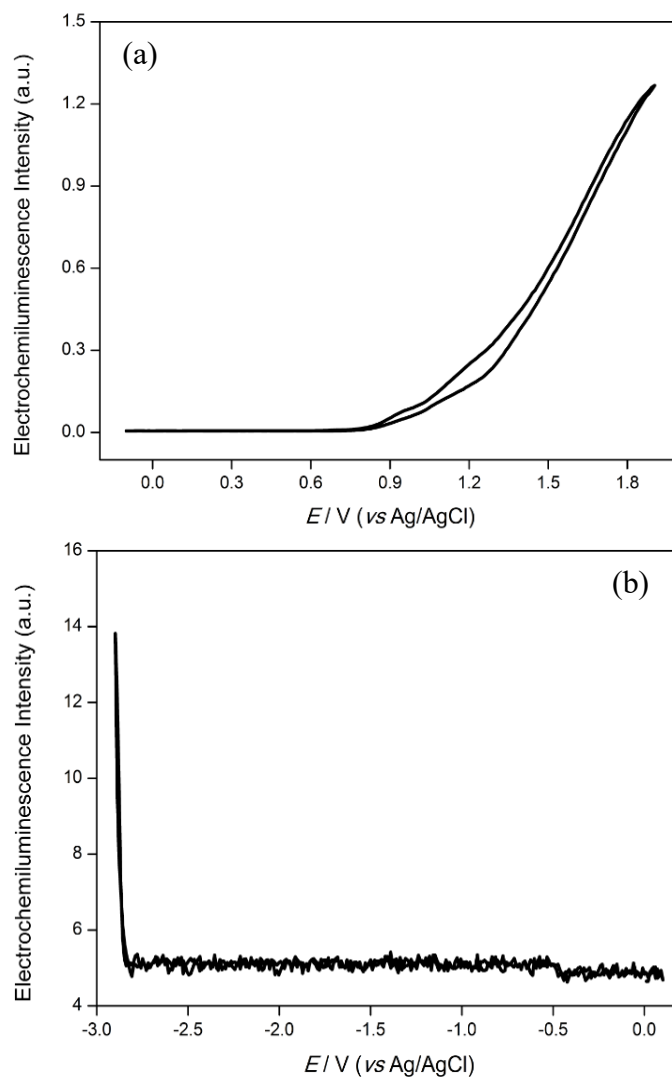


Figure 4.6. Cyclic voltammetric experiments illustrating ECL emission of $5 \mu\text{M}$ $[\text{Ru}(\text{bpy})_3]^{2+}$ with 10 mM TPrA using PMT detection. Forward scan of positive potentials (a) and reverse scan of negative potentials (b).

In the mixed complex system of $\text{Ir}(\text{ppy})_3$, $[\text{Ru}(\text{bpy})_3]^{2+}$ and TPrA, the potentials at which emission began is similar to that in the camera experiments. In the forward sweep, an ECL

response was observed from approximately 0.55 V until 1.90 V (Figure 4.7 (a)). In the negative sweep, emission began at approximately -1.90 V. (Figure 4.7 (b)).

Traditional ECL experiments are conducted with either a PMT or CCD detector, and all emission is assumed to be at the surface of the working electrode. Using the response patterns for the single complexes, observed from the PMT, it would be assumed that emission was occurring in both anodic and cathodic pathways. However, due to previous camera work, it cannot be concluded that the emission in the negative sweeps are from a reductive-oxidative reaction when the images support an oxidative-reduction ECL response on the counter electrode.

In the mixed-complex system, where we know there is dual emission occurring, we can conclude that the PMT response will be a combination of both emissions (Figure 4.7).

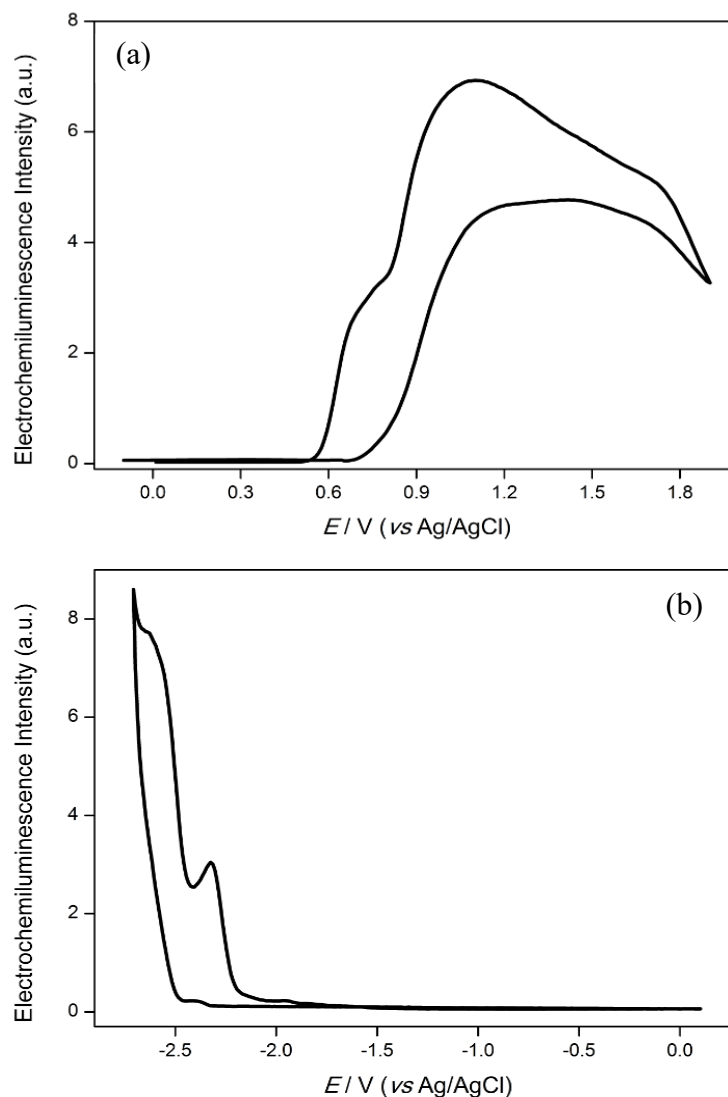


Figure 4.7. Cyclic voltammetric experiments illustrating ECL emission of 0.1 mM Ir(ppy)₃, 5 μM [Ru(bpy)₃]²⁺ with 10 mM TPrA using PMT detection. Forward scan of positive potentials (a) and reverse scan of negative potentials (b).

Referring back to the chronoamperometry experiments utilising a digital camera to visualise both the working and counter electrodes, for the simultaneous anodic and cathodic emission. Table 4.12 summarises the potentials at both the applied working electrode and the corresponding counter electrode for the Ir(ppy)₃, [Ru(bpy)₃]²⁺ and TPrA experiments. The asterisked values are where dual emission is observed and images are shown in Table 4.13 and Table 4.14.

When applying positive potentials of 1.50 V and greater, $[\text{Ru}(\text{bpy})_3]^{2+}$ elicits an ECL response on the working electrode while the corresponding counter electrode potential was high enough negative to elicit an ECL response from $\text{Ir}(\text{ppy})_3$ (Table 4.13). This discovery allows for dual emission of two complexes simultaneously at the two different electrodes and is the first visualisation of both anodic and cathodic ECL reactions in one cell at opposing electrodes, simultaneously, using co-reactant ECL.

Similar patterns are observed when applying high negative potentials (-2.80 V to -2.90 V): a green emission is observed at the working electrode while the opposing counter electrode potential is high enough to exhibit co-reactant ECL from $[\text{Ru}(\text{bpy})_3]^{2+}$ (Table 4.14)

Table 4.12. Summary of applied with corresponding counter electrode potentials in a 0.1 mM Ir(ppy)₃, 5 μM [Ru(bpy)₃]²⁺ and 10 mM TPrA solution. Values with asterisk donates dual emission visualised with red and green emission simultaneously.

Electrode	Electrode Potential E / V (vs Ag/AgCl)														
GC working	0.50	0.60	0.70	0.80	0.90	1.00	1.10	1.20	1.30	1.40	1.50*	1.60*	1.70*	1.80*	1.90*
Pt disk counter	-1.00	-1.83	-1.96	-2.10	-2.10	-2.05	-2.30	-2.30	-2.25	-2.20	-2.75*	-2.65*	-2.71*	-2.70*	-2.71*
GC working	-2.00	-2.10	-2.20	-2.30	-2.40	-2.50	-2.55	-2.60	-2.65	-2.70	-2.75	-2.80*	-2.85*	-2.90*	
Pt disk counter	0.55	0.56	0.57	0.58	0.60	0.63	0.59	0.60	0.61	0.62	0.63	0.65*	1.00*	2.60*	

Table 4.13. Images of dual emission in a 0.1 mM Ir(ppy)₃, 5 μM [Ru(bpy)₃]²⁺ and 10 mM TPrA solution at potentials 1.50 V and greater. Red/orange emission observed at the working electrode and green emission at the counter electrode. Images recorded with ISO 8000 and an aperture value F2.8.

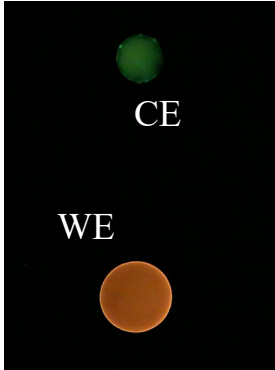
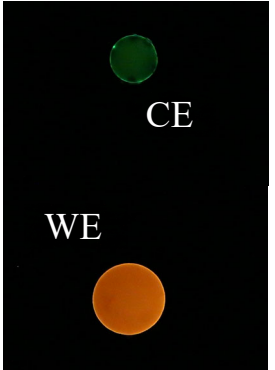
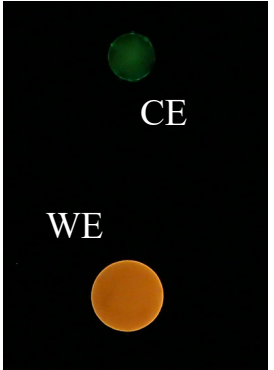
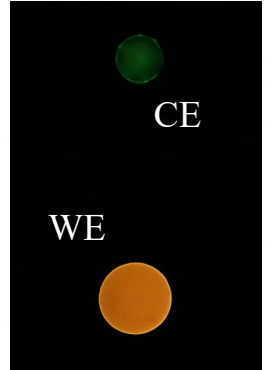
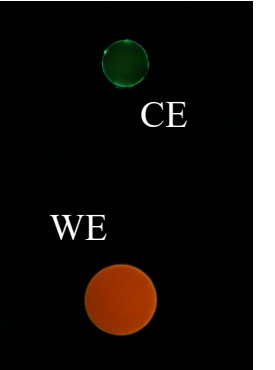
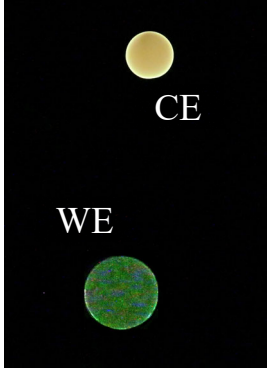
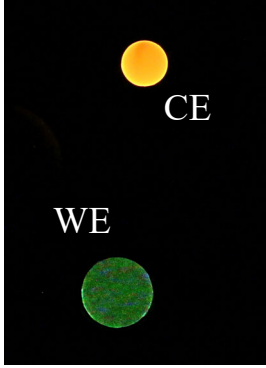
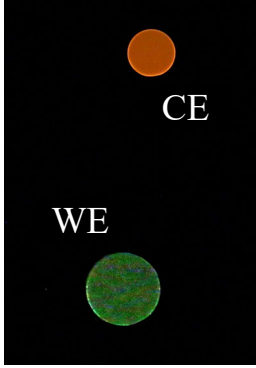
Electrode	Electrode Potential (<i>E</i>) / V vs Ag/AgCl				
GC working	1.50	1.60	1.70	1.80	1.90
Pt disk counter	-2.75	-2.65	-2.71	-2.70	-2.71
Photographs of ECL emission					

Table 4.14. Images of dual emission in a 0.1 mM Ir(ppy)₃, 5 μM [Ru(bpy)₃]²⁺ and 10 mM TPrA solution at potentials –2.80 V to –2.90 V Green emission observed at the working electrode and red/orange emission at the counter electrode. Images recorded with ISO 8000 and an aperture value F3.5.

Electrode	Electrode Potential (<i>E</i>) / V vs Ag/AgCl		
GC working	–2.80	–2.85	–2.90
Pt disk counter	0.65	1.00	2.60
Photographs of ECL emission			

Within single-complex systems, ECL was observed at only anodic potentials, but within this multi-complex system, the dual emission at both working and counter electrodes illustrates simultaneous anodic and cathodic ECL reactions occurring within one cell.

The mechanisms of ECL from metal complex luminophores with TPrA co-reactant at anodic potentials are well established, but the ECL observed at high cathodic potentials from the mixed system containing Ir(ppy)₃, [Ru(bpy)₃]²⁺ and TPrA has not previously been reported and is yet to be elucidated. This ECL, observed both at the working electrode when high cathodic potentials were directly applied (Table 4.14), and at the counter electrode upon application of high anodic potentials at the working electrode (Table 4.13), was green in colour, consistent with emission from the Ir(ppy)₃ luminophore.

When applying high cathodic potentials to the solution of Ir(ppy)₃ and TPrA in the absence of [Ru(bpy)₃]²⁺ (Table 4.5), ECL was not observed at the counter electrode, indicating the

involvement of the ruthenium complex in this unexpected emission from Ir(ppy)₃. At a similar potential to that required for the reduction of Ir(ppy)₃ (-2.32 V vs Ag/AgCl, Table 4.1), the [Ru(bpy)₃]²⁺ complex undergoes a fourth reduction (-2.45 V). Unlike the first three reductions of [Ru(bpy)₃]²⁺, that involve reversible electron transfers onto the three bipyridine ligands (Figure 4.3 (e)), the fourth reduction is irreversible (at the voltammetric scan rate of 0.1 V s⁻¹). It is possible that the instability of the [Ru(bpy)₃]²⁻ species plays a role in the observed ECL of Ir(ppy)₃ at high cathodic potentials. It should be noted, however, that the ECL was not observed until potentials more negative than those required to generate the reduced [Ir(ppy)₃]⁻ and [Ru(bpy)₃]²⁻ species. When cathodic potentials were applied at the working electrode, the green emission was not observed until -2.80 V vs Ag/AgCl, that also implicates high energy intermediates generated by reduction/degradation of the solvent in this light-emitting reaction process.

4.4 Conclusions

Initial experiments involved cyclic voltammetric sweeps at both anodic and cathodic potentials to gain information regarding three metal chelates (Ir(ppy)_3 , $[\text{Ir(df-ppy)}_2(\text{ptb})]^+$ and $[\text{Ru(bpy)}_3]^{2+}$) and TPrA for their redox electron-transfer processes. Utilising TPrA as the model co-reactant and a digital camera to visualise ECL location, the three single-complex systems displayed only oxidative-reduction ECL and emission was not observed within cathodic potentials. In the mixed-complex system of $[\text{Ir(df-ppy)}_2(\text{ptb})]^+$ and $[\text{Ru(bpy)}_3]^{2+}$, the TPrA co-reactant displayed oxidative-reduction ECL on the working electrode when positive potentials were applied and at the counter electrode when negative potentials were applied to the working. Similar to the single-complex systems, no emission was visualised at the cathodic potentials that limited the scope for dual emission.

Replacing $[\text{Ir(df-ppy)}_2(\text{ptb})]^+$ with Ir(ppy)_3 it was possible to extend the range of emission potentials as the Ir(ppy)_3 and $[\text{Ru(bpy)}_3]^{2+}$ have greater potential resolution, while remaining spectrally resolved. Applying high positive potentials resulted in an emission from $[\text{Ru(bpy)}_3]^{2+}$ at the working electrode with simultaneous ECL emission from Ir(ppy)_3 on the counter electrode, on the resulting negative potentials. The opposite occurred when high negative potentials were applied that indicates simultaneous anodic and cathodic ECL reactions within the one vessel. These anodic and cathodic ECL emissions were then supported by image RGB values, CCD spectrometry and PMT detections.

While the anodic pathways are well known within TPrA co-reactant ECL, the cathodic emission from the Ir(ppy)_3 is unexpected and could be a result of the instability of the $[\text{Ru(bpy)}_3]^{2-}$ species or high energy intermediates generated by reduction/degradation of the solvent.

The ability to observe multiple responses from one co-reactant provides greater selectivity that is particularly important for forensically relevant compounds. The greater selectivity provides the ability to distinguish between different analytes that could prove useful in forensic samples that contain more than one active ingredient, which is often the case. The luminophore selectivity that is available for synthetic cannabinoid compounds is explored within chapter 5.

CHAPTER FIVE:

DETERMINATION OF SYNTHETIC CANNABINOIDS IN REAL SAMPLES

Chapter overview

This chapter utilises electrochemiluminescence (ECL) for the detection of a number of synthetic cannabinoid compounds. Cyclic voltammetry experiments were performed on thirteen synthetic cannabinoids to determine oxidation and reduction potentials. Nine synthetic cannabinoid standards were reacted with one of two metal chelates, Ir(ppy)₃ and [Ru(bpy)₃]²⁺, and the ECL emission was recorded using a photomultiplier tube (PMT) as the photodetector. Further from the nine standards five were selected for chronoamperometry experiments utilising a DSLR digital camera to determine location of anodic and/or cathodic ECL response. Several herbal blends containing synthetic cannabinoids, that were purchased pre-ban, were tested in order for viability of this technique to be used on real world samples. Importantly, extraction of the synthetic cannabinoid from the herbal substrate was not necessary as the plant material posed no interferences to ECL emission signals. Dual emission, on both the counter and working electrodes, using both reagents simultaneously, seems plausible however this research focused on initial screening of real samples rather than a fundamental bi-detection system.

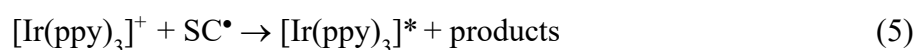
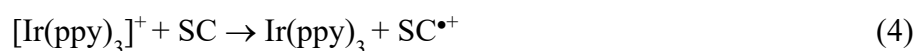
An important aspect of the synthetic cannabinoid samples is that the analyte is sprayed onto the surface of the herbal substrate and it is likely that the surface interface is a key part to consider for selective detection. As a side project to this PhD program work was done to help identify if the nature of the sample matrix that afforded direct detection of the synthetic cannabinoids with solid-state nuclear magnetic resonance (SSNMR) spectroscopy. This work is presented in this chapter because like the ECL no sample pre-treatment is required and as such may be a complementary non-destructive analytical process for analysis of precious forensic samples.

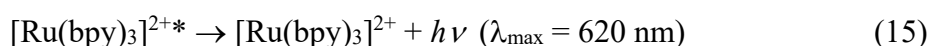
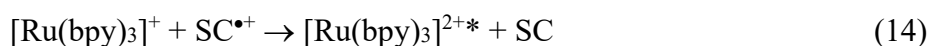
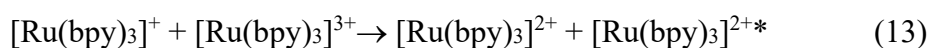
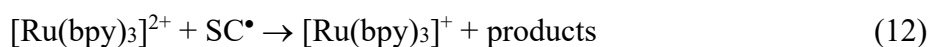
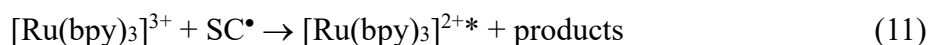
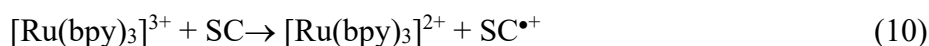
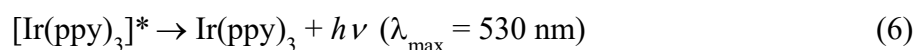
5.1 Introduction

There are hundreds of known compounds classified as a synthetic cannabinoid each containing an indole or indazole core structure [64]. Therefore each synthetic cannabinoid contains at least one tertiary amine as a key feature along with the variation at the tail, linker or head functional groups. This amine moiety can be explored with ECL detection methods given the nature of the nitrogen having the potential to oxidise and reduce. The individual structures of thirteen synthetic cannabinoids within this chapter, and their IUPAC names are tabulated in the results and discussion section.

Similar to in chapter 4, an anhydrous organic environment was utilised as some synthetic cannabinoids and the iridium(III) complex were insoluble in water, and to gain the maximum solvent window range possible (approximately -2.90 V to $+1.90$ V). Once again, a counter electrode with a lower effective surface area was employed in order for higher current densities and higher resistance at the electrode surface, and provided a wider range of potentials at the counter electrode.

Oxidation of single complex systems containing Ir(ppy)_3 or $[\text{Ru(bpy)}_3]^{2+}$ with one synthetic cannabinoid follows reaction equations 1-6 and 7-15 respectively. Similar to in chapter 4 however TPrA is replaced by a synthetic cannabinoid compound as the co-reactant (represented by SC).





The previous work on counter electrode emission can be exploited for applications such as a rapid screening tool for illicit substances detection. Dual emission systems have been reported in both annihilation [149] and co-reactant [148] ECL with $\text{Ir}(\text{ppy})_3$ and $[\text{Ru}(\text{bpy})_3]^{2+}$ using TPrA as the model compound. So far, research has been focused towards the fundamental processes however synthetic cannabinoids have potential to be the first instance of an application for the dual emission systems. Seizure samples are often mixtures of active ingredients [166, 209] therefore detection of two compounds simultaneously at two different electrodes can be a viable method of screening without the need for sample extractions or separations.

Alongside the ECL experiments a SSNMR identification method is explored as it has shown promising results for generating structural information of compounds without sample

destruction, and requires a smaller sample size compared to other analytical approaches (generally between 2 mg and 100 mg) [210]. The solid-state technique is not as widely used as solution-state in NMR experiments due to lower resolution however cross polarisation (CP) and magic angle spinning (MAS) can be applied to rectify this issue [211]. Cross polarisation (CP) involves transferring abundant nuclei (such as ^1H and ^{19}F) to polarise rare nuclei (^{13}C and ^{15}N) that improves the signal to noise ratio as well as reduces analysis time [212, 213]. Magic angle spinning (MAS) results in better resolution by spinning the rotor at a magic angle in respect to the magnetic field, improving resolution by narrowing the spectral lines [214].

Solution-state NMR has been utilised for the identification of forensically important compounds however it has been applied as a secondary screening after other analytical techniques such as direct analysis in real time mass spectrometry (DART-MS) [215], silica-gel column chromatography and thin layer chromatography (TLC) [88]. In 2009, Lindigkeit *et al.* developed a method for solution-state NMR analysis of synthetic cannabinoids however it required an extensive extraction process, followed by isolation, concentration and separation *via* TLC, then collection and dissolution in an appropriate solvent [88]. This process can take up to 4 hours for one sample that highlights the need for a rapid approach and is not suitable within a forensic context. Similarly, in 2016, Marino *et al.* developed a ^1H NMR method for a rapid detection of ten synthetic cannabinoid compounds however it served as a secondary screening after DART-MS identifications and was not a stand-alone method [215].

Although the solution-state NMR experiments are successful in identifying the synthetic cannabinoid compounds there is limited scope for a rapid technique and the sample is not reusable after extensive preparations. Solid-state NMR however can provide a non-destructive technique for structural identification and sample can be reused for further analysis if needed and as such may be complementary to the ECL approach described in this thesis.

5.2 Experimental

5.2.1 Chemicals

Reagents used were of analytical grade standard unless otherwise stated. Synthetic cannabinoid standards PB-22, 5F-AKB48, AM-1220, XLR-11, AM-2201, UR-144, JWH-302, MDMB-CHMICA, AB-CHMINACA were purchased from National Measurement Institute (Melbourne, Victoria, Australia). Synthetic cannabinoid standards BB-22, STS-135, THJ-018, THJ-2201 were purchased in the United Kingdom pre-ban and all work on these standards was completed at the University of Strathclyde in Glasgow, UK.

Twelve herbal substrates containing synthetic cannabinoids (brands: Atomic Bomb, Bombay Blue, Code Black, Cloud 9, Malibu, Puff, Red Dot, Special K, Stoner, Storm, Supernova, and Voodoo) were purchased at various local Victorian stores prior to legislation bans. The synthetic cannabinoid model substrate material damiana (*Turnera Diffusa*) was purchased at Happy Herb in Geelong, Victoria.

For all SSNMR experiments, samples (~100 mg) were ground to a fine powder and packed into a 4 mm o.d. MAS NMR rotor for experimental analysis.

Refer for chapter 4 experimental for further chemical information.

5.2.2 Instrumentation

5.2.2.1 Electrochemiluminescence (ECL)

Refer to chapter 3 and 4 experimental for electrochemical instrumentation and a schematic manifold.

5.2.2.2 Solid-state nuclear magnetic resonance (SSNMR) spectroscopy

All SSNMR was completed on a Bruker Avance III 300 MHz Wide Bore with a 4.0 mm MAS HX probe (Preston, Victoria, Australia) and were examined at a 10 kHz MAS spinning rate. ^{13}C CPMAS was carried out at 7.05 T on all samples with a minimum of 2000 scans and a 5 second recycle delay. Direct ^{13}C MAS was carried out on two samples (Damiana and Bombay Blue) at T_1 relaxation times of 2 seconds or 60 seconds. ^{19}F was only carried out on nine selected samples with a minimum scan time of 2 hours.

5.3 Results and discussion

5.3.1 Electrochemiluminescence (ECL) detection

Initial experiments involved cyclic voltammetric (CV) sweeps to understand specific redox processes and to observe oxidation and reduction potentials of the thirteen synthetic cannabinoid standards as well as the individual metal complexes. An example CV of one synthetic cannabinoid (5F-AKB48) is represented in Figure 5.1.

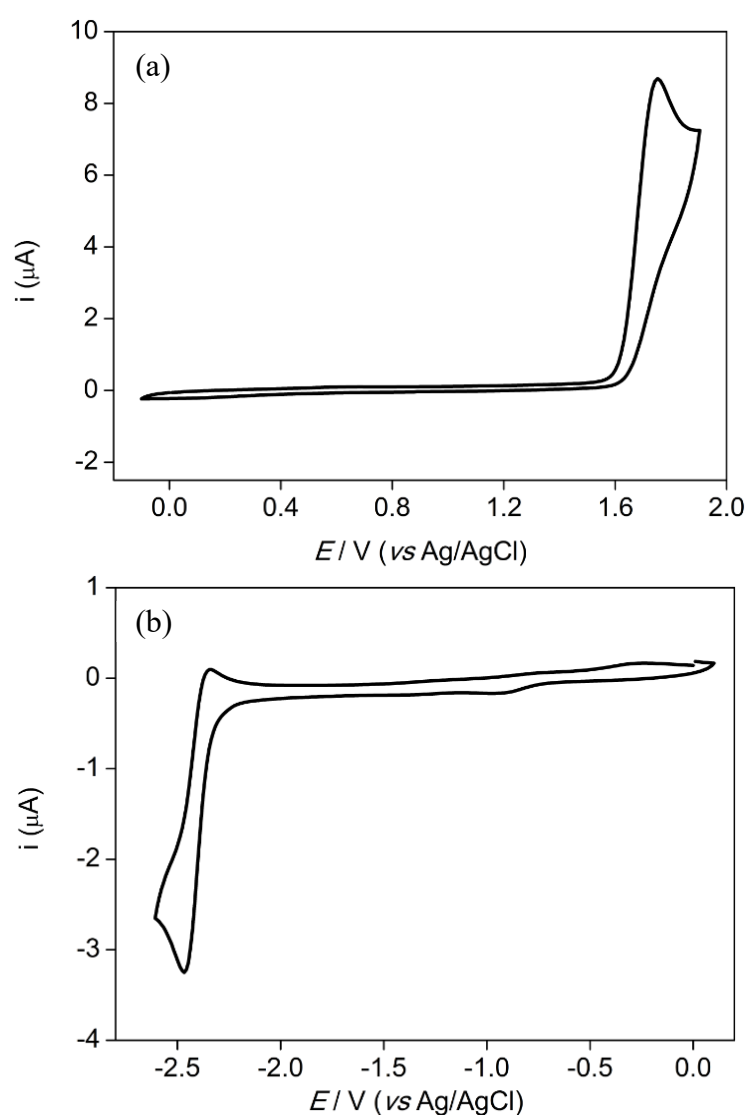


Figure 5.1. Cyclic voltammetry showing oxidation (a) and reduction (b) potentials of a synthetic cannabinoid standard: 5F-AKB48 (1 mM in freshly distilled acetonitrile with TBAPF₆ as the supporting electrolyte).

Referenced to Ag/AgCl, Ir(ppy)₃ has an oxidation potential of 0.67 V and a reduction peak at -2.33 V. [Ru(bpy)₃]²⁺ oxidises at 1.24 V and has numerous reductions at -1.38 V, -1.58 V, -1.83 V and -2.45 V. See chapter 4 results and discussion for specific oxidation and reduction products. A typical synthetic cannabinoid CV contained an irreversible oxidation peak at potentials greater than 1.30 V and reduction peaks varied with the majority illustrating an irreversible product. There are a select few synthetic cannabinoid compounds that displayed slightly reversible reduction products and are summarised below.

All thirteen synthetic cannabinoid standards were prepared at 1 mM concentrations in freshly distilled acetonitrile and have displayed oxidation potentials within this electroactive window, while ten exhibited at least one reduction peak (Table 5.1). In summary 5F-AKB48 exhibited one irreversible oxidation peak and one slightly reversible reduction product (Figure 5.1). AB CHMINACA displayed one irreversible oxidation product and two irreversible reduced species. AM-1220 had one irreversible oxidation product, one slightly reversible reduction product (-1.99 V) and one irreversible reduction species. AM-2201 displayed one irreversible oxidation product, one slightly reversible reduction product (-2.03 V) and two irreversible reduction species. BB-22 exhibited one irreversible oxidation peak and one irreversible reduction product. JWH-302 illustrated one irreversible oxidation product and no reduction peaks were observed. MDMB-CHMICA followed the same trend as JWH-302 with one irreversible oxidation product and no reduction species. PB-22 had two irreversible oxidation products and one irreversible reduced species. THJ-018 exhibited one irreversible oxidation product, one slightly reversible reduction (-1.74 V) and three irreversible reduction products. THJ-2201 displayed the same trend as THJ-018 with one irreversible oxidation product, one slightly reversible reduction (-1.73 V) and three irreversible reduction products. UR-144 exhibited the same trend as JWH-302 and MDMB-CHMICA with one irreversible oxidation product and no reduction species. XLR-11 had one irreversible oxidation product and one

irreversible reduction species. All oxidation and reduction potentials were referenced to Ag/AgCl and are displayed in Table 5.1.

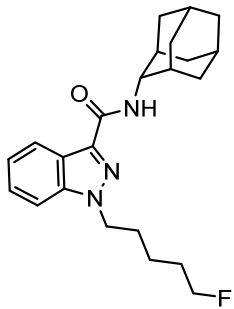
Table 5.1. Summary of oxidation and reduction potentials for the three metal complexes and synthetic cannabinoid standards. All potentials referenced to Ag/AgCl. Experiments conducted in freshly distilled acetonitrile with 0.1 M TBAPF₆ and 1 mM of the synthetic cannabinoid or [Ru(bpy)₃]²⁺. For Ir(ppy)₃ experiments, a concentration of 0.2 mM was employed.

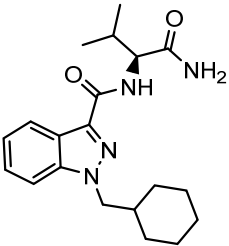
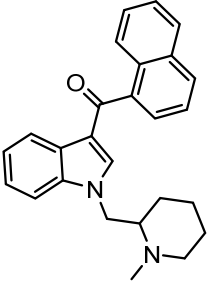
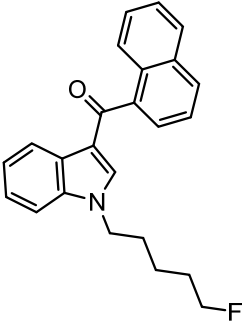
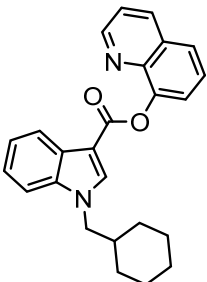
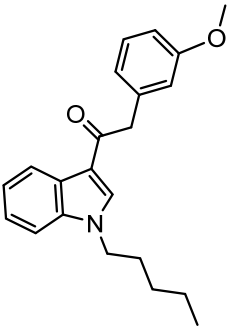
	$E_{\text{ox}}/\text{V vs Ag/AgCl}$	$E_{\text{red}}/\text{V vs Ag/AgCl}$
Ir(ppy) ₃	0.67	-2.33
[Ru(bpy) ₃] ²⁺	1.24	-1.38, -1.58, -1.83, -2.45
5F-AKB48	1.75	-2.41
AB-CHMINACA	1.85	-2.41, -2.54
AM-1220	1.66	-1.99, -2.35
AM-2201	1.54	-2.03, -2.26, -2.57
BB-22	1.66	-2.04
JWH-302	1.51	
MDMB-CHMICA	1.32	
PB-22	1.43, 1.59	-2.13
STS-135	1.36	-2.78
THJ-018	1.81	-1.74, -2.06, -2.48, -2.64
THJ-2201	1.82	-1.73, -2.08, -2.60, -2.71
UR-144	1.42	
XLR-11	1.39	-2.62

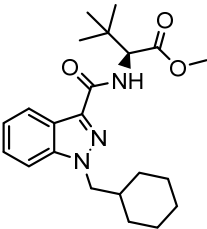
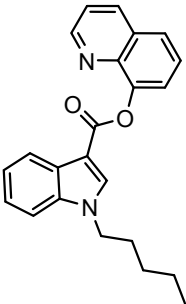
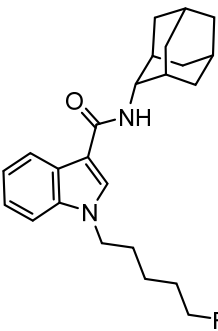
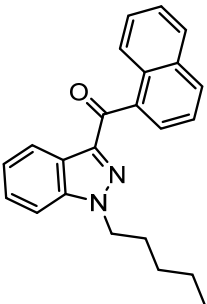
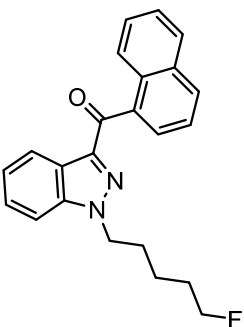
THJ-018 and THJ-2201 have comparable oxidation and reduction potentials and this can be attributed to their structural similarities. The difference between these two compounds is the presence of a fluorinated pentyl chain tail on THJ-2201 (Table 5.2). 5F-AKB48 and STS-135

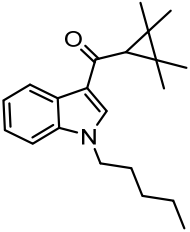
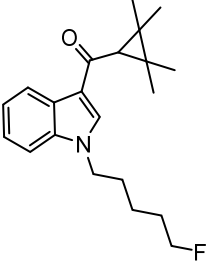
are also structurally similar with an indazole and indole core, respectively. The indazole structure (5F-AKB48) requires more energy to oxidise however it is more easily reduced compared to the indole. AM-2201 and THJ-2201 have the same structural similarity with an indole and indazole core, respectively. The same pattern is observed with the indazole (THJ-2201) requiring more energy to oxidise but can be reduced with lower potentials compared to the indole. AB-CHMINACA and MDMB-CHMICA are structurally similar with differences observed in the head of the structure. AB-CHMINACA has a carboxamide and MDMB-CHMICA has a methyl ester. The methyl ester is easier oxidised but cannot be reduced, while the carboxamide containing a nitrogen has potential for reduction. UR-144 and XLR-11 differ by the fluorinated pentyl chain tail present on XLR-11. This fluorination gives the compound potential to be reduced while UR-44 has no reduction potentials. All chemical structures and IUPAC names for the thirteen synthetic cannabinoid standards are shown in Table 5.2.

Table 5.2. Chemical structures and IUPAC names for the thirteen synthetic cannabinoid: 5F-AKB48, AB-CHMINACA, AM-1220, AM-2201, BB-22, JWH-302, MDMB-CHMICA, PB-22, STS-135, THJ-018, THJ-2201, UR-144 and XLR-11.

Structure	Common name(s)	IUPAC name
	5F-AKB48	<i>N</i> -(adamantan-1-yl)-1-(5-fluoropentyl)-1 <i>H</i> -indazole-3-carboxamide

	<p>AB-CHMINACA <i>N</i>-[(1<i>S</i>)-1-(aminocarbonyl)-2-methylpropyl]-1-(cyclohexylmethyl)-1<i>H</i>-indazole-3-carboxamide</p>
	<p>AM-1220 [1-[(1-methyl-2-piperidinyl)methyl]-1<i>H</i>-indol-3-yl]-1-naphthalenyl-methanone</p>
	<p>AM-2201 1-[(5-fluoropentyl)-1<i>H</i>-indol-3-yl]-(naphthalen-1-yl)methanone</p>
	<p>BB-22 1-(cyclohexylmethyl)-8-quinolinyl ester-1<i>H</i>-indole-3-carboxylic acid</p>
	<p>JWH-302 2-(3-methoxyphenyl)-1-(1-pentyl-1<i>H</i>-indol-3-yl)-ethanone</p>

	<p>MDMB-CHMICA</p>	<p><i>N</i>-[[1-(cyclohexylmethyl)-1<i>H</i>-indol-3-yl]carbonyl]-3-methyl-<i>L</i>-valine, methyl ester</p>
	<p>PB-22</p>	<p>1-pentyl-1<i>H</i>-indole-3-carboxylic acid 8-quinolinyl ester</p>
	<p>STS-135</p>	<p>1-(5-fluoropentyl)-<i>N</i>-tricyclo[3.3.1.1.3,7]dec-1-yl-1<i>H</i>-indole-3-carboxamide</p>
	<p>THJ-018</p>	<p>1-naphthalenyl(1-pentyl-1<i>H</i>-indazol-3-yl)-methanone</p>
	<p>THJ-2201</p>	<p>[1-(5-fluoropentyl)-1<i>H</i>-indazol-3-yl]-1-naphthalenyl-methanone</p>

	UR-144	(1-pentylindol-3-yl)-(2,2,3,3-tetramethylcyclopropyl)methanone
	XLR-11	(1-(5-fluoropentyl)-1 <i>H</i> -indol-3-yl)(2,2,3,3-tetramethylcyclopropyl)methanone

Nine synthetic cannabinoid standards were subjected to cyclic voltammetric scans with either Ir(ppy)₃ or [Ru(bpy)₃]²⁺ and the ECL response was observed with a PMT as the photodetector. These nine were identified as prominent compounds detected by forensic services within recent seizure samples. Seven of the nine compounds elicited an ECL response with either one or both metal complexes. Forward and reverse sweeps were performed to determine the range of potentials that gave a response for each particular analyte. 5F-AKB48, AM-1220 and PB-22 exhibited an ECL response for the two metal complexes when both anodic and cathodic potentials were applied. BB-22, STS-135 and XLR-11 only gave an ECL response with the iridium centered complex while UR-144 responded to both anodic and cathodic sweeps of the Ir(ppy)₃ and only the cathodic potentials with [Ru(bpy)₃]²⁺. The ECL emission potentials for each synthetic cannabinoid with the metal complexes is summarised in Table 5.3. An example of the ECL emission is displayed in Figure 5.2 and Figure 5.3.

Table 5.3. Summaries of the potential range over which ECL was observed for each synthetic cannabinoid (5 mM) with either 0.1 mM Ir(ppy)₃ or 5 mM [Ru(bpy)₃]²⁺ luminophores, in both forward and reverse CV sweeps. Asterisk donates no ECL emission observed with PMT detection.

Synthetic cannabinoid	Ir(ppy) ₃		[Ru(bpy) ₃] ²⁺	
	Forward (V)	Reverse (V)	Forward (V)	Reverse (V)
5F-AKB48	1.55 to 1.90	-2.16 to -2.90	1.61 to 1.76	-2.37 to -2.70
AM-1220	0.59 to 1.12	-1.70 to -2.33	1.12 to 1.90	-1.41 to -2.10
BB-22	1.61 to 1.90	-1.00 to -2.45	*	*
PB-22	0.59 to 1.90	-2.01 to -2.54	1.01 to 1.90	-1.56 to -1.95
STS-135	0.64 to 1.22	-2.18 to -2.50	*	*
THJ-018	*	*	*	*
THJ-2201	*	*	*	*
UR-144	1.34 to 1.52	-2.22 to -2.46	*	-1.37 to -1.97
XLR-11	*	-2.17 to -2.54	*	*

Utilising a PMT as the photodetector is excellent for initial screenings to establish ECL emission potentials however it does not illustrate the location of where emission is taking place. Counter electrode emission has been observed numerous times within this research and prior literature. Therefore, is it necessary to utilise a digital camera to illustrate where the emission is occurring, at either the working or counter electrode that corresponds to specific mechanistic processes. The aid of a digital camera also contributes to the portability of the system when applying it in the field, as it does not require a high voltage power supply or amplifier that is necessary for a PMT photodetector.

The two synthetic cannabinoids (THJ-18 and THJ-2201) that did not elicit an ECL response with either metal complex require very high energies in order for oxidation or reduction processes to occur therefore a negative result for these two was expected.

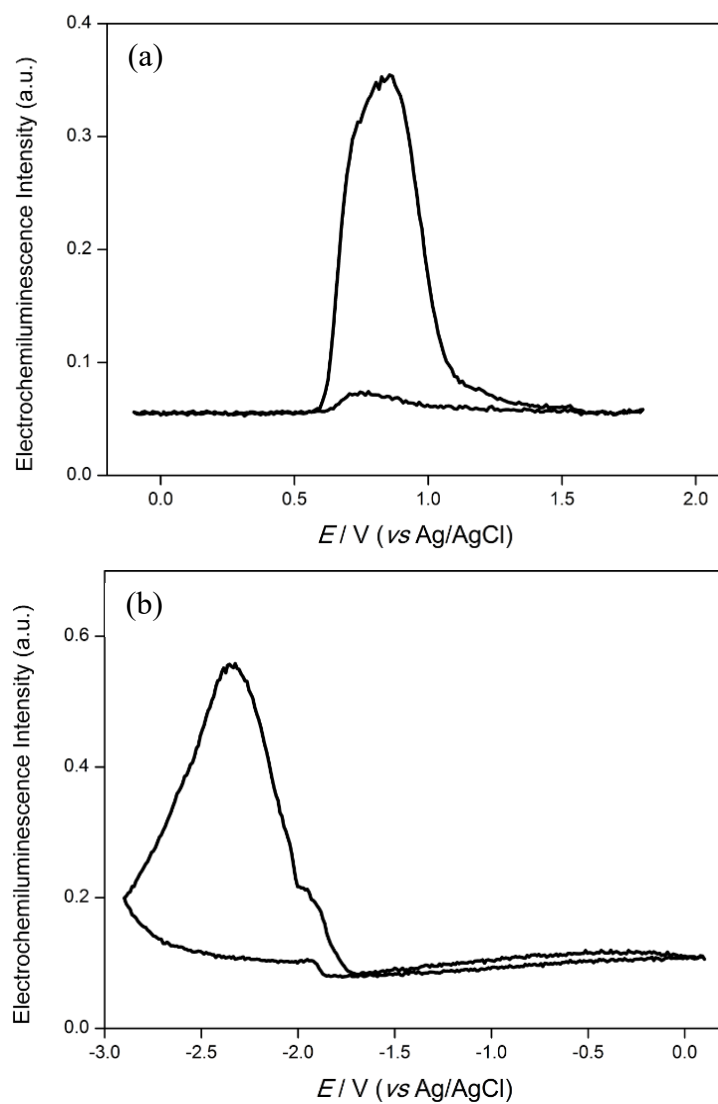


Figure 5.2. Typical ECL response for 0.1 mM Ir(ppy)₃ with 5 mM AM-1220 in freshly distilled acetonitrile. When scanning from 0 V to 1.80 V vs Ag/AgCl and then back to 0 V (a), and scanning from 0 V to -2.90 V vs Ag/AgCl and then back to 0 V (b). Both scans at a rate of 100 mV s⁻¹ with a GC working electrode and Pt disk counter electrode.

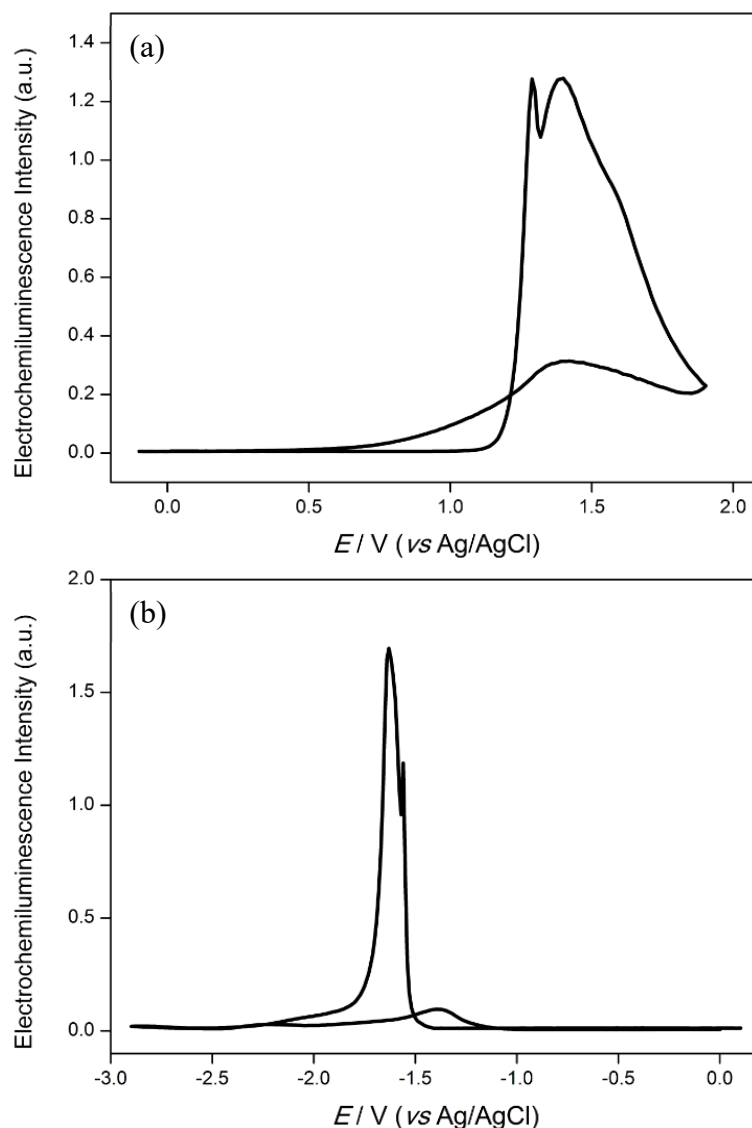


Figure 5.3. Typical ECL response for 5 mM $[\text{Ru}(\text{bpy})_3]^{12+}$ with 5 mM AM-1220 in freshly distilled acetonitrile. When scanning from 0 V to 1.90 V vs Ag/AgCl and then back to 0 V (a), and scanning from 0 V to -2.90 V vs Ag/AgCl and then back to 0 V (b). Both scans at a rate of 100 mV s^{-1} with a GC working electrode and Pt disk counter electrode.

The five synthetic cannabinoids that were prominent within Australian samples were observed under a Canon EOS 6D DSLR digital camera and ECL emissions were photographed, determining whether the emission was occurring at the working and/or counter electrode. Four of the five synthetic cannabinoids gave responses with both metal complexes when anodic and cathodic potentials were applied. Reacting 5F-AKB48 with $\text{Ir}(\text{ppy})_3$, emission was observed at

the cathodic potentials on the counter electrode when positive potentials were applied and on the working electrode when negative potentials were applied. 5F-AKB48 with $[\text{Ru}(\text{bpy})_3]^{2+}$ exhibited the opposite response with oxidative-reduction ECL emission at the working electrode when positive potentials applied and at the counter electrode when negative potentials applied to the working.

AM-1220 illustrated oxidative-reduction ECL emission with both $\text{Ir}(\text{ppy})_3$ and $[\text{Ru}(\text{bpy})_3]^{2+}$. Emission was observed at the working electrode when positive potentials were applied and at the counter electrode when negative potentials were applied. PB-22 exhibited a similar trend to AM-1220 with oxidative-reduction ECL emission at the working electrode when positive potentials were applied and at the counter electrode when negative potentials were applied. 5F-AKB48, AM-1220 and PB-22 exhibited similar responses with the digital camera and PMT detections. Slight differences in ECL emission potentials could be due to the changing counter electrode potentials and being unable to monitor them with cyclic voltammetric experiments for the PMT detections.

UR-144 had oxidative-reduction ECL as well as emission at the cathodic potentials with $\text{Ir}(\text{ppy})_3$ and only emission at the cathodic potentials with $[\text{Ru}(\text{bpy})_3]^{2+}$. When positive potentials were applied to UR-144 with $[\text{Ru}(\text{bpy})_3]^{2+}$, emission was photographed at the counter electrode that does not correspond with PMT results.

XLR-11 did not elicit an ECL response with $[\text{Ru}(\text{bpy})_3]^{2+}$ but an emission with $\text{Ir}(\text{ppy})_3$ was observed. This corresponds well with previous ECL responses by PMT detection. In the PMT experiments, emission was observed at only the cathodic potentials for XLR-11, unlike here where emission was observed at both anodic and cathodic potentials. This specific PMT is sensitive to wavelengths in the red coloured region, while the distinct green emission observed for $\text{Ir}(\text{ppy})_3$ may not be detectable by this PMT with small emission signals. XLR-11 emission

was observed at the counter electrode when positive potentials were applied and at the working electrode when negative potentials were applied. This suggests that XLR-11 only exhibits an ECL response within cathodic potentials. All the emission potentials for these five synthetic cannabinoids with both metal complexes is summarised in Table 5.4.

Table 5.4. Summary of camera ECL emissions observed with five synthetic cannabinoids and two metal complexes. Numbers without brackets indicate potential that was applied and numbers within brackets indicate where emission was observed. Applied potentials were chosen based off previous CV results. All experiments were in freshly distilled acetonitrile, synthetic cannabinoid and $[\text{Ru}(\text{bpy})_3]^{2+}$ concentrations were always 5 mM and $\text{Ir}(\text{ppy})_3$ was 0.1 mM. Asterisks are where no ECL emission was observed.

Synthetic cannabinoid	$\text{Ir}(\text{ppy})_3$		$[\text{Ru}(\text{bpy})_3]^{2+}$	
	Forward (V)	Reverse (V)	Forward (V)	Reverse (V)
5F-AKB48	1.50 to 1.90 (-1.69 to -2.28)	-2.10 to -2.90 (-2.10 to -2.90)	1.50 to 1.70 (1.50 to 1.70)	-2.00 to -2.50 (2.78 to 2.94)
AM-1220	0.60 to 1.00 (0.60 to 1.00)	-1.20 to -1.90 (0.61 to 0.80)	1.10 to 1.90 (1.10 to 1.90)	-1.40 to -2.60 (1.19 to 2.40)
PB-22	0.90 to 1.90 (0.90 to 1.90)	-0.80 to -2.00 (0.82 to 1.58)	1.10 to 1.90 (1.10 to 1.90)	-1.40 to -2.00 (1.27 to 2.50)
UR-144	0.70 to 0.90 (0.70 to 0.90)	-2.00 to -2.60 (0.85-0.95) and (-2.20 to -2.60)	1.20 to 1.40 (-1.52 to -1.86)	-1.50 to -1.90 (-1.50 to -1.90)
XLR-11	1.40 to 1.90 (-1.94 to -2.25)	-2.20 to -2.70 (-2.20 to -2.70)	*	*

Images of the digital camera ECL emissions for AM-1220 is shown in Table 5.5 to Table 5.8, as examples of the characteristic photographs. AM-1220 having only oxidative-reduction ECL emissions from both $\text{Ir}(\text{ppy})_3$ and $[\text{Ru}(\text{bpy})_3]^{2+}$.

Table 5.5. Potentials applied at the GC working electrode and measured at the Pt disk counter electrode, and photographs of the ECL at the working electrode with 0.1 mM Ir(ppy)₃ and 5 mM AM-1220. Images recorded with ISO 8000 and an aperture value F2.8.

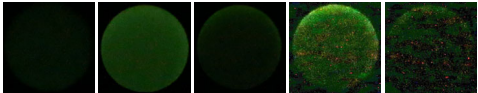
Electrode	Electrode Potential (<i>E</i>) / V vs Ag/AgCl						
GC working	0.50	0.60	0.70	0.80	0.90	1.00	1.10
Pt disk counter	-0.56	-0.61	-1.31	-1.94	-2.17	-2.45	-2.63
Photographs of GC emission							

Table 5.6. Potentials applied at the GC working electrode and measured at the Pt disk counter electrode, and photographs of the ECL at the counter electrode with 0.1 mM Ir(ppy)₃ and 5 mM AM-1220. Images recorded with ISO 8000 and an aperture value F2.8.

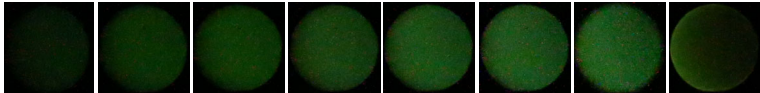
Electrode	Electrode Potential (<i>E</i>) / V vs Ag/AgCl									
GC working	-1.10	-1.20	-1.30	-1.40	-1.50	-1.60	-1.70	-1.80	-1.90	-2.00
Pt disk counter	0.57	0.61	0.62	0.62	0.63	0.64	0.67	0.66	0.80	1.81
Photographs of Pt disk emission										

Table 5.7. Potentials applied at the GC working electrode and measured at the Pt disk counter electrode, and photographs of the ECL at the working electrode with 5 mM [Ru(bpy)₃]²⁺ and 5 mM AM-1220. Images recorded with ISO 8000 and an aperture value F2.8.

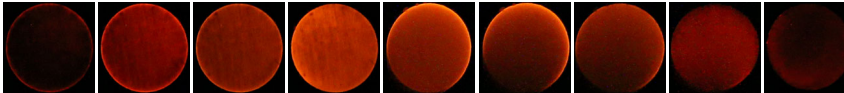
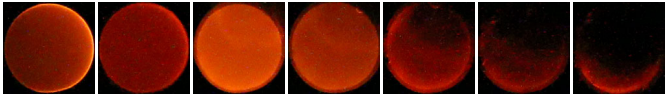
Electrode	Electrode Potential (<i>E</i>) / V vs Ag/AgCl									
GC working	1.00	1.10	1.20	1.30	1.40	1.50	1.60	1.70	1.80	1.90
Pt disk counter	-1.43	-1.61	-1.73	-1.81	-1.88	-1.59	-1.59	-1.52	-1.45	-1.56
Photographs of GC emission										

Table 5.8. Potentials applied at the GC working electrode and measured at the Pt disk counter electrode, and photographs of the ECL at the counter electrode with 5 mM [Ru(bpy)₃]²⁺ and 5 mM AM-1220. Images recorded with ISO 8000 and an aperture value F2.8.

Electrode	Electrode Potential (<i>E</i>) / V vs Ag/AgCl								
GC working	-1.30	-1.40	-1.60	-1.80	-2.00	-2.20	-2.40	-2.60	-2.70
Pt disk counter	0.89	1.19	1.70	2.10	2.02	2.08	2.22	2.40	2.73
Photographs of Pt disk emission									

Once the location of working and counter electrode ECL emissions and the potentials that resulted in an ECL response for each synthetic cannabinoid standard was established, real samples were exploited to similar testing. Twelve herbal substrates that contain synthetic cannabinoids and were obtained pre-ban from local stores in Victoria were examined utilising cyclic voltammetric experiments at both anodic and cathodic potentials with a PMT detector. Prior research at Deakin University has identified the synthetic cannabinoid present in each brand [62] and is shown in Table 5.9. One brand (Code Black) contained a synthetic cannabinoid that was not available to purchase (A-796,260) so the effect it presents on ECL emission remains unknown. One brand (Voodoo) also contains a synthetic cannabinoid that is unknown.

In order to develop a rapid screening for these forensically important substances, rubbing the herbal substrate directly onto the surface of the electrodes was explored with no extraction techniques necessary. All twelve of the herbal substrates containing synthetic cannabinoids gave an ECL response with one or both of the metal complexes. The plant material without synthetic cannabinoid was purchased and used as a blank to determine if the herbal substrate alone contains any substances that may exhibit an ECL response and result in a false positive. The ECL responses for the blank herb (Damiana) as well as the twelve brands is summarised in Table 5.10.

Table 5.9. Twelve brand names of commercially purchased samples with the common and IUPAC names of each synthetic cannabinoid present.

Brand	Common name(s)	IUPAC name
Atomic Bomb	PB-22, 5F-PB-22	1-pentyl-1 <i>H</i> -indole-3-carboxylic acid 8-quinolinyl ester, 1-pentyfluoro-1 <i>H</i> -indole-3-carboxylic acid 8-quinolinyl
Bombay Blue	XLR-11	(1-(5-fluoropentyl)-1 <i>H</i> -indol-3-yl)(2,2,3,3-tetramethylcyclopropyl)methanone
Code Black	UR-144, A-796,260	(1-pentylindol-3-yl)-(2,2,3,3-tetramethylcyclopropyl)methanone, [1-(2-morpholin-4-ylethyl)-1 <i>H</i> -indol-3-yl]-(2,2,3,3-tetramethylcyclopropyl)methanone
Cloud 9	UR-144, XLR-11	(1-pentylindol-3-yl)-(2,2,3,3-tetramethylcyclopropyl)methanone, (1-(5-fluoropentyl)-1 <i>H</i> -indol-3-yl)(2,2,3,3-tetramethylcyclopropyl)methanone
Malibu	5F-AKB48	<i>N</i> -(adamantan-1-yl)-1-(5-fluoropentyl)-1 <i>H</i> -indazole-3-carboxamide
Puff	UR-144	(1-pentylindol-3-yl)-(2,2,3,3-tetramethylcyclopropyl)methanone
Red Dot	AM-2201	1-[(5-fluoropentyl)-1 <i>H</i> -indol-3-yl]-(naphthalen-1-yl)methanone
Special K	UR-144, XLR-11	(1-pentylindol-3-yl)-(2,2,3,3-tetramethylcyclopropyl)methanone, (1-(5-fluoropentyl)-1 <i>H</i> -indol-3-yl)(2,2,3,3-tetramethylcyclopropyl)methanone
Stoner	PB-22, 5F-PB-22	1-pentyl-1 <i>H</i> -indole-3-carboxylic acid 8-quinolinyl ester, 1-pentyfluoro-1 <i>H</i> -indole-3-carboxylic acid 8-quinolinyl
Storm	PB-22, 5F-PB-22	1-pentyl-1 <i>H</i> -indole-3-carboxylic acid 8-quinolinyl ester, 1-pentyfluoro-1 <i>H</i> -indole-3-carboxylic acid 8-quinolinyl
Supernova	PB-22	1-pentyl-1 <i>H</i> -indole-3-carboxylic acid 8-quinolinyl ester
Voodoo	Unknown	

Table 5.10. Summaries of the potential range for each synthetic cannabinoid with either 0.2 mM Ir(ppy)₃ or 1 mM [Ru(bpy)₃]²⁺ metal complex in freshly distilled acetonitrile with TBAPF₆, in both forward and reverse CV sweeps. Asterisk donates no ECL emission observed with PMT detection.

Brand	Ir(ppy) ₃		[Ru(bpy) ₃] ²⁺	
	Forward (V)	Reverse (V)	Forward (V)	Reverse (V)
Damiana	*	*	*	*
Atomic Bomb	1.58 to 1.90	-2.14 to -2.90	1.17 to 1.90	-1.33 to -1.77 and -2.28 to -2.63
Bombay Blue	*	-2.11 to -2.90	1.15 to 1.49	-1.26 to -1.72 and -2.30 to -2.56
Code Black	*	-2.14 to -2.69	1.17 to 1.50	-1.27 to -1.62 and -2.31 to -2.57
Cloud 9	*	-2.13 to -2.90	1.19 to 1.44	-1.28 to -1.66 and -2.28 to -2.56
Malibu	*	-2.16 to -2.90	1.16 to 1.48	-1.33 to -2.57
Puff	1.50 to 1.90	-2.15 to -2.90	1.21 to 1.90	-1.24 to -1.61 and -2.32 to -2.50
Red Dot	*	-1.93 to -2.90	1.20 to 1.90	-2.25 to -2.66
Special K	*	-2.11 to -2.90	*	*
Stoner	*	-2.15 to -2.90	1.18 to 1.90	*
Storm	*	-2.17 to -2.90	1.13 to 1.90	-1.32 to -1.72 and -2.32 to -2.60
Supernova	*	-2.10 to -2.90	1.16 to 1.90	-1.11 to -1.68 and -2.29 to -2.57
Voodoo	*	-1.83 to -2.90	1.17 to 1.90	-1.33 to -1.69

Damiana was purchased as the blank herbal substrate in order to determine whether the plant material would respond with either metal complex to elicit light. In these cyclic voltammetric experiments utilising PMT detection, no ECL emission was observed for the Damiana

substrate. This is a promising result as it limits the likelihood of false positives from this substrate and ensures that no sample pre-treatment is required prior to analysis.

All twelve synthetic cannabinoid samples exhibited similar ECL responses with the Ir(ppy)₃ complex, with only two responding to anodic potentials, and all eliciting an ECL response at cathodic potentials. Eleven out of the twelve cannabinoid samples also exhibited a response with [Ru(bpy)₃]²⁺, while the brand Special K displayed no ECL emission at either anodic or cathodic potentials. Special K is known to contain both UR-144 and XLR-11 synthetic cannabinoid compounds and although the UR-144 standard observed an ECL response with [Ru(bpy)₃]²⁺, the XLR-11 standard did not respond to either anodic or cathodic potentials in this single-complex system. This result suggests that the majority of the herbal substrate brand Special K contains XLR-11, with only trace amounts of UR-144 present that are undetectable *via* PMT.

With the approach taken here by directly rubbing the plant material onto the surface of the electrodes, it is not possible to determine the concentration of the synthetic cannabinoid, therefore this method is strictly qualitative. The response to anodic and cathodic ECL emissions suggest that this approach may be developed into a potential rapid screening method for specific synthetic cannabinoids. Regeneration and cleaning of electrodes is not time consuming compared to other analytical techniques, therefore it does not interfere with the possibility of a potential rapid screening method.

As this method requires no sample extraction, it eliminates the sample preparation steps currently required in forensic analysis of these substances and will improve sample output times that is important when handling forensically important compounds where timely processing is critical for court proceedings.

Example ECL emission trace for one brand is shown in Figure 5.4 and Figure 5.5.

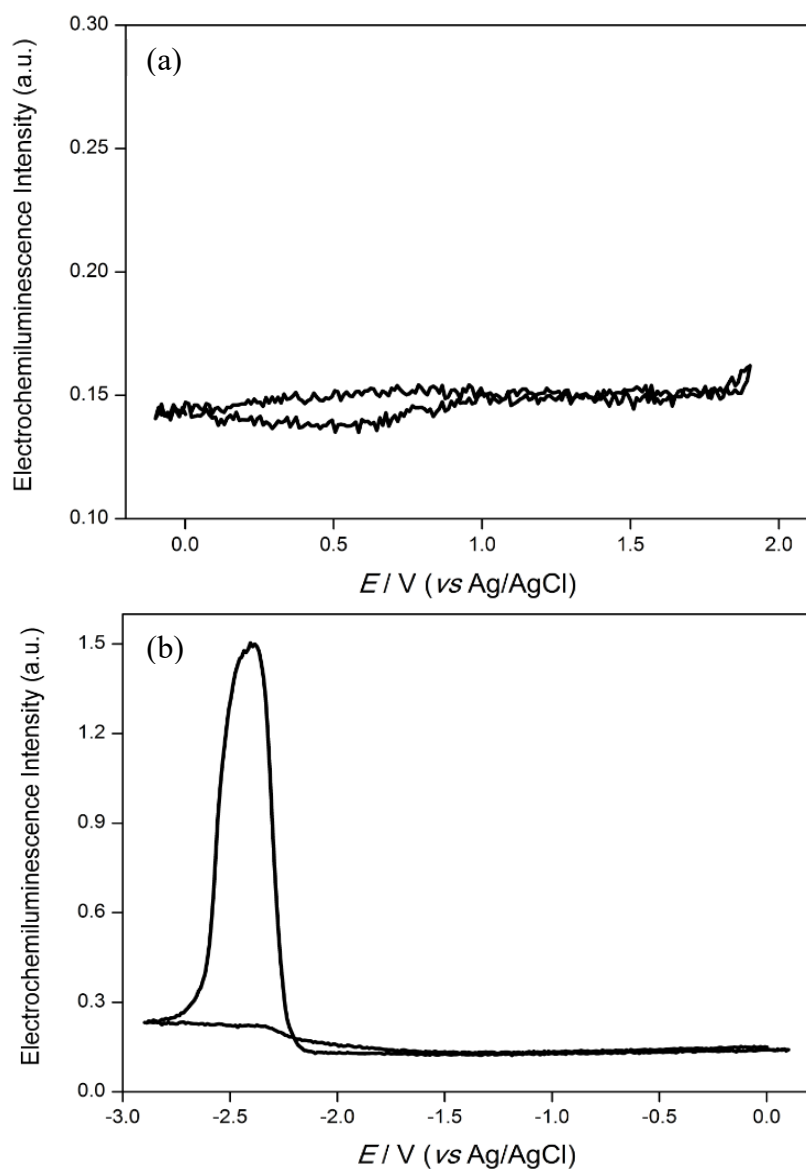


Figure 5.4. Typical ECL response for 0.2 mM Ir(ppy)₃ with Code Black in freshly distilled acetonitrile. When scanning from 0 V to 1.90 V vs Ag/AgCl and then back to 0 V (a), and scanning from 0 V to -2.90 V vs Ag/AgCl and then back to 0 V (b). Both scans at a rate of 100 mV s⁻¹ with a GC working electrode and Pt disk counter electrode.

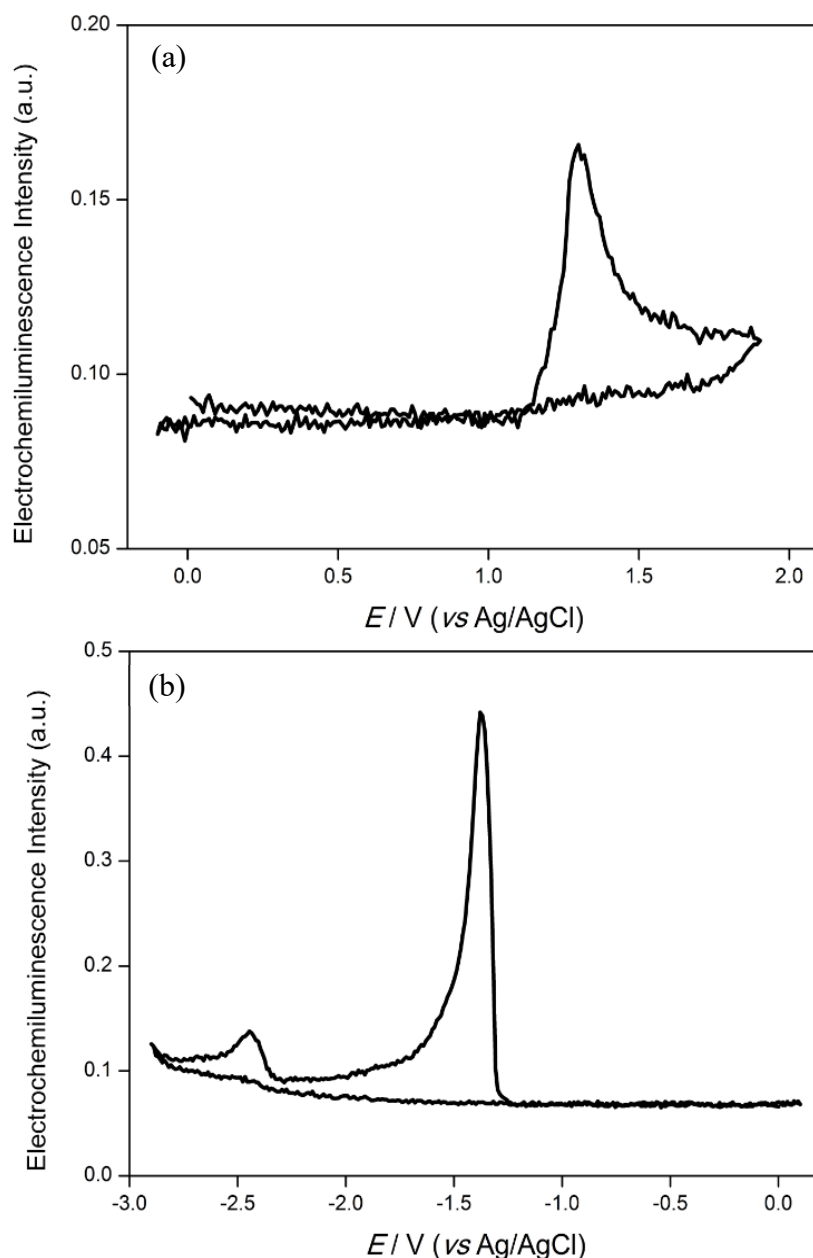


Figure 5.5. Typical ECL response for 1 mM $[\text{Ru}(\text{bpy})_3]^{2+}$ with Code Black in freshly distilled acetonitrile. When scanning from 0 V to 1.90 V vs Ag/AgCl and then back to 0 V (a), and scanning from 0 V to -2.90 V vs Ag/AgCl and then back to 0 V (b). Both scans at a rate of 100 mV s^{-1} with a GC working electrode and Pt disk counter electrode.

The fundamental cyclic voltammetry and chronoamperometry experiments completed using synthetic cannabinoid standards are crucial in order to understand anodic and cathodic reaction mechanisms for these particular compounds. As each structure contains at least one amine

moiety it was likely for redox processes to occur at this functional group when subjected to an applied potential. Traditional ECL detection methods including a PMT and CCD spectrometer weren't sufficient to locate where emission is occurring and to identify the anodic or cathodic ECL emission potentials. As a result of this, images of the ECL emission were taken using a DSLR camera. It is important to note that this is a preliminary investigation and the standards used in these experiments were limited to what was available to purchase within Australia and the UK at the time of the research. This approach looks to be very promising for forensic screening and it would be worth pursuing this technology with the full range (hundreds) of known synthetic cannabinoid compounds.

The results from these standard experiments indicate that the majority of the synthetic cannabinoid compounds should elicit either an anodic or cathodic ECL response that is detectable *via* a portable DSLR camera. The potential portability of this system is crucial for an at-scene screening tool for use by forensic personnel.

It is also important to note that these results illustrate a rapid screening tool for herbal substrate samples containing synthetic cannabinoids that corresponds to the substances seized by law enforcement agencies. These samples require no extraction of the active ingredient as the substrate does not interfere with ECL emission responses. In a forensic context, this is particularly important as identification of illicit substances need to be accurate and completed in an appropriate time frame. To date, there is no rapid screening tool for these NPS and this technique shows promising results to be used for the development of an at-scene screening method.

5.3.2 Solid-state nuclear magnetic resonance (SSNMR) spectroscopy detection

Removing the need for an extraction step for an analyte of forensic interest affords the opportunity to develop robust at scene detection systems. The lack of extraction required for the ECL correlates well with a project on SSNMR completed in collaboration with Dr Niki Burns [62].

Solid-state nuclear magnetic resonance (SSNMR) spectroscopy has been explored to identify specific synthetic cannabinoid compounds present on the surface of the herbal substrate. Solid-state nuclear magnetic resonance spectroscopy is a non-destructive method and has been tested for the ability to identify synthetic cannabinoids *via* ^{13}C and ^{19}F magic angle spinning (MAS) and ^1H - ^{13}C cross-polarisation (CP) magic angle spinning (MAS) experiments. Initial experiments were carried out comparing Damiana as the blank substrate and Bombay Blue (XLR-11) as the synthetic cannabinoid. Sample preparation involved grinding the herbal substances (~100 mg) into a fine powder and packing into a 4 mm o.d. MAS NMR rotor for experimental analysis, with no extraction technique required. Figure 5.6 illustrates normalised ^{13}C CPMAS spectra of Damiana and the synthetic cannabinoid brand Bombay Blue.

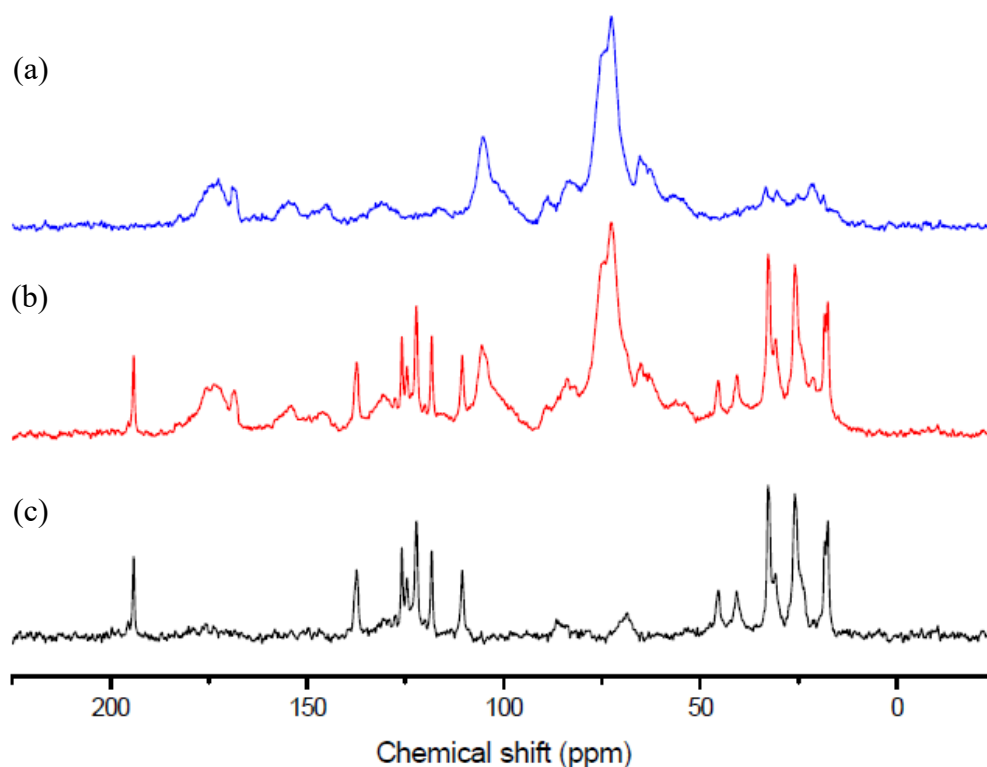


Figure 5.6. Normalised spectra with ^{13}C CPMAS SSNMR experiments of: (a) Damiana herbal substrate, (b) synthetic cannabinoid brand Bombay Blue (containing XLR-11) and (c) Bombay Blue spectra with Damiana subtracted. All ^{13}C CPMAS experiments were obtained with 7.05 T with a MAS rate of 10 kHz, a CP contact time of 4 ms, 16384 scans acquired and a recycled delay of 5 seconds (23 hour per spectrum). Image from reference [62].

Figure 5.6 (a) corresponds to Damiana, while (b) is the brand Bombay Blue that contains synthetic cannabinoid XLR-11. Figure 5.6 (c) is the Bombay Blue spectra with Damiana subtracted, illustrating the XLR-11 synthetic cannabinoid without the herbal substrate. The key structural components are shown as the following: peaks between 0 ppm and 50 ppm refer to aliphatic hydrocarbons, peaks between 100 ppm and 150 ppm refer to the aromatic carbons and the peak at 195 ppm refers to the carbonyl ($\text{C}=\text{O}$ ketone).

The ^{13}C CPMAS experiments were conducted on all remaining synthetic cannabinoid brands and differentiation between specific compounds was determined. Samples containing UR-144, XLR-11 or AM-2201 presented a ketone peak at 195 ppm, 5F-AKB48 had an amide peak at

160 ppm and PB-22 had an ester present at 170 ppm. As ^{13}C CPMAS experiments are not quantitative, an effort to quantify synthetic cannabinoid concentrations were trialled with direct ^{13}C MAS experiments, without the cross polarisation from ^1H . The T_1 relaxation time for the herbal substrate was longer than that of the synthetic cannabinoid, therefore different recycle delay times could be used to selectively observe the signal from the cannabinoid. A short delay of 2 seconds effectively showed the XLR-11 without the substrate while a longer delay of 60 seconds, showed both components. Figure 5.7 illustrates the synthetic cannabinoid brand Bombay Blue with a 2 second and 60 second delay times.

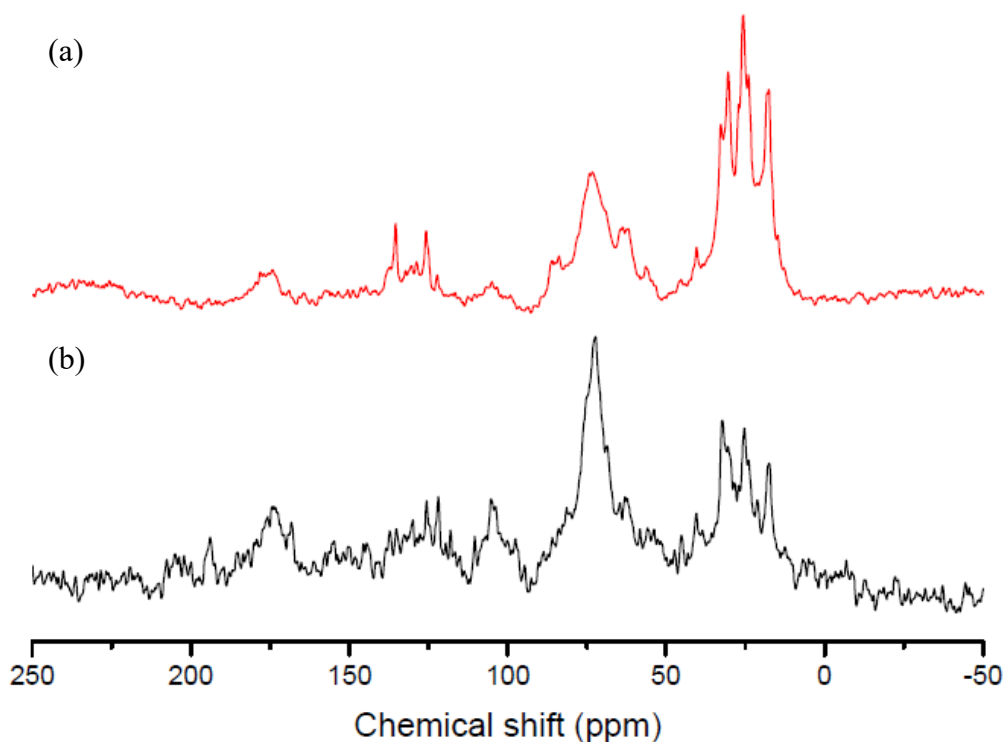


Figure 5.7. Synthetic cannabinoid brand Bombay Blue with direct ^{13}C MAS SSNMR experiments at different recycle delay times: (a) 2 seconds (16384 scans) illustrating XLR-11 without the herbal substrate and (b) 60 seconds (6165 scans) with both components. Image from reference [62].

Although the direct ^{13}C MAS approach is quite time consuming, it has the potential for quantification of the synthetic cannabinoid component.

Once the collaborative component of the work was completed with Niki Burns one key aspect needed to be further explored and it was important to use an approach to test the idea of the potential crystalline nature of the synthetic cannabinoids on the Damiana substrate. This was explored in order to see if it is the nature of the crystal formation that leads to the relatively sharp ^{13}C peak widths observed in the SSNMR spectra generated. To explore the crystallinity of the synthetic cannabinoid present on the surface of the herbal substrate, the ^1H T_1 relaxation times were determined for the synthetic cannabinoid, with and without the plant material, which was also compared to a starting material compound (indole-3-carboxaldehyde). See Figure 5.8 for the chemical structures. The T_1 value for the synthetic cannabinoid brand Bombay Blue (that has been shown to contain XLR-11) was 1.3 seconds, with the XLR-11 standard having a T_1 of 1.8 seconds and indole-3-carboxaldehyde that represents the core of the structure illustrated a T_1 time of 1.1 seconds. The ^1H T_1 for Bombay Blue was measured indirectly from the ^{13}C nuclei *via* a CP method to avoid interference from the ^1H signal generated from the plant material, while XLR-11 and the indole were measured directly from the ^1H signal.

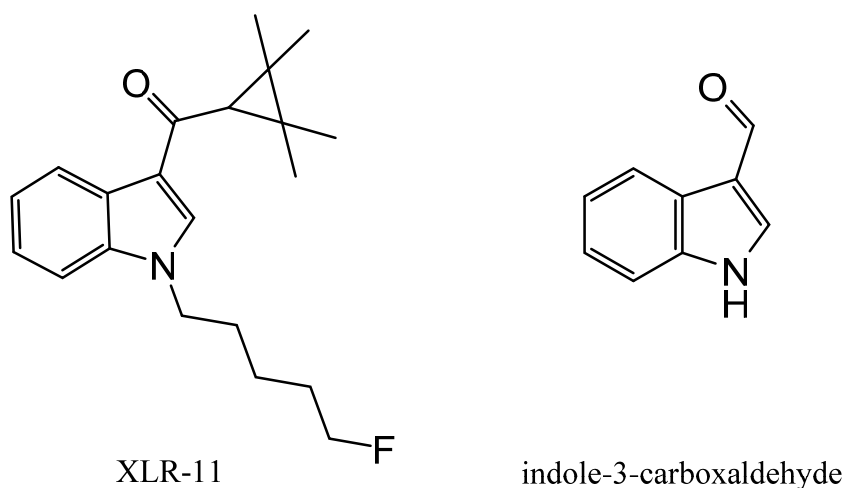


Figure 5.8. Chemical structures of the synthetic cannabinoid XLR-11 and a starting material indole-3-carboxaldehyde.

The consistency of the T_1 relaxation times between the commercial synthetic cannabinoid herbal product sample and the crystalline XLR-11 standard suggests that the synthetic cannabinoid sprayed onto the plant material may form crystalline aggregations on the surface rather than being fully absorbed into the substrate. The smaller T_1 time for the Bombay Blue compared to the XLR-11 could potentially be attributed to a smaller crystal size, as smaller crystals tend to display shorter T_1 values due to efficient relaxation at the crystal surface.

An alternative explanation for the narrow peaks present in a ^{13}C CP MAS NMR experiment of Bombay Blue compared to XLR-11, is the mobility of isolated molecules absorbed by the herbal substrate and shown in Figure 5.9.

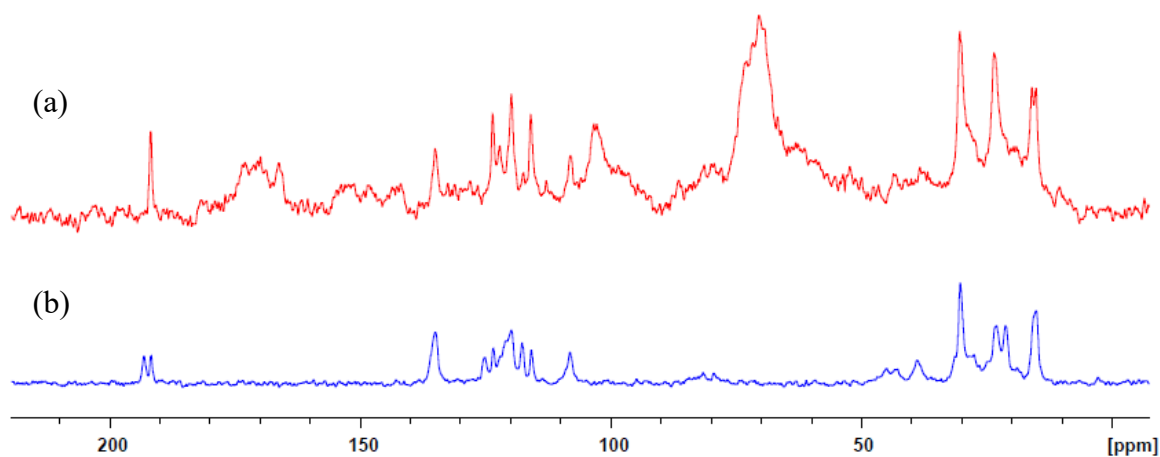


Figure 5.9. Normalised spectra with ^{13}C CPMAS SSNMR experiments of: (a) synthetic cannabinoid brand Bombay Blue (containing XLR-11) and (b) XLR-11 standard. All ^{13}C CPMAS experiments were obtained with 7.05 T with a MAS rate of 10 kHz, a CP contact time of 4 ms, 16384 scans acquired and a recycled delay of 5 seconds (23 hour per spectrum).

The peaks at approximately 195 ppm illustrate a difference between the crystalline standard and the synthetic cannabinoid that has been sprayed onto the herbal substrate. The presence of a split peak in the standard indicates two molecular conformations within a single crystal structure whereas the absence of these split peaks in Bombay Blue suggest the absorption of the molecules within the herbal substrate rather than crystalline aggregates on the surface material.

The SSNMR results between the T_1 relaxation times and the observed CP peaks are therefore unfortunately unable to determine whether the cannabinoids exist as crystalline aggregates or isolated absorbed molecules and these results highlight the complexity of these herbal substrates and the crystallinity of the synthetic cannabinoid sprayed onto the plant material remains a complex problem. Further investigation into the conformation of the synthetic cannabinoid is required and could potentially be resolved with techniques such as scanning electron microscopy (SEM) or crystal structure determination with XRD. Never-the-less the SSNMR approach presented here is an excellent tool for aiding the structural elucidation of

synthetic cannabinoids directly from the real world sample without requiring an extraction process.

A number of the synthetic cannabinoid brands that contain low concentrations of the active ingredient, were not resolved within an appropriate timeframe with the ^1H - ^{13}C CPMAS. Therefore, a ^{19}F MAS technique was utilised to identify the synthetic cannabinoids that contain a fluorinated alky chain tail. Brands containing XLR-11, AM-2201, 5F-PB-22 and 5F-AKB48 resulted in a peak at -218 ppm, that is characteristic of a primary alkyl fluoride. No ^{19}F signals were detected on brands that contain synthetic cannabinoids without fluorine substitutes, which was expected. Figure 5.10 illustrates the spectra obtained for nine brands as well as the Damiana substrate with ^{19}F MAS experiments.

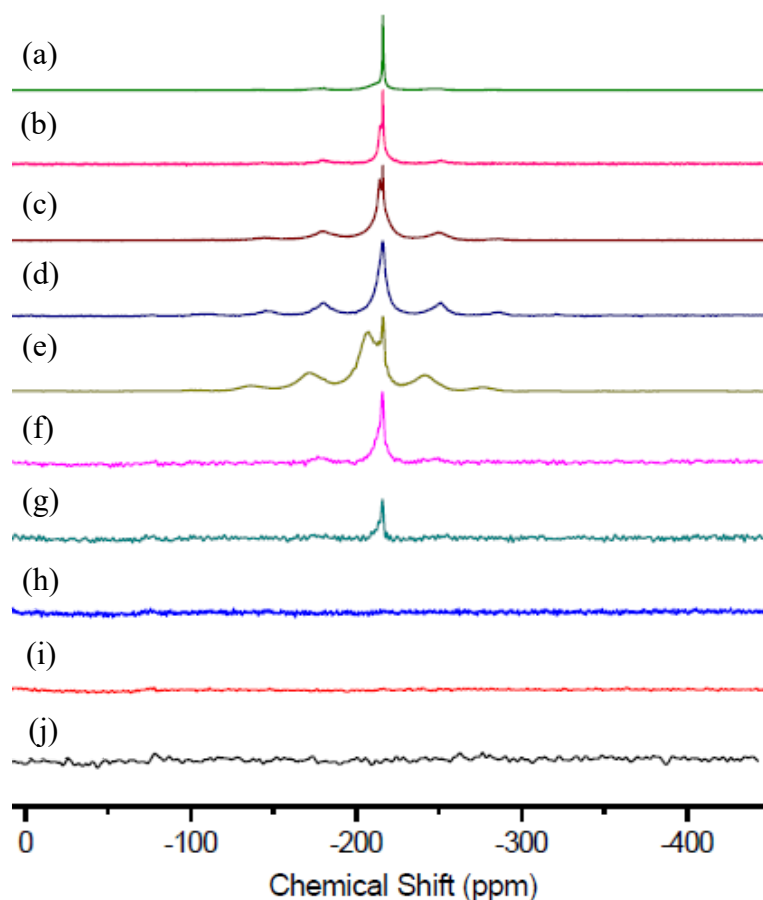


Figure 5.10. Normalised ^{19}F MAS SSNMR spectra from different synthetic cannabinoid brands. (a) Malibu (5F-AKB48), (b) Cloud 9 (UR-144 and XLR-11), (c) Bombay Blue (XLR-11), (d) Red Dot (AM-2201), (e) Voodoo (Unknown), (f) Atomic Bomb (5F-PB-22 and PB-22), (g) Code Black (UR-144), (h) Puff (UR-144), (i) Supernova (PB-22) and (j) Damiana. All ^{19}F spectra was acquired at 7.05 T and 10 kHz MAS using a 2 μs excitation pulse and 51200 scans with a 2 second recycle delay (28 hour per spectrum). Image from reference [62].

The methods currently used for forensic analysis of synthetic cannabinoids involve extensive sample preparation with no option for a non-destructive technique. The ECL methodology illustrated above and these SSNMR experiments, provide a simple alternative technique that is non-destructive, requires minimal sample preparation and is specific to certain atoms or functional groups present. Utilising both ^{13}C CPMAS and ^{19}F MAS SSNMR experiments, key structural components can be readily identified. For both ECL and SSNMR techniques the

non-destructive techniques allows for sample integrity that can be used for further forensic investigations.

Forensic samples are often seized in small quantities therefore the ability to develop a method that is non-destructive and requires minimal amounts for analysis, is particularly important. The United Nations Office of Drugs and Crime (UNODC) recommendations for the analysis of synthetic cannabinoid compounds in herbal substrates require an extraction followed by a separation technique (either gas or liquid chromatography) as well as identification through mass spectrometry (MS) [67]. These methods require extensive preparation which removes the option for sample re-use, while SSNMR provides a method that requires no extraction or separation and affords sample integrity.

The development of new NMR technologies also allows for a portable screening tool, as commercial benchtop NMR instruments have recently become available [216], allowing for the opportunity advancement of an at-scene identification method.

5.4 Conclusions

Thirteen synthetic cannabinoid compounds were subjected to cyclic voltammetry experiments to gain an understanding of their individual redox processes for an ECL detection system. Forward and reverse sweeps were performed to obtain oxidation and reduction potentials for all thirteen synthetic cannabinoid standards. Nine of the thirteen compounds were subjected to cyclic voltammetry experiments with either an Ir(ppy)₃ or [Ru(bpy)₃]²⁺ luminophore and both anodic and cathodic ECL response was monitored with a PMT as the photodetector. Seven out of the nine exhibited an ECL response with either one or both metal complexes which indicates that ECL may be a viable detection system for these substances.

Utilising a PMT detector, emission is assumed to be emanating from solution near the surface of the working electrode. A forward sweep indicates an oxidative-reduction (anodic) ECL response and negative sweep indicates a reductive-oxidative (cathodic) ECL response. The ECL emission from five standards was visualised with chronoamperometry experiments under a DSLR camera to locate whether the emission is occurring at the working and/or the counter electrode, and to confirm these reaction pathways. Two of the five synthetic cannabinoids (AM-1220 and PB-22) exhibited only oxidative-reduction ECL emission with both metal complexes. When positive potentials were applied, emission was seen at the working electrode whilst negative potentials applied at the working electrode resulted in emission at the counter electrode where the corresponding positive potential is located. XLR-11 only exhibited a response within cathodic potentials when reacted with the iridium centered complex and no ECL emission was visualised with the ruthenium based luminophore. Interestingly, 5F-AKB48 and UR-144 illustrated both anodic and cathodic ECL responses therefore could potentially be further explored for a dual emission system with both metal complexes present.

Twelve herbal brands with known synthetic cannabinoids present, were subjected to cyclic voltammetric experiments in both anodic and cathodic potentials with PMT detection. No extraction of the active component was necessary which is ideal in a forensic context with on-the-spot testing. The ECL responses from these samples corresponded with the standard responses however slight variations in ECL emission patterns could be due to the unknown concentration of active ingredient present in each substrate. All twelve herbal blends gave a response, with no interference from the substrate, from either one or both metal luminophores, which confirms the viability of ECL detection for seizure samples containing synthetic cannabinoids.

Solid-state NMR was explored alongside ECL to illustrate a secondary technique that is non-destructive to the herbal substrate and requires little sample preparation. Specific functional groups were identified through ^{13}C CPMAS and ^{19}F MAS SSNMR experiments that illustrated carbons or the fluorinated alkyl chain present on the synthetic cannabinoid substances. The herbal substrate could be subtracted from the spectra, leaving the corresponding synthetic cannabinoid peaks. This is particularly important as it confirms a secondary option for the identification of synthetic cannabinoids with little sample preparation and is non-destructive, allowing for further analysis if needed.

Further experiments were completed to determine if the synthetic cannabinoid compounds that are sprayed onto the herbal substrate is present as a crystalline aggregate on the surface of the plant material or absorbed by the substrate. The results between T_1 relaxation times and ^{13}C CPMAS experiments illustrate the complexity of the herbal substrates and requires further analysis.

CHAPTER SIX:

CONCLUDING REMARKS AND FUTURE WORK

6.1 Concluding remarks

Post-column chemiluminescence (CL) detection is a viable method for methylenedioxy ring substituted amphetamine type stimulants however was not as selective for synthetic cannabinoid compounds. A secondary ruthenium centered CL reagent was selective towards synthetic cannabinoids at expense of the stability. Understanding and optimising the stability issues with the secondary reagent could potentially introduce a new CL reagent that is selective to species the traditional reagents cannot detect.

Fundamental co-reactant electrochemiluminescence (ECL) was explored using TPrA to better understand the reaction mechanisms of three metal complexes. This research began with the traditional PMT detections however it was important to utilise a digital camera to determine location of ECL emission. Determining the location of the emission it was possible to illustrate whether anodic or cathodic processes occurred and to clarify some confusion within previous literature surrounding 'cathodic' ECL.

Once the fundamental electron-transfer processes were understood for the metal complexes it was applied by utilising a synthetic cannabinoid co-reactant. Both PMT and digital camera detection illustrated that synthetic cannabinoid compounds can act as a co-reactant with enough energy to generate an excited state metal complex and result in the emission of light. Therefore, ECL is deemed a viable detection method and can be applied as a screening tool for synthetic cannabinoid compounds, without the need for a sample extraction.

Solid-state nuclear magnetic resonance (SSNMR) spectroscopy was ran alongside ECL experiments as a complementary method that may offer a non-destructive approach to directly elucidate synthetic cannabinoids. Specific structures were identified through ^{13}C CPMAS and ^{19}F MAS experiments while crystallinity on the surface of the herbal substrate was explored

via T₁ and ¹³C CPMAS experiments which confirms the complexity of the herbal substrates and requires further analysis.

6.2 Future work

There is no limit to expanding on the work presented in this thesis as chemistry and forensically important compounds are constantly evolving and new techniques are emerging. A few recommendations for future directions are suggested below.

Chapter 2 investigated utilising chemiluminescence detection for amphetamine type stimulants and synthetic cannabinoids. A mixture of three synthetic cannabinoids was separated using HPLC with post-column chemiluminescence detection. It is recommended to explore the chemiluminescence stability issues with the bis(acetonitrile)bis(2,2'-bipyridine)ruthenium(II) reagent. The acetonitrile complex was more selective towards the synthetic cannabinoid compounds however lack of stability was a major downfall for utilising bis(acetonitrile)bis(2,2'-bipyridine)ruthenium(II) as a potential new chemiluminescence reagent. Producing a stable reagent with bis(acetonitrile)bis(2,2'-bipyridine)ruthenium(II) could expand chemiluminescence selectivity with indole or indazole based compounds. It would also be worth exploring the possibility of testing herbal substrates that contain synthetic cannabinoids to see if this technique is viable for real world samples.

Chapter 4 investigated dual emission systems for electrochemiluminescence detections at two simultaneous electrodes. Successful dual emission was observed with a [Ru(bpy)₃]²⁺ and Ir(ppy)₃ system with a TPrA co-reactant. As there are numerous iridium and ruthenium centered metal chelates that may be more selective towards other target compounds, it would be worth exploring dual emission systems with different iridium or ruthenium complexes *via*

a comprehensive systematic study. Other highly reactive co-reactants could also be explored as a model compound for application purposes.

One issue that arose in chapter 4 is the inability to monitor counter electrode potentials when cyclic voltammetric experiments were performed. The ability to monitor these potentials would benefit the PMT data that corresponds only to potentials that were applied.

Chapter 5 investigated electrochemiluminescence detection for synthetic cannabinoid compounds. Not all standards were subjected to PMT and digital camera detections due to time restraints so it would be worth expanding this library of data. Dual emission seemed viable for specific synthetic cannabinoid compounds however was never performed. It would be interesting to explore if dual emission can occur for these compounds and then further explore bi-detection systems with more than one compound present. The herbal substrates containing synthetic cannabinoids were tested with PMT detection however camera images were not obtained. These images would be useful in order to determine rough concentrations of active ingredients corresponding to the amount of light emitted.

Chapters 3, 4 and 5 all explored ECL detection using platinum and glassy carbon electrodes which can be quite expensive. Ideally, a cheaper option would be explored such as screen printed or miniaturised planar electrodes, however for systems that require organic solvents this can be quite difficult. It would be worth investigating the solubility of reagents as well as potential aqueous environments to introduce cheaper electrode options.

Chapter 5 also explored utilising SSNMR to identify specific atoms within the synthetic cannabinoid structure and their crystallinity on the surface of the herbal substrate. The results between ^1H T_1 experiments and ^{13}C CP MAS illustrate the complexity of the plant material and

crystal structure determination through XRD or imaging through SEM is suggested for further investigations.

REFERENCES

1. UNODC, *World Drug report - Analysis of Drug Markets*. United Nations Office on Drugs and Crime, 2018. **3**.
2. Schloenhardt, A., *The market for amphetamine-type stimulants and their precursors in Oceania*. 2007, Australian Institute of Criminology.
3. *Phenethylamines*. Illicit Drug Data Report, 2003-04: p. 1-10.
4. Fowler, G., Kinner, S., Krenske, L., *Containing ecstasy: analytical tools for profiling an illegal drug market*. 2007, National Drug Strategy.
5. UNODC, *Amphetamine, methamphetamine and their ring-substituted analogues in seized materials*. United Nations Office on Drugs and Crime, 2006.
6. King, L.A., *Generic controls: Group-specific*. The Misuse of Drugs Act: A Guide for Forensic Scientists, 2003: p. 29-37.
7. Allen, A. and R. Ely, *Review: Synthetic Methods for Amphetamine*. 2010, North West Association of Forensic Scientists.
8. Lee, J.S., et al., *Analysis of the impurities in the methamphetamine synthesized by three different methods from ephedrine and pseudoephedrine*. Forensic Science International, 2006. **161**(2-3): p. 209-215.
9. Choe, S., et al., *Estimation of the synthetic routes of seized methamphetamines using GC-MS and multivariate analysis*. Forensic Sci Int, 2016. **259**: p. 85-94.
10. Skinner, H., *Methamphetamine synthesis via hydriodic acid/red phosphorus reduction of ephedrine*. Forensic Sci Int, 1990. **48**: p. 123-134.
11. Qi, Y., I.D. Evans, and A. McCluskey, *Australian Federal Police seizures of illicit crystalline methamphetamine ('ice') 1998-2002: impurity analysis*. Forensic Sci Int, 2006. **164**(2-3): p. 201-10.
12. *Australian Illicit Drug Report: Amphetamines*. 1998-99, Australian Bureau of Criminal Intelligence. p. 47-59.
13. UN, *List of precursors and chemicals frequently used in the illicit manufacture of narcotic drugs and psychotropic substances under international control*. 2018, United Nations International Narcotics Control Board: Vienna.
14. King, L.A., *Future developments*. The Misuse of Drugs Act: A Guide for Forensic Scientists, 2003: p. 73-85.

15. Government, N., *Schedule 4 (Prescribed Restricted Substances)*. 2014, NSW Ministry of Health.
16. Government, V.S., *SafeScript*. 2018, Department of Health & Human Services.
17. Andrighetto, L., *Platform Technology Towards the Chemical Fingerprinting of Methamphetamine from Ephedrine Pathways*. 2016, Deakin University.
18. EMCDDA, *Amphetamine, methamphetamine and MDMA — Production and precursors*. EU Drug Markets Report, 2016.
19. Shulgin, A. and A. Shulgin, *PIHKAL - A Chemical Love Story*. 1991, United States: Transform Press.
20. Murnane, K.S., et al., *Discriminative stimulus effects of psychostimulants and hallucinogens in S(+)-3,4-methylenedioxymethamphetamine (MDMA) and R(-)-MDMA trained mice*. J. Pharmacol. Exp. Ther., 2009. **331**(2): p. 717-723.
21. Murnane, K.S., et al., *Endocrine and neurochemical effects of 3,4-methylenedioxymethamphetamine and its stereoisomers in rhesus monkeys*. J. Pharmacol. Exp. Ther., 2010. **334**(2): p. 642-650.
22. Iversen, L.W., R., *Speed, Ecstasy, Ritalin: The Science of Amphetamines*. 2006: Oxford University Press.
23. Silins, E., Bleeker, A., Martin, G., *Ecstasy: Facts and Fiction*. 2008, National Drug and Alcohol Research Centre.
24. Bernschneider-Reif, S., F. Oxler, and R.W. Freudenmann, *The origin of MDMA (Ecstasy) separating the facts from the myth*. Die Pharmazie - An International Journal of Pharmaceutical Sciences, 2006. **61**(11): p. 966-972.
25. Grinspoon, L. and J.B. Bakalar, *Can drugs be used to enhance the psychotherapeutic process?* Am. J. Psychother., 1986. **40**(3): p. 393-404.
26. Parrott, A.C., *Human psychopharmacology of Ecstasy (MDMA): a review of 15 years of empirical reseach*. Hum. Psychopharmacol., 2001. **16**(8): p. 557-577.
27. NIDA, *MDMA (Ecstasy Abuse)*. National Institute on Drug Abuse, 2017.
28. ACIC, *Illicit Drug Data Report*. Australian Criminal Intelligence Commission, 2014-15.
29. Commission, T.A.C., *Illicit Drug Data Report 2010-11*. 2012, Commonwealth Government of Australia: Canberra.
30. Rogers, P. and J. Williams, *National amphetamine-type stimulant strategy : background paper / by National Drug Research Institute ; Australian Institute of*

- Criminology ; report prepared for the Department of Health and Ageing*. 2007, National Drug Research Institute: Australian Institute of Criminology.
31. *Get the facts about drugs*. 2008, United Nations Office on Drugs and Crime: Vienna. p. 7.
 32. McCann, U.D. and G.A. Ricaurte, *Effects of MDMA on the Human Nervous System*. 2014: p. 475-497.
 33. McGuire, P., *Long term psychiatric and cognitive effects of MDMA use*. Toxicology Letters, 2000. **112-113**: p. 153-156.
 34. McCann, U.D., et al., *Positron emission tomographic evidence of toxic effect of MDMA ("Ecstasy") on brain serotonin neurons in human beings*. The Lancet, 1998. **352**(9138): p. 1433-1437.
 35. *Amphetamine-Type Stimulants*, in *Illicit Drug Data Report 2010-11*. 2012, Australian Crime Commission: Canberra. p. 23-43.
 36. Houck, M.S., J., *Fundamentals of Forensic Science*. 2nd ed. 2010, Oxford: Academic Press.
 37. Bell, S., *Forensic Chemistry*. 1st ed. 2006, New Jersey: Pearson Education.
 38. UN, *Recommended Methods for Testing Illicit Ring-Substituted Amphetamine Derivatives*. United Nations Division of Narcotic Drugs, 1987.
 39. Cole, M.D., *The Analysis of Controlled Substances*. 2003: John Wiley & Sons.
 40. Quinn, C., Black, E., Dunn, M. & Degenhardt, L., *Methylamphetamine in Victoria 2004-2007: Forms and purity*. 2008, National Drug and Alcohol Research Centre: Sydney.
 41. NIDA, *MDMA (Ecstasy/Molly)*. National Institute on Drug Abuse, 2018.
 42. UNODC, *World Drug Report*. United Nations Office on Drugs and Crime, 2017.
 43. ACIC, *Illicit Drug Data Report*. Australian Criminal Intelligence Commission, 2016-2017.
 44. O'Neal, C.L., D.J. Crouch, and A.A. Fatah, *Validation of twelve chemical spot tests for the detection of drugs of abuse*. Forensic Sci Int, 2000. **109**: p. 189-201.
 45. Connaughton, M. *The VICE MDMA census*. 2017.
 46. Hodges, C., *The use of Fourier Transform Raman spectroscopy in the forensic identification of illicit drugs and explosives*. Spectrochimica Acta, 1990. **46A**(2): p. 303-307.

47. *FT-IR Spectroscopy: Attenuated Total Reflectance*, P. Elmer, Editor. 2005: Shelton, USA.
48. Mills III, T., et al., *Instrumental Data for Drug Analysis*. Vol. 1. 2005: Taylor & Francis.
49. Sindicich, N. and L. Burns, *Australian Trends in Ecstasy and Related Drug Markets 2012*. EDRS Drug Trends Bulletin, 2012.
50. Schneider, R.C. and K.A. Kovar, *Analysis of ecstasy with a monolithic reversed-phase column*. *Chromatographia*, 2003. **57**(5-6): p. 287-291.
51. Sadeghipour, F., et al., *Rapid determination of amphetamines by high-performance liquid chromatography with UV detection*. *Journal of Chromatography A*, 1997. **761**(1–2): p. 71-78.
52. Sadeghipour, F. and J.L. Veuthey, *Sensitive and selective determination of methylenedioxyated amphetamines by high-performance liquid chromatography with fluorimetric detection*. *Journal of Chromatography A*, 1997. **787**(1–2): p. 137-143.
53. Adamovics, J., *Analysis of Addictive and Misused Drugs*. 1995, New York: Marcel Dekker Inc.
54. Nakashima, K., Ikeda, R., Wada, M., *Analytical studies on the development of High-Performance Liquid Chromatography methods with Fluorescence or Chemiluminescence Detections and their practical applications*. The Japan Society for Analytical Chemistry, 2009. **25**: p. 21-31.
55. Pavlova, V. and S. Petrovska-jovanoviæ, *Analytical study of amphetamine and methamphetamine by reversed-phase high-performance liquid chromatography method*. *Chemistry*, 2007. **16**(3): p. 226-239.
56. Pavlova, V. and S. Petrovska-Jovanović, *Simultaneous determination of amphetamine, methamphetamine, and caffeine in seized tablets by high-performance liquid chromatography*. *Acta Chromatographica*, 2007. **18**: p. 157-167.
57. Valento, M. and J. Lebin, *Emerging drugs of abuse: synthetic cannabinoids, phenylethylamines (2C drugs), and synthetic cathinones*. 2017, Elsevier Inc. p. 203-211.
58. D'Ambra, T.E., et al., *Conformationally restrained analogs of pravadoline: Nanomolar potent, enantioselective, (aminoalkyl)indole agonists of the cannabinoid receptor*. *Journal of Medical Chemistry*, 1992. **35**(1): p. 124-135.

59. Winstock, A.R. and M.J. Barratt, *Synthetic cannabis: A comparison of patterns of use and effect profile with natural cannabis in a large global sample*. Drug and Alcohol Dependence, 2013. **131**: p. 106-111.
60. Allsop, D.J., et al., *Quantifying the clinical significance of cannabis withdrawal*. PLoS One, 2012. **7**(9): p. e44864.
61. Kevin, R.C., *The psychopharmacology of novel synthetic cannabinoids*. 2017, The University of Sydney.
62. Burns, N., *Identification and Isolation of Drugs in Complex Samples*. 2017, Deakin University.
63. Seely, K.A., et al., *Marijuana-based drugs: Innovative therapeutics or designer drugs of abuse?* Molecular Interventions, 2011. **11**(1): p. 36.
64. EMCDDA, *Synthetic cannabinoids in Europe*. 2016, European Monitoring Centre for Drugs and Drug Addiction.
65. EMCDDA, *Understanding the 'Spice' Phenomenon*. 2009, European Monitoring Centre for Drugs and Drug Addiction.
66. ACMD, *Consideration of the major cannabinoid agonists*. Advisory Council on the Misuse of Drugs, 2009.
67. UNODC, *Synthetic cannabinoids in herbal products*. United Nations Office on Drugs and Crime, 2011.
68. Carlsson, A., et al., *Prediction of designer drugs: synthesis and spectroscopic analysis of synthetic cannabinoid analogues of 1H-indol-3-yl(2,2,3,3-tetramethylcyclopropyl)methanone and 1H-indol-3-yl(adamantan-1-yl)methanone*. Drug Test Anal, 2016. **8**(10): p. 1015-1029.
69. Bretteville-Jensen, A.L., et al., *Synthetic cannabinoids and cathinones: prevalence and markets*. Forensic Sci Rev, 2013. **25**(7).
70. Carlsson, A., *Synthetic and spectroscopic characterization of emerging synthetic cannabinoids and cathinones*. 2016, Linkoping University: Sweden.
71. Namera, A., et al., *Comprehensive review of the detection methods for synthetic cannabinoids and cathinones*. Forensic Toxicol, 2015. **33**(2): p. 175-194.
72. *Synthetic Cannabinoids Are Prohibited In Victoria*. Department of Health - State Government Victoria, 2012.
73. *Drugs, Poisons and Controlled Substances (Drugs of Dependence - Synthetic Cannabinoids) Regulations 2013*. Chief Parliamentary Council, 2013.

74. *Drugs, Poisons and Controlled Substances Miscellaneous Amendment Bill*. Parliament of Victoria, 2017.
75. Vandrey, R., et al., *A survey study to characterize use of Spice products (synthetic cannabinoids)*. Drug and Alcohol Dependence, 2012. **120**(1-3): p. 238-241.
76. Tracy, D.K., D.M. Wood, and D. Baumeister, *Novel psychoactive substances: types, mechanisms of action, and effects*. BMJ, 2017. **356**: p. i6848.
77. Gurney, S.M.R., et al., *Pharmacology, Toxicology, and Adverse Effects of Synthetic Cannabinoid Drugs*. Forensic Sci Rev, 2014. **26**(53): p. 54-77.
78. Lapoint, J., et al., *Severe toxicity following synthetic cannabinoid ingestion*. Clin. Toxicol. (Phila), 2011. **49**: p. 760-764.
79. Buser, G.L., R.R. Gerona, and B.Z. Horowitz, *Acute kidney injury associated with smoking synthetic cannabinoid*. Clin. Toxicol. (Phila), 2014. **52**: p. 664-673.
80. McQuade, D., et al., *First European case of convulsions related to analytically confirmed use of the synthetic cannabinoid receptor agonist AM-2201*. Eur. J. Clin. Pharmacol., 2013. **69**: p. 373-376.
81. Adamowicz, P., E. Meissner, and M. Maslanka, *Fatal intoxication with new synthetic cannabinoids AMB-FUBINACA and EMB-FUBINACA*. Clin Toxicol (Phila), 2019: p. 1-6.
82. Behonick, G., et al., *Four postmortem case reports with quantitative detection of the synthetic cannabinoid, 5F-PB-22*. J Anal Toxicol, 2014. **38**(8): p. 559-62.
83. Shanks, K.G., et al., *Case reports of synthetic cannabinoid XLR-11 associated fatalities*. Forensic Sci Int, 2015. **252**: p. e6-9.
84. Paul, A.B.M., et al., *Teens and Spice: A Review of Adolescent Fatalities Associated with Synthetic Cannabinoid Use*. J Forensic Sci, 2018. **63**(4): p. 1321-1324.
85. Institute, P., *Australia's Annual Overdose Report*. 2018.
86. de la Asuncion-Nadal, V., et al., *Identification and determination of synthetic cannabinoids in herbal products by dry film attenuated total reflectance-infrared spectroscopy*. Talanta, 2017. **167**: p. 344-351.
87. Penn, H.J., et al., *Detection of synthetic cannabinoids in herbal incense products*. Clin Biochem, 2011. **44**(13): p. 1163-1165.
88. Marino, M., L. Huang, and B. Voyer, *Nuclear Magnetic Resonance Implemented Synthetic Indole and Indazole Cannabinoid Detection, Identification, and Quantification*. Faculty Works: Biology, Chemistry, and Environmental Studies, 2014.

89. Marginean, I., W.F. Rowe, and I.S. Lurie, *The role of ultra high performance liquid chromatography with time of flight detection for the identification of synthetic cannabinoids in seized drugs*. Forensic Sci Int, 2015. **249**: p. 83-91.
90. Uchiyama, N., et al., *URB-754: a new class of designer drug and 12 synthetic cannabinoids detected in illegal products*. Forensic Sci Int, 2013. **227**(1-3): p. 21-32.
91. Stewart, K., Beecher, G. & Hare, P., *Rapid Analysis of Discrete Samples: The use of nonsegmented, continuous flow*. Analytical Biochemistry, 1976. **70**: p. 167-173.
92. Ruzicka, J.H., E.H, *Analytica Chimica Acta*, 1975. **78**(1): p. 145-157.
93. Roda, A., Mirasoli, M., Roda, B. & Reschiglian, P., *Flow-assisted analysis, in Chemiluminescence and Bioluminescence : Past, Present and Future*, A. Roda, Editor. 2011, Royal Society of Chemistry: Cambridge. p. 191-227.
94. Mansour, F.R. and N.D. Danielson, *Reverse flow-injection analysis*. TrAC Trends in Analytical Chemistry, 2012. **40**: p. 1-14.
95. Chi, Y., et al., *Flow injection analysis system equipped with a newly designed electrochemiluminescent detector and its application for detection of 2-thiouracil*. Anal. Chem., 2006. **78**: p. 1568-1573.
96. Valcarcel, M.L.d.C., M., *Flow injection analysis: A useful alternative for solving analytical problems*. Journal of Analytical Chemistry, 1990. **337**: p. 662-666.
97. Hansen, E.W., J., *Flow injection/Sequential injection analysis*, in *Ewing's Analytical Instrumentation Handbook*. 2005, Marcel Dekker.
98. Neves, M.M.P.S., et al., *A Miniaturized Flow Injection Analysis System for Electrogenenerated Chemiluminescence Based Assays*. ChemElectroChem, 2017. **4**: p. 1686-1689.
99. Calokerinos, A.P., L., *Chemiluminescence in Flow Injection Analysis*, in *Chemiluminescence in Analytical Chemistry*, A.M.B. García-Campaña, W.R.G., Editor. 2001, Marcel Dekker: New York. p. 321-348.
100. Terry, J.M., *Enhancing the chemiluminescence determinations of biologically and forensically important molecules*. 2012, Deakin University.
101. McMaster, M.C., *LC/MS - A Practical User's Guide*. 2005, New Jersey: John Wiley & Sons.
102. Snyder, L.R., J.J. Kirkland, and J.L. Glajch, *Practical HPLC method development*. 2nd ed. 1997, United States: John Wiley & Sons.

103. Rofael, H.Z. and M.S. Abdel-Rahman, *Development and validation of a high-performance liquid chromatography method for the determination of cocaine, its metabolites and ketamine*. Journal of Applied Toxicology, 2002. **22**(2): p. 123-128.
104. Francis, P.S. and J.L. Adcock, *Liquid-Phase Chemiluminescence Detection for HPLC, in Hyphenated and Alternative Methods of Detection in Chromatography*. 2011, CRC Press. p. 221-250.
105. Theakstone, A.G., et al., *Chemiluminescence detection of MDMA in street drug samples using tris(2,2'-bipyridine)ruthenium(III)*. Drug Test Anal, 2015. **7**(5): p. 428-32.
106. Barnett, N.W. and P.S. Francis, *Chemiluminescence*. 2005, Elsevier, Ltd. p. 506-511.
107. Barnett, N.W. and P.S. Francis, *Luminescence*. 2005, Elsevier, Ltd. p. 305-315.
108. Adcock, J.L., et al., *Chemiluminescence detectors for liquid chromatography*. Drug Test Anal, 2011. **3**(3): p. 139-44.
109. Adcock, J.L., et al., *Chemiluminescence and electrochemiluminescence detection of controlled drugs*. Drug Test Anal, 2011. **3**(3): p. 145-60.
110. Meseguer Lloret, S., et al., *Sensitive determination of aliphatic amines in water by high-performance liquid chromatography with chemiluminescence detection*. Journal of Chromatography A, 2004. **1035**(1): p. 75-82.
111. Gorman, B.A., P.S. Francis, and N.W. Barnett, *Tris(2,2'-bipyridyl)ruthenium(II) chemiluminescence*. Analyst, 2006. **131**(5): p. 616-39.
112. Gerardi, R.D., N.W. Barnett, and S.W. Lewis, *Analytical applications of tris(2,2'bipyridyl)ruthenium(III) as a chemiluminescent reagent*. Anal Chim Acta, 1999. **378**: p. 1-41.
113. McDermott, G.P., et al., *Stable tris(2,2'-bipyridine)ruthenium(III) for chemiluminescence detection*. Anal Chem, 2011. **83**(13): p. 5453-7.
114. Terry, J.M., et al., *Chemiluminescence detection of amino acids and related compounds using acidic potassium permanganate, manganese(IV) or tris(2,2'-bipyridine)ruthenium(III)*. Talanta, 2012. **99**: p. 1051-6.
115. Gámiz-Gracia, L., et al., *Chemiluminescence detection in liquid chromatography: Applications to clinical, pharmaceutical, environmental and food analysis—A review*. Analytica Chimica Acta, 2009. **640**(1-2): p. 7-28.

116. Roda, A., Guardigli, M., Michelini, E., Mirasoli, M. & Pasini, P., *Analytical bioluminescence and chemiluminescence*. American Chemical Society, 2003. **75**(21): p. 462A-470A.
117. Gerardi, R., Barnett, N. & Jones, P., *Two chemical approaches for the production of stable solutions of tris(2,2'-bipyridyl)ruthenium(III) for analytical chemiluminescence*. *Analytica Chimica Acta*, 1999. **388**: p. 1-10.
118. Terry, J.M., et al., *Chemiluminescence detection of heroin in illicit drug samples*. *Talanta*, 2013. **116**: p. 619-625.
119. Richter, M., *Electrochemiluminescence (ECL)*. *Chem. Rev.*, 2004. **104**: p. 3003-3036.
120. Knight, A.W., *A review of recent trends in analytical applications of electrogenerated chemiluminescence*. *TrAC Trends in Analytical Chemistry*, 1999. **18**(1): p. 47-62.
121. Miao, W., *Electrogenerated Chemiluminescence and Its Biorelated Applications*. *Chem. Rev.*, 2008. **108**(7): p. 2506-2553.
122. Marinesco, S. and N. Dale, *Microelectrode Biosensors*, ed. *Neuromethods*. Vol. 80. 2013.
123. Doeven, E.H., et al., *Red-green-blue electrogenerated chemiluminescence utilizing a digital camera as detector*. *Anal Chem*, 2014. **86**(5): p. 2727-32.
124. Yang, H., et al., *Electrochemiluminescence: A New Diagnostic and Research Tool*. *Bio/Technology*, 1994. **12**(2): p. 193-194.
125. Doeven, E.H., et al., *Mobile phone-based electrochemiluminescence sensing exploiting the 'USB On-The-Go' protocol*. *Sensors and Actuators B: Chemical*, 2015. **216**: p. 608-613.
126. Delaney, J.L., et al., *Reprint of: Use of a mobile phone for potentiostatic control with low cost paper-based microfluidic sensors*. *Anal Chim Acta*, 2013. **803**: p. 123-7.
127. Choi, J.-P. and A.J. Bard, *Electrogenerated chemiluminescence (ECL) 79*. *Analytica Chimica Acta*, 2005. **541**(1-2): p. 141-148.
128. Hercules, D.M., *Chemiluminescence Resulting from Electrochemically Generated Species*. *Science*, 1964. **145**(3634): p. 808-809.
129. Santhanam, K.S.V. and A.J. Bard, *Chemiluminescence of Electrogenerated 9,10-Diphenylanthracene Anion Radical*. *J. Am. Chem. Soc.*, 1965. **87**: p. 139-140.
130. Zweig, A., A.H. Maurer, and B.G. Roberts, *Oxidation, reduction, and electrochemiluminescence of donor-substituted polycyclic aromatic hydrocarbons*. *J. Org. Chem*, 1967. **32**(5): p. 1322-1329.

131. Su, M., W. Wei, and S. Liu, *Analytical applications of the electrochemiluminescence of tris(2,2'-bipyridyl)ruthenium(II) coupled to capillary/microchip electrophoresis: A review*. *Analytica Chimica Acta*, 2011. **704**(1-2): p. 16-32.
132. Miao, S.S., et al., *Electrochemiluminescence biosensor for determination of organophosphorous pesticides based on bimetallic Pt-Au/multi-walled carbon nanotubes modified electrode*. *Talanta*, 2016. **158**: p. 142-151.
133. Fu, X., et al., *A dual-potential electrochemiluminescence ratiometric sensor for sensitive detection of dopamine based on graphene-CdTe quantum dots and self-enhanced Ru(II) complex*. *Biosensors & Bioelectronics*, 2016. **90**: p. 61-68.
134. Gao, W., et al., *Artemisinin-Luminol Chemiluminescence for Forensic Bloodstain Detection Using a Smart Phone as a Detector*. *Anal Chem*, 2017. **89**(11): p. 6160-6165.
135. Kadimisetty, K., et al., *Automated multiplexed ECL Immunoarrays for cancer biomarker proteins*. *Anal Chem*, 2015. **87**(8): p. 4472-8.
136. Zhao, Z., et al., *Development of a Simple Multiplex Electrochemiluminescence (ECL) Assay for Screening Pre-Type 1 Diabetes and Multiple Relevant Autoimmune Diseases*. 2018.
137. Rizwan, M., N.F. Mohd-Naim, and M.U. Ahmed, *Trends and Advances in Electrochemiluminescence Nanobiosensors*. *Sensors*, 2018. **18**(1): p. 166.
138. Forster, R.J., P. Bertoncello, and T.E. Keyes, *Electrogenerated chemiluminescence*. *Annu. Rev. Anal. Chem.*, 2009. **2**: p. 359-385.
139. Tokel, N.E. and A.J. Bard, *Electrogenerated chemiluminescence. IX. Electrochemistry and emission from systems containing tris(2,2'-bipyridine)ruthenium(II) dichloride*. *J. Am. Chem. Soc.*, 1972. **94**(8): p. 2862-2863.
140. Paris, J.P. and W.W. Brandt, *Charge transfer luminescence of a ruthenium(ii) chelate*. *J. Am. Chem. Soc.*, 1959. **81**(18): p. 5001-5002.
141. Kerr, E., et al., *Considering the chemical energy requirements of the tri-n-propylamine co-reactant pathways for the judicious design of new electrogenerated chemiluminescence detection systems*. *Analyst*, 2016. **141**: p. 62-69.
142. Miao, W., J.-P. Choi, and A.J. Bard, *Electrogenerated Chemiluminescence 69: The Tris(2,2'-bipyridine)ruthenium(II), (Ru(bpy)₃²⁺)/Tri-n-propylamine (TPrA) System Revisited - A New Route Involving TPrA Cation Radicals*. *J Am Chem Soc*, 2002. **124**: p. 14478-14485.
143. Bond, A.M., et al., *Electroanalytical Methods*. 2nd ed. 2010, Berlin: Springer.

144. Bard, A.J. and L.R. Faulkner, *Electrochemical Methods, Fundamentals and Applications*. 1980, New York: Joh Wiley & Sons.
145. Barbante, G.J., *Electrochemiluminescence of ruthenium polypyridyl complexes in solution and solid-state*. 2011, La Trobe University.
146. Stojek, Z., *Electroanalytical Methods*, F. Scholz, Editor. 2010, Springer: Berlin.
147. Balzani, V., et al., *Luminescent and Redox-Active Polynuclear Transition Metal Complexes*. Chem Rev, 1996. **96**: p. 759-833.
148. Bruce, D. and M. Richter, *Green electrochemiluminescence from ortho-metalated tris(2-phenylpyridine)iridium(III)*. Anal. Chem., 2002. **74**: p. 1340-1342.
149. Soulsby, L.C., et al., *Electrochemically, Spectrally, and Spatially Resolved Annihilation-Electrogenerated Chemiluminescence of Mixed-Metal Complexes at Working and Counter Electrodes*. ChemElectroChem, 2018. **5**(12): p. 1543-1547.
150. Nelson, J.H., *Nuclear Magnetic Resonance Spectroscopy*. 2003, United States: Pearson Education.
151. Rabi, I.I., et al., *The Molecular Beam Resonance Method for Measuring Nuclear Magnetic Moments* Phys. Rev., 1939. **55**: p. 526-535.
152. Bloch, F., W.W. Hansen, and M. Packard, *Nuclear Induction*. Phys. Rev., 1946. **69**: p. 127.
153. Becker, E.D., *A brief history of nuclear magnetic resonance*. Analytical Chemistry, 1993. **65**(6): p. 295-302.
154. Burns, N.K., et al., *Extraction, identification and detection of synthetic cannabinoids found pre-ban in herbal products in Victoria, Australia*. Forensic Chemistry, 2018. **7**: p. 19-25.
155. Macomber, R.S., *A complete introduction to modern NMR spectroscopy*. 1998, United States: John Wiley & Sons.
156. Saito, T., et al., *Practical guide for accurate quantitative solution state NMR analysis*. Metrologia, 2004. **41**: p. 213-218.
157. Rossini, A.J., et al., *Dynamic Nuclear Polarization Enhanced Solid-State NMR Spectroscopy of Functionalised Metal-Organic Frameworks*. Angew Chem, 2012. **124**(1): p. 137-131.
158. Wang, W., et al., *Formation and Decomposition of Surface Ethoxy Species on Acidic Zeolite Y*. ChemPhysChem, 2005. **6**(8): p. 1467-1469.

159. Dybowski*, C. and S. Bai, *Solid-state NMR spectroscopy*. Analytical Chemistry, 2008. **80**(12): p. 4295-4300.
160. Peacock, A., et al., *Australian Drug Trends 2018: Key findings from the National Ecstasy and Related Drugs Reporting System (EDRS) interviews*. National Drug and Alcohol Research Centre, 2018.
161. GDS, *Global Drug Survey*. 2018.
162. Government, A., *National Drug Strategy Household Survey 2016*. 2017, Australian Institute of Health and Welfare.
163. Government, A., *National Drug Strategy Household Survey detailed report 2013*. 2014, Australian Institute of Health and Welfare.
164. Barratt, M.J., V. Cakic, and S. Lenton, *Patterns of synthetic cannabinoid use in Australia*. Drug and Alcohol Review, 2012. **32**(2): p. 141-146.
165. Sindicich, N.B., L., *Australian Drug Trends Series No 100*, in *Australian Trends in Ecstasy and Related Drug Markets 2012*. 2013, National Drug and Alcohol Research Centre: Sydney.
166. Parrott, A.C., *Is ecstasy MDMA? A review of the proportion of ecstasy tablets containing MDMA, their dosage levels, and the changing perceptions of purity*. Psychopharmacology (Berl), 2004. **173**(3-4): p. 234-41.
167. Sherlock K. , W.K., Hay A. W. M. , Conner M., *Analysis of illicit ecstasy tablets: implications for clinical management in the accident and emergency department*. Journal of accident and emergency medicine, 1999. **16**(3): p. 194-197.
168. Waite, R.J., et al., *Chemiluminescence detection of piperazine designer drugs and related compounds using tris(2,2'-bipyridine)ruthenium(III)*. Talanta, 2013. **116**: p. 1067-1072.
169. Nakamura, S., et al., *A sensitive semi-micro column HPLC method with peroxyoxalate chemiluminescence detection and column switching for determination of MDMA-related compounds in hair*. Anal Bioanal Chem, 2007. **387**(6): p. 1983-90.
170. Holland, B.J., et al., *Chemiluminescence detection of cannabinoids and related compounds with acidic potassium permanganate*. Drug Test Anal, 2012. **4**(7-8): p. 675-9.
171. Wiley, J.L., et al., *Hijacking of Basic Research: The Case of Synthetic Cannabinoids*, M.R.R. Press, Editor. 2011, National Institute of Health.

172. CDC, *About Synthetic Cannabinoids*. 2017, US Department of Health & Human Services.
173. Yoshikawa, N., et al., *Emission property and DFT calculation for the 3MLCT luminescence of Ru(bpy)₂(L)₂⁺ complex*. Journal of Molecular Structure, 2016. **1117**: p. 49-56.
174. Adcock, J.L., et al., *Determination of glyphosate mono-isopropylamine salt in process samples using flow injection analysis with tris(2,2'-bipyridyl)ruthenium(II) chemiluminescence detection*. Talanta, 2004. **64**(2): p. 534-537.
175. Costin, J.W., P.S. Francis, and S.W. Lewis, *Selective determination of amino acids using flow injection analysis coupled with chemiluminescence detection*. Analytica Chimica Acta, 2003. **480**(1): p. 67-77.
176. Zuccato, E. and S. Castiglioni, *Illicit drugs in the environment*. Philos Trans A Math Phys Eng Sci, 2009. **367**(1904): p. 3965-78.
177. Cole, J.C., et al., *The content of ecstasy tablets: implications for the study of their long-term effects*. Addiction, 2002. **97**: p. 1531-1536.
178. Lee, J.S., et al., *Determination of impurities in illicit methamphetamine seized in Korea and Japan*. Anal Chim Acta, 2008. **619**(1): p. 20-5.
179. Nasiri Khonsari, Y. and S. Sun, *Recent trends in electrochemiluminescence aptasensors and their applications*. Chem Commun (Camb), 2017. **53**(65): p. 9042-9054.
180. Li, L., Y. Chen, and J.J. Zhu, *Recent Advances in Electrochemiluminescence Analysis*. Anal Chem, 2017. **89**(1): p. 358-371.
181. Bouffier, L., et al., *Generation of electrochemiluminescence at bipolar electrodes: concepts and applications*. Anal Bioanal Chem, 2016. **408**(25): p. 7003-11.
182. Doeven, E.H., et al., *Potential-Resolved Electrogenerated Chemiluminescence for the Selective Detection of Multiple Luminophores*. ChemPlusChem, 2015. **80**(3): p. 456-470.
183. Stewart, A.J., J. Hendry, and L. Dennany, *Whole blood electrochemiluminescent detection of dopamine*. Anal Chem, 2015. **87**(23): p. 11847-11853.
184. Guo, W., et al., *Potential-Resolved Multicolor Electrochemiluminescence for Multiplex Immunoassay in a Single Sample*. J Am Chem Soc, 2018. **140**(46): p. 15904-15915.
185. Voci, S., et al., *Surface-Confined Electrochemiluminescence Microscopy of Cell Membranes*. J Am Chem Soc, 2018. **140**(44): p. 14753-14760.

186. Valenti, G., et al., *Single Cell Electrochemiluminescence Imaging: From the Proof-of-Concept to Disposable Device-Based Analysis*. J Am Chem Soc, 2017. **139**(46): p. 16830-16837.
187. Svir, I., et al., *Strong and Unexpected Effects of Diffusion Rates on the Generation of Electrochemiluminescence by Amine/Transition-Metal(II) Systems*. ChemElectroChem, 2015. **2**(6): p. 811-818.
188. Sentic, M., et al., *Mapping electrogenerated chemiluminescence reactivity in space: mechanistic insight into model systems used in immunoassays*. Chem. Sci., 2014. **5**(6): p. 2568-2572.
189. Ege, D., W.G. Becker, and A.J. Bard, *Electrogenerated chemiluminescent determination of Ru(bpy)₃(2+) at low levels*. Anal Chem, 1984. **56**: p. 2413-2417.
190. Russell, R., A.J. Stewart, and L. Dennany, *Optimising electrogenerated chemiluminescence of quantum dots via co-reactant selection*. Anal Bioanal Chem, 2016(408): p. 7129-7136.
191. Stewart, A.J., K. Brown, and L. Dennany, *Cathodic Quantum Dot Facilitated Electrochemiluminescent Detection in Blood*. Anal Chem, 2018. **90**(21): p. 12944-12950.
192. Santa Cruz, T.D., D.L. Akins, and R.L. Birke, *Chemiluminescence and Energy Transfer in Systems of Electrogenerated Aromatic Anions and Benzoyl Peroxide*. J. Am. Chem. Soc., 1975. **98**: p. 1677-1682.
193. Hsu, C.-W., et al., *Pyrazolo[4,3-h]quinoline Ligand-Based Iridium(III) Complexes for Electrochemiluminescence*. Chem. Asian. J., 2017. **12**: p. 1649-1658.
194. Cao, W., et al., *Novel tris(2,2'-bipyridine)ruthenium(ii) cathodic electrochemiluminescence in aqueous solution at a glassy carbon electrode*. Chemical Communications, 2002(14): p. 1540-1541.
195. Yuan, B., H. Du, and T. You, *A novel tris(2,2'-bipyridine)ruthenium(II)/tripropylamine cathodic electrochemiluminescence in acetonitrile for the indirect determination of hydrogen peroxide*. Talanta, 2009. **79**(3): p. 730-733.
196. Kerr, E., et al., *New perspectives on the annihilation electrogenerated chemiluminescence of mixed metal complexes in solution*. Chem Sci, 2016. **7**(8): p. 5271-5279.

197. Dennany, L., T.E. Keyes, and R.J. Forster, *Surface confinement and its effects on the luminescence quenching of a ruthenium-containing metallopolymer*. *Analyst*, 2008. **133**(6): p. 753-9.
198. Doeven, E.H., et al., *Selective excitation of concomitant electrochemiluminophores: tuning emission color by electrode potential*. *Angew Chem Int Ed Engl*, 2012. **51**(18): p. 4354-7.
199. Danis, A.S., et al., *Simultaneous Electrochemical and Emission Monitoring of Electrogenenerated Chemiluminescence through Instrument Hyphenation*. *Anal Chem*, 2019. **91**(3): p. 2312-2318.
200. Barbante, G.J., et al., *Control of excitation and quenching in multi-colour electrogenerated chemiluminescence systems through choice of co-reactant*. *Chemistry*, 2014. **20**(43): p. 14026-14031.
201. Thompson, D.W., A. Ito, and T.J. Meyer, *[Ru(bpy)₃]²⁺* and other remarkable metal-to-ligand charge transfer (MLCT) excited states*. *Pure and Applied Chemistry*, 2013. **85**(7): p. 1257-1305.
202. Suzuki, K., et al., *Reevaluation of absolute luminescence quantum yields of standard solutions using a spectrometer with an integrating sphere and a back-thinned CCD detector*. *Phys Chem Chem Phys*, 2009. **11**(42): p. 9850-60.
203. Mavre, F., et al., *A theoretical and experimental framework for understanding electrogenerated chemiluminescence (ECL) emission at bipolar electrodes*. *Anal. Chem.*, 2009. **81**: p. 6218-6225.
204. Doeven, E.H., et al., *A potential-controlled switch on/off mechanism for selective excitation in mixed electrochemiluminescent systems*. *Chem. Sci.*, 2013. **4**(3): p. 977-982.
205. Elgrishi, N., et al., *A Practical Beginner's Guide to Cyclic Voltammetry*. *Journal of Chemical Education*, 2017. **95**(2): p. 197-206.
206. Yin, X.-B., S. Dong, and E. Wang, *Analytical applications of the electrochemiluminescence of tris (2,2'-bipyridyl) ruthenium and its derivatives*. *TrAC Trends in Analytical Chemistry*, 2004. **23**(6): p. 432-441.
207. Badocca, D., F. Zanon, and P. Pastore, *Use of Ru(bpy)₃²⁺/tertiary aliphatic amine system fast potential pulses electrochemiluminescence at ultramicroelectrodes coupled to electrochemical data for evaluating E° of amine redox couples*. *Electrochim. acta*, 2006. **51**(28): p. 6442-6450.

208. Zhou, M., et al., *Direct voltammetric evidence for a reducing agent generated from the electrochemical oxidation of tripropylamine for electro-chemiluminescence of ruthenium tris(bipyridine) complexes?* Chemphyschem, 2003. **4**(11): p. 1241-3.
209. Vaiano, F., et al., *A novel screening method for 64 new psychoactive substances and 5 amphetamines in blood by LC-MS/MS and application to real cases.* J Pharm Biomed Anal, 2016. **129**: p. 441-449.
210. Paradowska, K. and I. Wawer, *Solid-state NMR in the analysis of drugs and naturally occurring materials.* J Pharm Biomed Anal, 2014. **93**: p. 27-42.
211. Ashbrook, S.E., D.M. Dawson, and V.R. Seymour, *Recent developments in solid-state NMR spectroscopy of crystalline microporous materials.* Phys Chem Chem Phys, 2014. **16**(18): p. 8223-8242.
212. Schaefer, J. and E.O. Stejskal, *Carbon-13 nuclear magnetic resonance of polymers spinning at the magic angle.* Journal of the American Chemical Society, 1976. **98**(4): p. 1031-1032.
213. Albert, K. and E. Bayer, *Characterization of bonded phases by solid-state NMR spectroscopy.* Journal of Chromatography A, 1991. **544**: p. 345-370.
214. Sperger, D.M. and E.J. Munson, *Analysis of structural variability in pharmaceutical excipients using solid-state NMR spectroscopy.* AAPS PharmSciTech, 2011. **12**(3): p. 821-833.
215. Marino, M., et al., *Rapid Identification of Synthetic Cannabinoids in Herbal Incenses with DART-MS and NMR.* J Forensic Sci, 2016. **61**(S1): p. S82-S91.
216. Ariando, D., et al., *An autonomous, highly portable NMR spectrometer based on a low-cost System-on-Chip (SoC).* Journal of Magnetic Resonance, 2019. **299**: p. 74-92.